Volume 1 Issue 2 • December 2015
ISSN (Print): 2424-7847 | ISSN (Online): 2424-7855

Advances in Modern ONCOLOGY Research

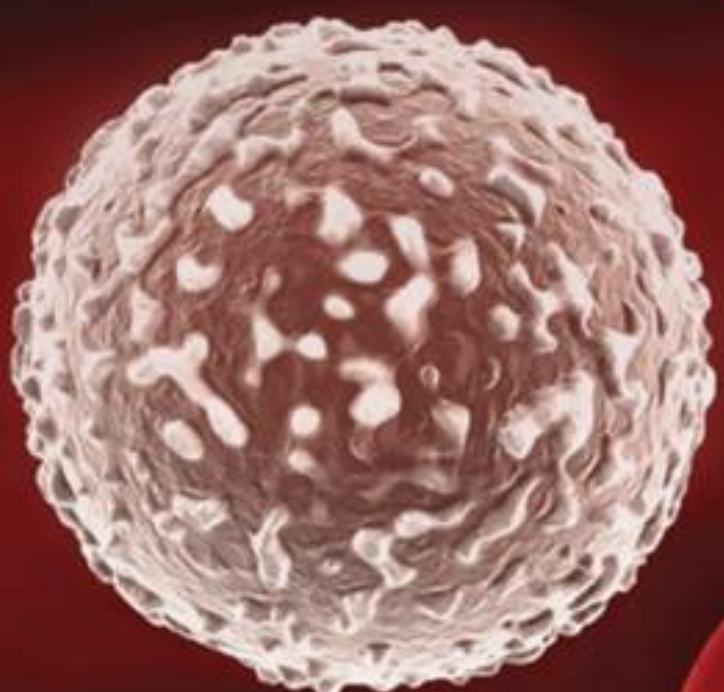

www.advmodoncolres.com

Pisco Med Publishing

Advances in Modern Oncology Research
Volume 1 Issue 2 • December 2015

Editorial Board

Managing Editor

Kho Siew Leng
sl.kho@piscomed.com
Advances in Modern Oncology Research
Editorial Office

Advances in Modern Oncology Research

December 2015 • Volume 1 • Issue 2 • Pages 79–150

Advances in Modern Oncology Research

www.advmodoncolres.com

Contents

Advances in Modern Oncology Research

doi: 10.18282/amor.v1.i2.86

EDITORIAL

Health economics of breast cancer management: An oversight

Omar Abdel-Rahman

Clinical Oncology Department, Faculty of Medicine, Ain Shams University, Cairo, Egypt

***Keywords*:** breast cancer; resource utilization; health economics

***Citation*:** Abdel-Rahman O. Health economics of breast cancer management: an oversight. Adv Mod Oncol Res 2015; 1(2): 79; http://dx.doi.org/10.18282/amor.v1.i2.86.

*Correspondence to: Omar Abdel-Rahman, Clinical Oncology Department, Faculty of Medicine, Ain Shams University, Lotfy Elsayed Street, Cairo, 113331, Egypt, omar.abdelrhman@med.asu.edu.eg.

Received: 13th November 2015; **Accepted:** 21st November 2015; **Published Online:** 30th November 2015

Cancer is a global health problem with profound healthcare, social and economic consequences. Breast cancer tops the list of cancer cases in women and approximately 1 in 8 women is diagnosed with this disease[1]. In the past two decades, major breakthroughs have been achieved in the treatment of breast cancer. Every year, researchers explore newer therapeutics which pave the way towards better treatment outcomes. However, these new therapeutics pose an extra burden on the already compromised economies all over the world. Moreover, the implementation of properly qualified breast cancer centers, comprehensive multidisciplinary teams and the institution of quality assurance measures to help foster a standard of care for breast cancer management require considerable costs[2]. The proper assessment of aspects relevant to breast cancer health economics should be conducted after joint discussion between breast cancer physicians and experts in health economics and quality of medical care[3].

A frequently overlooked issue in measuring the advances in breast cancer management has been the impact of these advances on healthcare resource utilization. In the current issue of *Advances in Modern Oncology Research*, a population-based study evaluating the economic burden of patients with inoperable advanced breast cancer receiving early or late capecitabine or trastuzumab as second-line treatment, is being presented[4]. The authors found that early or late capecitabine or trastuzumab administration after first-line anthracycline or taxane-based treatments did not exhibit a change in healthcare resource utilization. In addition, the 1-year healthcare costs did not differ significantly for patients treated with early or late capecitabine. However, patients receiving trastuzumab continue to face an economic burden. Such findings are particularly relevant for the decision-making process in low- and middle-income countries when dealing with breast cancer treatment on a national basis. I believe that further health economic studies are eagerly needed to guide proper decisions in breast cancer management.

Conflict of interest

The author declared no potential conflict of interest with respect to the research, authorship, and/or publication of this article.

References

1. Abdel-Rahman O, ElHalawani H. Adjuvant systemic treatment for elderly breast cancer patients; addressing safety concerns. Expert Opin Drug Saf 2014; 13(11): 1443–1467.
2. Lux M, Hildebrandt T, Beyer-Finkler E, et al. Relevance of health economics in breast cancer treatment – the view of certified breast centres and their patients. Breast Care 2013; 8(1): 15–21.
3. Jacobs VR, Bogner G, Schausberger CE, et al. Relevance of health economics in breast cancer treatment: integration of economics in the management of breast cancer at the clinic level. Breast Care 2013; 8(1): 7–14.
4. Liu C. Economic burden of patients with inoperable advanced breast cancer receiving early or late capecitabine or trastuzumab as second-line treatment: a population-based study. Adv Mod Oncol Res 2015; 1(2): 80–87.

Advances in Modern Oncology Research

doi: 10.18282/amor.v1.i2.50

TRENDS IN ONCOLOGY

Economic burden of patients with inoperable advanced breast cancer receiving early or late capecitabine or trastuzumab as second-line treatment: A population-based study

Chieh-Yu Liu

Institute of Nurse-Midwifery, School of Nursing, National Taipei University of Nursing and Health Sciences, Taipei City, Taiwan, Republic of China

***Abstract*:** This study investigates the economic burden and healthcare resource utilization of receiving early or late capecitabine and trastuzumab as second-line anthracycline- or taxane-based treatments for inoperable advanced breast cancer (IABC). Data was retrieved from the National Health Insurance Research Database of Taiwan. The demographic characteristics, healthcare resource utilization, and economic burden of patients with IABC receiving capecitabine and trastuzumab for 0–3, 3–6, 6–9 and 9–12 months after anthracycline- or taxane-based treatments were analyzed. 1,629 women newly diagnosed with IABC were recruited. IABC incidence rates reduced from 9.75% in 2004 to 7.35% in 2006. However, the proportion of patients receiving capecitabine or trastuzumab after anthracycline- or taxane-based treatments increased. Inpatient admissions (times/year), length of hospital stay (days/year), and outpatient visits (visits/year) did not differ significantly for the 2004–2005, 2005–2006 and 2006–2007 cohorts of patients with IABC receiving capecitabine and trastuzumab at different time points. The 1-year healthcare cost and outpatient, inpatient, and total costs (USD/year) differed significantly for trastuzumab but not for capecitabine. The conclusion indicated that early or late capecitabine or trastuzumab administration after first-line anthracycline or taxane-based treatments did not exhibit a change in healthcare resource utilization. In addition, the 1-year healthcare costs did not differ significantly for patients with IABC receiving early or late capecitabine. However, patients with IABC receiving trastuzumab continue to face an economic burden.

***Keywords*:** inoperable breast cancer; capecitabine; trastuzumab; healthcare resources; economic burden

***Citation*:** Liu CY. Economic burden of patients with inoperable advanced breast cancer receiving early or late capecitabine or trastuzumab as second-line treatment: A population-based study. Adv Mod Oncol Res 2015; 1(2): 80–87; http://dx.doi.org/10.18282/amor.v1.i2.50.

*Correspondence to: Chieh-Yu Liu, Institute of Nurse-Midwifery, School of Nursing, National Taipei University of Nursing and Health Sciences, 365, Ming-Te Road, Peitou District 112, Taipei City, Taiwan, Republic of China, chiehyu@ntunhs.edu.tw.

Received: 24th September 2015; **Accepted:** 21st October 2015; **Published Online:** 2nd December 2015

Globally, breast cancer is the most prevalent malignant cancer among women. Although new therapies have been proposed in recent years for possibly prolonging survival, studies regarding economic burden are scant, particularly for inoperable advanced breast cancer (IABC). Capecitabine and trastuzumab have been widely used in advanced breast cancer (ABC) treatments[1]. Capecitabine (trade name: Xeloda®), an orally administered fluoropyrimidine carbamate, has been proven effective in monotherapy for metastatic breast cancer, metastatic colorectal cancer, and adjuvant colon cancer in recent years[2-4]. In addition, trastuzumab (trade names: Herclon®, Herceptin®), a monoclonal antibody that interferes with the HER2/neu receptor, has been proven to improve clinical outcome and prolong the survival of patients with HER2-positive breast cancer and is

the standard drug for both adjuvant and metastatic cancers[5-7]. However, irrespective of whether patients with IABC receive targeted therapies, the economic burden has always been a critical concern for patients with breast cancer as well as for healthcare policy makers and health insurance providers[8].

The economic burden of patients with ABC has now been recognized and widely investigated in the United States and the European countries[9-11]. However, few studies have focused on the economic burden of IABC, probably because the IABC population is smaller than that of operable ABC. Patients with IABC may require several conventional cytotoxic treatments, and if these treatments fail, the patients may receive targeted therapies, which further increased their economic burden[12-14]. Sixteen-week intense chemotherapy has been reported to be safe and is well-tolerated by patients with IABC[15] and similar results were obtained in a Phase II study on dose-dense sequential doxorubicin and docetaxel for such patients[16]. With the failure of conventional cytotoxic treatments, the economic burden and healthcare resource utilization of early or late second-line targeted therapies are crucial. However, this concern has rarely been addressed.

In Taiwan, breast cancer has been the most prevalent cancer among females since 2007[17]. The Bureau of National Health Insurance (BNHI) reimburses the costs of capecitabine and trastuzumab only when the first-line treatment using anthracycline-plus-taxane-based treatment fails. Therefore, the economic burden and healthcare resource utilization for patients with IABC receiving first-line cytotoxic treatments can be estimated. Although numerous studies have investigated the economic burden for early-stage breast cancer[18-20], only a few have investigated the economic burden of patients with newly diagnosed IABC. Furthermore, few studies have reported the economic burden and healthcare resource utilization of early or late targeted therapy after first-line cytotoxic treatments. Anthracyclines and taxanes are frequently used in treating adjuvant and first-line metastatic or advanced cancers[21,22], and capecitabine and trastuzumab are frequently used in monotherapy and in combination for ABC[6,23–25]. In this study, the demographic characteristics, healthcare resource utilization, and economic burden of patients with IABC receiving capecitabine and trastuzumab at 0–3, 3–6, 6–9, and 9–12 months after anthracycline- or taxane-based treatments were investigated using the population-based BNHI database in Taiwan.

Materials and methods

Data

The data used in this study were retrieved from the National Health Insurance Research Database (NHIRD) of Taiwan on the basis of the following inclusion and exclusion criteria.

Inclusion criteria:

(1) Age: patients aged ≥18 years.

(2) IABC diagnosis: At least two eligible ABC diagnoses (or one ABC-related hospitalization) occurring on different days between 1st January 2004 and 31st December 2006. ABC was identified using the International Classification of Diseases, 9th Revision, Clinical Modification (ICD-9-CM) with diagnosis code 174.xx.

Among these patients, only those recently diagnosed with cancer, not having any cancer diagnosis in the previous year (clean period), and possessing a catastrophic illness card (CIC) issued by the BNHI for breast cancer were included in this study.

The patients were recently diagnosed with ABC and sequentially received chemotherapeutic treatment for more than eight months with used chemotherapeutic drugs (e.g., anthracycline, taxane, and fluorouracil) and did not undergo breast surgery for the following 1 year.

Exclusion criteria

Excluded are patients who received any form of breast surgery within one year of being recently diagnosed with ABC.

A retrospective cohort study was conducted on the basis of the NHIRD claims data to estimate the medical costs and the healthcare resource utilization of patients with IABC. Six cohorts were formed according to their year of diagnosis: cohorts A, B, and C were the capecitabine cohorts and D, E, and F were the trastuzumab cohorts for 2004–2005, 2005–2006, and 2006–2007, respectively. For each year's cohort, we further classified patients with IABC into 4 groups: receiving capecitabine or trastuzumab subsequently to anthracycline-plus-taxane-based treatments for 0–3, 3–6, 6–9, and 9–12 months. All patients with IABC were identified, except those who did not enroll in the BNHI or those making out-of-pocket healthcare payments.

Statistical analysis

Descriptive profiles were used for estimating the average annual direct medical costs for patients receiving capecitabine and trastuzumab after anthracycline- and taxane-based treatments. Continuous and other numeric

doi: 10.18282/amor.v1.i2.50

variables are presented as means and standard deviation. Categorical variables are presented as the number of observations and frequency (%). In addition, a Charlson comorbidity index (CCI) score was computed for evaluating the concurrent illnesses in each patient during the study period and was used for adjusting the expected medical resource utilization and medical costs associated with major comorbidities. A general linear model (GLM) was employed for comparing the differences in the medical costs and medical resource utilization in patients receiving capecitabine and trastuzumab at different time points. The outcome variables in this study were inpatient hospital admissions (IPD admissions, times/year), length of hospital stay (LOS, d/year), the number of outpatient visits (OPD visits, times/year), inpatient medical costs (IPD costs, USD), outpatient medical costs (OPD costs, USD), and total medical costs (USD). The covariates were age, CCI scores, and radiotherapy (RT) administration. In addition, statistical models of healthcare expenditure, as an outcome or response variable, were estimated using log-transformed dollars[26,27]. All statistical analyses were conducted using SAS (Version 8.1, SAS Institute Incorporation). Two-tailed tests of hypotheses were considered, and $p < 0.05$ was considered statistically significant.

Ethics statement

This study was approved by the Institutional Review Board of the School of Nursing, National Taipei University of Nursing and Health Sciences (CN-IRB-2011-063). The data in this study was retrieved from the NHIRD, which is maintained and managed by the National Health Research Institutes. The NHIRD contains de-identified secondary data of patients and medical facilities, and these data were scrambled twice to protect patient privacy. The informed consent requirement was waived by the review board as only secondary data were analyzed in this study.

Results

We identified and adopted 1,629 women who were recently diagnosed with IABC and sequentially received chemotherapies in 2004, 2005, and 2006 for more than 8 months after the initial diagnosis (N = 602, 520, 507 for 2004, 2005, and 2006, respectively as shown in *Table 1*). The IABC incidence rates reduced from 9.75% in 2004 to 7.35% in 2006. However, the proportion of patients receiving capecitabine sequential to anthracycline-plus-taxane-based regimens (ATC) and trastuzumab sequential to anthracycline-plus-taxane-based regimens (ATT) increased in the recent years (from 25.42% in 2004 to 57.79% in 2006). For patients with IABC on ATC at different time points (0–3, 3–6, 6–9 and 9–12 months as shown in *Table 2*), the age and CCI score distribution did not differ significantly among cohorts of A, B, and C. A borderline significant difference was observed in patients receiving RT in cohort A (p = 0.05). However, no such differences were observed for cohorts B and C. Meanwhile, for patients with IABC on ATT at different time points (0–3, 3–6, 6–9 and 9–12 months as shown in *Table 2*), the distribution of age, RT administration, and CCI scores did not significantly differ among cohorts of D, E, and F.

Regarding healthcare resource utilization, patients on ATC at different time points (0–3, 3–6, 6–9 and 9–12 months as shown in *Table 3*) were analyzed using GLM after adjustment for age, RT administration, and CCI scores. IPD admissions, LOS, and OPD visits did not significantly differ among cohorts of A, B, and C. Similarly, for patients on ATT, the IPD admissions, LOS, and OPD visits did not differ significantly among cohorts of D, E and F. Furthermore, the 1-year healthcare cost for patients on ATC at different time points (0–3, 3–6, 6–9 and 9–12 months as shown in *Table 4*) were evaluated using GLM after an adjustment of age, RT administration, and CCI scores. The OPD, IPD, and total costs did not

Table 1 Incidence of breast cancer (BC) and inoperable advanced breast cancer (IABC) patients from 2004 to 2006

Year	Women all cancer incidence[1] (*N*)	BC incidence[1] (*N*)	IABC incidence[2] (*N*)	IABC BC Incidence (%)	ATC[3] *N* (%)	ATT[4] *N* (%)	(ATC+ATT) IABC (%)
		(A)	(B)	(C) = (B)/(A)	(D)	(E)	(G) = (D+E)/(B)
2004	28821	6176	602	9.75	88 (14.6%)	65 (10.8%)	25.42
2005	29476	6593	520	7.89	134 (25.8%)	96 (18.5%)	44.23
2006	31276	6895	507	7.35	129 (25.4%)	164 (32.3%)	57.79
Total	89573	19664	1629	8.28	351 (21.5%)	325 (20.0%)	41.50

[1]The incidence data were from the Taiwan Cancer Registration System, Bureau of Health Promotion, Department of Health, Executive Yuan, Taiwan, Republic of China
[2] Data estimated from this study
[3]ATC: IABC patients receiving capecitabine subsequent to anthracycline and taxane
[4]ATT: IABC patients receiving trastuzumab subsequent to anthracycline and taxane

doi: 10.18282/amor.v1.i2.50

Table 2 Demographic information of study sample (arranged by time of receiving capecitabine/trastuzumab)

Cohort (A)	Capecitabine 2004–2005 (*N* = 88)						Trastuzumab 2004–2005 (*N* = 65)					
	Time of receiving capecitabine						Cohort (D)	Time of receiving trastuzumab				
	N	0–3 mo	3–6 mo	6–9 mo	9–12 mo	*p* value	*N*	0–3 mo	3–6 mo	6–9 mo	9–12 mo	*p* value
Age[1]												
Age ≥50	42	23	7	7	5	0.3817	35	20	7	7	1	0.6636
Age <50	46	24	14	4	4		30	17	9	3	1	
Receiving RT[1]												
Yes	37	20	13	3	1	0.050	36	22	9	4	1	0.6417
No	51	27	8	8	8		29	15	7	6	1	
CCI score ($\bar{x}$ ± SD)[2]	42 ± 23	43 ± 24	34 ± 15	48 ± 38	48 ± 22	0.4060	40 ± 18	41 ± 18	40 ± 14	41 ± 27	57 ± 15	0.7838
Cohort (B)	2005–2006 (*N* = 134)						Cohort (E)	2005–2006 (*N* = 96)				
Age[1]												
Age ≥50	92	57	20	6	9	0.6191	60	38	11	4	7	0.4873
Age <50	42	26	9	5	2		36	21	4	3	8	
Receiving RT[1]												
Yes	42	33	5	2	2	0.0790	43	28	5	3	7	0.8412
No	92	50	24	9	9		63	31	10	4	8	
CCI score ($\bar{x}$ ± SD)[2]	46 ± 26	46 ± 29	51 ± 25	35 ± 19	41 ± 17	0.4118	52 ± 25	54 ± 28	58 ± 23	45 ± 21	44 ± 18	0.3612
Cohort (C)	2006–2007 (*N* = 129)						Cohort (F)	2006–2007 (*N* = 164)				
Age[1]												
Age ≥50	75	39	21	11	4	0.5261	96	71	12	7	6	0.5606
Age <50	54	35	11	5	3		68	49	12	2	5	
Receiving RT[1]												
Yes	26	15	6	4	1	0.9615	49	41	5	2	1	0.2422
No	103	59	26	12	6		115	79	19	7	10	
CCI score ($\bar{x}$ ± SD)[2]	50 ± 27	51 ± 29	47 ± 21	55 ± 31	49 ± 27	0.7494	50 ± 30	50 ± 31	52 ± 23	53 ± 35	52 ± 25	0.7697

[1]analyzed by χ^2 test, [2]analyzed by one-way ANOVA

significantly differ among cohorts A, B, and C. However, for patients on ATT at different time points (0–3, 3–6, 6–9, and 9–12 months as shown in *Table 4*), the IPDs costs of cohort D were significantly higher in the '9–12 months' group than that in the other groups (Scheffe post-hoc comparison $p < 0.05$). Similarly, OPD and total costs of cohort F differed significantly in the 0–3 and 3–6 months groups compared with the other groups (Scheffe post-hoc comparison $p < 0.05$). OPD, IPD, and total costs did not significantly differ in cohort E.

Discussion

In this study, we used data of a population-representative database for estimating the incidence of IABC and proportion of patients receiving capecitabine and trastuzumab after anthracycline- or taxane-based treatments between 2004 and 2006. Furthermore, we investigated whether demographic characteristics, healthcare resource utilization, and healthcare differed for the different time points of receiving second-line capecitabine and trastuzumab. A review of relevant literature revealed that this is the first study to investigate the economic burden of patients with IABC.

The obtained results showed that the IABC incidence rates reduced from 2004 to 2006, possibly because of the annual increase in early screening and detection[28,29]. However, the proportion of capecitabine or trastuzumab administration has increased in the recent years, indicating that higher patients with IABC are receiving ATT and ATC. In addition, the demographic characteristics of receiving early or late capecitabine and trastuzumab did

doi: 10.18282/amor.v1.i2.50

Table 3 Healthcare resources utilization of inoperable advanced breast cancer patients receiving capecitabine and trastuzumab

	Capecitabine					Trastuzumab				
	Cohort (A): 2004–2005 (*N* = 88)					Cohort (D): 2004–2005 (*N* = 65)				
	0–3 mo	3–6 mo	6–9 mo	9–12 mo	*p* value	0–3 mo	3–6 mo	6–9 mo	9–12 mo	*p* value
IPD admissions (times/year)	8.1 ± 0.5	7.2 ± 0.6	6.7 ± 1.2	5.6 ± 2.2	0.4831	9.3 ± 0.6	9.1 ± 0.9	8.9 ± 1.4	15.9 ± 2.6	0.1114
Length of hospital stay (days/year)	114.2 ± 21.8	64.5 ± 27.3	62.1 ± 57.8	83.9 ± 100.2	0.5220	228.1 ± 86.5	106.6 ± 152.7	96.24 ± 204.9	200.6 ± 407.2	0.8781
OPD visits (times/year)	38.2 ± 1.2	39.8 ± 2.0	34.9 ± 2.5	33.4 ± 2.5	0.1830	37.8 ± 1.6	37.8 ± 2.3	36.9 ± 2.9	40.8 ± 7.6	0.9717
	Cohort (B): 2005–2006 (*N* = 134)					Cohort (E): 2005–2006 (*N* = 96)				
IPD admissions (times/year)	8.2 ± 0.4	6.3 ± 0.9	5.3 ± 1.5	8.4 ± 1.5	0.1189	7.5 ± 0.5	7.1 ± 1.1	7.1 ± 1.5	7.8 ± 0.9	0.9557
Length of hospital stay (days/year)	68.1 ± 11.5	50.4 ± 29.9	127.3 ± 47.1	62.3 ± 48.5	0.5883	96.9 ± 38.5	63.7 ± 90.6	21.9 ± 120.6	51.5 ± 77.6	0.9040
OPD visits (times/year)	40.1 ± 1.3	41.7 ± 2.1	41.3 ± 3.5	41.9 ± 3.5	0.8928	43.1 ± 1.5	50.2 ± 2.9	40.9 ± 5.4	49.1 ± 3.2	0.0715
	Cohort (C): 2006–2007 (*N* = 129)					Cohort (F): 2006–2007 (*N* = 164)				
IPD admissions (times/year)	8.99 ± 0.78	9.95 ± 1.24	10.54 ± 1.51	9.28 ± 2.98	0.8114	9.71 ± 0.41	9.64 ± 1.19	7.81 ± 1.87	11.05 ± 2.62	0.7424
Length of hospital stay (days/year)	81.09 ± 26.29	87.23 ± 42.12	31.56 ± 51.23	69.97 ± 101.85	0.8317	61.52 ± 11.25	13.06 ± 33.09	139.2 ± 51.85	31.89 ± 72.18	0.2440
OPD visits (times/year)	43.79 ± 1.22	41.89 ± 1.86	45.34 ± 2.72	41.67 ± 3.99	0.6951	45.44 ± 1.15	43.57 ± 2.46	42.42 ± 4.28	41.63 ± 3.42	0.6419

Note: All estimations have been adjusted for age, receiving radiotherapy or not and Charlson comorbidity index (CCI)

Table 4 One-year healthcare cost of inoperable advanced breast cancer patients receiving capecitabine and trastuzumab

	Capecitabine					Trastuzumab				
	Cohort (A): 2004–2005 (*N* = 88)					Cohort (D): 2004–2005 (*N* = 65)				
	0–3 mo	3–6 mo	6–9 mo	9–12 mo	*p* value	0–3 mo	3–6 mo	6–9 mo	9–12 mo	*p* value
OPD cost (NTD$/year)	12086 ± 1365	13038 ± 2251	10647 ± 2791	9334 ± 2766	0.4288	16606 ± 2730	16492 ± 3907	21983 ± 5134	19242 ± 13509	0.8461
IPD cost (NTD$/year)	24967 ± 2579	19117 ± 3386	23583 ± 6824	11894 ± 12085	0.2717	24478 ± 2229	32479 ± 3914	18257 ± 5537	59910 ± 10315	0.0488*
Total cost (NTD$/year)	27686 ± 2202	19171 ± 3341	22916 ± 4637	22614 ± 5179	0.9526	34527 ± 2807	39316 ± 4366	27939 ± 5404	54229 ± 12077	0.1074
	Cohort (B): 2005–2006 (*N* = 134)					Cohort (E): 2005–2006 (*N* = 96)				
OPD cost (NTD$/year)	14655 ± 866	14631 ± 1353	12116 ± 2331	13403 ± 2319	0.9617	20430 ± 1354	16743 ± 2610	16206 ± 4930	14558 ± 2947	0.3067
IPD cost (NTD$/year)	20637 ± 1836	19349 ± 4354	31728 ± 7473	25427 ± 7578	0.6077	23777 ± 3646	38267 ± 8742	11082 ± 11750	28362 ± 7293	0.2426
Total cost (NTD$/year)	22383 ± 1391	22855 ± 2351	21401 ± 3833	23897 ± 3838	0.9131	35866 ± 3076	37903 ± 6138	29751 ± 8945	33757 ± 6156	0.8233
	Cohort (C): 2006–2007 (*N* = 129)					Cohort (F): 2006–2007 (*N* = 164)				
OPD cost (NTD$/year)	16137 ± 873	16356 ± 1322	12289 ± 1940	14032 ± 2844	0.4761	22485 ± 1091	22081 ± 2330	17253 ± 4054	13711 ± 3244	0.0303*
IPD cost (NTD$/year)	24510 ± 1285	22735 ± 1958	21334 ± 2764	24549 ± 4160	0.8242	24951 ± 1296	20043 ± 3765	19753 ± 5978	14119 ± 8364	0.2093
Total cost (NTD$/year)	32722 ± 3252	24365 ± 5220	33263 ± 6237	43776 ± 12499	0.4766	31594 ± 1192	30766 ± 2664	24173 ± 4352	21992 ± 3974	0.0211*

Note: All estimations have been adjusted for age, receiving radiotherapy or not and Charlson comorbidity index (CCI)

* indicates significant *p* values.

doi: 10.18282/amor.v1.i2.50

not significantly differ among the 0–3, 3–6, 6–9, and 9–12 months subgroups. In this study, we classified patients into two subgroups (≥50 and <50 years) according to their age. The results indicated that early or late capecitabine or trastuzumab administration did not significantly differ between these two subgroups. Regarding healthcare resource utilization, the IPD admissions, LOS, and OPD visits did not significantly differ among those receiving early or late capecitabine or trastuzumab, implies that early or late second-line treatment in patients with IABC did not increase the healthcare service utilization. The mean of total 1-year healthcare costs of patients with IABC receiving ATC and ATT ranged from USD22,634 (cohort B) to USD39,003 (cohort D) and these values were higher than the mean of annual cost of patients with general breast cancer (approximately USD16,364) in Taiwan[30]. However, no significant differences in OPD, IPD, and total costs were observed in cohorts A, B, and C at different time points which implies that early or late administration of capecitabine did not affect the healthcare costs. For patients receiving trastuzumab, the IPD cost was significantly higher for the late-use group (9–12 months, cohort D as shown in *Table 4*) compared with the other groups. However, the OPD and total costs were significantly higher for the early-use groups (0–3 and 3–6 months in cohort F as shown in *Table 4*). This implies that physicians may prescribe trastuzumab for aggressive treatment or that the patients may prefer to receive trastuzumab combined with other chemotherapeutic treatments if first-line anthracycline- or taxane-based treatments fail.

The results in this study should be interpreted with caution. Although this study was mainly to study the economic burden of IABC patients receiving capecitabine or trastuzumab followed by anthracycline-plus-taxane-based treatments for 0–3, 3–6, 6–9, and 9–12 months, other treatments such as eribulin[31], vinorelbine and gemcitabine[32] were also proposed in recent years. Due to lack of studies, it is difficult to collect economic burden data of such treatments, which can be done in the future studies. Besides, due to the nature of secondary database study, the side effects and corresponding additional cost to the disease management and hospital stay were not recorded in NHIRD database, which can be regarded as a study limitation. This study is a parallel group study of healthcare resource utilization and the economic burden of patients with IABC receiving capecitabine and trastuzumab and whether any differences exist between early or late capecitabine and trastuzumab administration. The definition of IABC was based on the operational definition coined using the ICD-9-CM codes and BNHI drug codes for capecitabine and trastuzumab. The BNHI programme in Taiwan reimbursed capecitabine and trastuzumab as the second- or third-line treatments only if the first-line anthracycline- or taxane-based treatments have failed. In addition, every patient with breast cancer was issued a CIC based on pathological and imaging evidences. Therefore, the definition of IABC employed for patient recruitment is valid. In addition, the OPD, IPD, and total costs were calculated on the basis of the 1-year healthcare cost of receiving second-line capecitabine and trastuzumab, not for 5 years[33] or for lifetime[18], which is usually used for healthcare cost estimation. In addition, the cost estimates in this study may be conservative because the healthcare costs were estimated using NHIRD data, which is a claim-based database. Moreover, we did not consider the 'out-of-pocket' healthcare costs. The economic burden of IABC on patients receiving early or late second-line capecitabine or trastuzumab after the first-line anthracycline- or taxane-based treatments substantially influences the overall cost of breast cancer care. Therefore, our results facilitate the development of cost-effective evaluations of breast cancer therapies. Furthermore, this study serves as a valuable reference for framing reimbursement policies for patients availing IABC treatment.

Conclusion

Early or late capecitabine or trastuzumab administration after the failure of first-line anthracycline- or taxane-based treatments did not affect healthcare resource utilization. The one-year healthcare costs of early or late capecitabine administration did not differ significantly for patients with IABC. However, the economic burden remains a concern for patients receiving early or late trastuzumab.

Author contributions

Liu CY planned the study design, performed data application and statistical analysis, and authored the manuscript.

Acknowledgments

The author thanks the National Health Research Institute for administration help and providing the National Health Insurance Research Database.

doi: 10.18282/amor.v1.i2.50

Conflict of interest

The author declared no potential conflict of interest with respect to the research, authorship, and/or publication of this article.

References

1. The Medical Letter: Capecitabine and trastuzumab for metastatic breast cancer. Med Lett Drugs Ther 1998; 40(1039): 106–108.
2. Ershler WB. Capecitabine monotherapy: Safe and effective treatment for metastatic breast cancer. Oncologist 2006; 11(4): 325–335.
3. Bunnell CA, Winer EP. Oral 5-FU analogues in the treatment of breast cancer. Oncology 1998; 12 (Suppl 7): 39–43.
4. Smorenburg CH, Bontenbal M, Verweij J. Capecitabine in breast cancer: Current status. Clin Breast Cancer 2001; 1(4): 288–293.
5. Kumler I, Tuxen MK, Nielsen DL. A systematic review of dual targeting in HER2-positive breast cancer. Cancer Treat Rev 2014; 40(2): 259–270.
6. Verma S, Joy AA, Rayson D, et al. HER Story: The next chapter in HER-2-directed therapy for advanced breast cancer. Oncologist 2013; 18(11): 1153–1166.
7. Fornier M, Esteva FJ, Seidman AD. Trastuzumab in combination with chemotherapy for the treatment of metastatic breast cancer. Semin Oncol 2000; 27(6 Suppl 11): 38–45; discussion 92–100.
8. Max W, Sung HY, Stark B. The economic burden of breast cancer in California. Breast Cancer Res Treat 2009; 116(1): 201–207.
9. Montero AJ, Eapen S, Gorin B, et al. The economic burden of metastatic breast cancer: a U.S. managed care perpective. Breast Cancer Res Treat 2012; 134(2): 815–822.
10. Foster TS, Miller JD, Boye ME, et al. The economic burden of metastatic breast cancer: a systematic review of literature from developed countries. Cancer Treat Rev 2011; 37(6): 405–415.
11. Barron JJ, Quimbo R, Nikam PT, et al. Assessing the economic burden of breast cancer in a US managed care population. Breast Cancer Res Treat 2008; 109(2): 367–377.
12. Lee SG, Jee YG, Chung HC, et al. Cost-effectiveness analysis of adjuvant therapy for node positive breast cancer in Korea: docetaxel, doxorubicin and cyclophosphamide (TAC) versus fluorouracil, doxorubicin and cyclophosphamide (FAC). Breast Cancer Res Treat 2009; 114(3): 589–595.
13. Okubo I, Kondo M, Toi M, et al. Cost-effectiveness of letrozole versus tamoxifen as first-line hormonal therapy in treating postmenopausal women with advanced breast cancer in Japan. Gan To Kagaku Ryoho 2005; 32(3): 351–363.
14. Lilliu H, Stevens D, Brun C, et al. Cost of treatment and follow up of breast cancer: A retrospective assessment in a comprehensive cancer centre. Bull Cancer 2002; 89(6): 635–642.
15. Armstrong DK, Fetting JH, Davidson NE, et al. Sixteen week dose intense chemotherapy for inoperable, locally advanced breast cancer. Breast Cancer Res Treat 1993; 28(3): 277–284.
16. Cooper BW, Radivoyevitch T, Overmoyer BA, et al. Phase II study of dose-dense sequential doxorubicin and docetaxel for patients with advanced operable and inoperable breast cancer. Breast Cancer Res Treat 2006; 97(3): 311–318.
17. Lang HC, Wu SL. Lifetime costs of the top five cancers in Taiwan. Eur J Health Econ 2012; 13(3): 347–353.
18. Boswell KA, Wang X, Shah MV, et al. Disease burden and treatment outcomes in second-line therapy of patients with estrogen receptor-positive (ER+) advanced breast cancer: a review of the literature. Breast 2012; 21(6): 701–706.
19. Marchetti M, Caruggi M, Colombo G. Cost utility and budget impact of third-generation aromatase inhibitors for advanced breast cancer: A literature-based model analysis of costs in the Italian National Health Service. Clin Ther 2004; 26(9): 1546–1561.
20. Simon MS, Ibrahim D, Newman L, et al. Efficacy and economics of hormonal therapies for advanced breast cancer. Drugs Aging 2002; 19(6): 453–463.
21. Qi WX, Tang LN, He AN, et al. Comparison between doublet agents versus single agent in metastatic breast cancer patients previously treated with an anthracycline and a taxane: A meta-analysis of four phase III trials. Breast 2013; 22(3): 314–319.
22. Feng QJ, Zhang F, Huang XY, et al. Effectiveness and complications of anthracycline and taxane in the therapy of breast cancer: a meta-analysis. Pathol Oncol Res 2014; 20(1): 179–184.
23. Chitapanarux I, Kamnerdsupaphon P, Tharavichitkul E, et al. Capecitabine and weekly paclitaxel as first-line therapy in Thai patients with metastatic breast cancer. Asia Pac J Clin Oncol 2012; 8(1): 76–82.
24. Stockler MR, Harvey VJ, Francis PA, et al. Capecitabine versus classical cyclophosphamide, methotrexate, and fluorouracil as first-line chemotherapy for advanced breast cancer. J Clin Oncol 2011; 29(34): 4498–

doi: 10.18282/amor.v1.i2.50

4504.
25. Zhu Q, DeFusco PA, Ricci AJ, et al. Breast cancer: assessing response to neoadjuvant chemotherapy by using US-guided near-infrared tomography. Radiology 2013; 266(2): 433–442.
26. Nichols L, Barton PL, Glazner J, et al. Diabetes, minor depression and health care utilization and expenditures: a retrospective database study. Cost Eff Resour Alloc 2007; 5: 4.
27. Ai C, Norton EC. Standard errors for the retransformation problem with heteroscedasticity. J Health Econ 2000; 19(5): 697–718.
28. Chuwa EW, Yeo AW, Koong HN, et al. Early detection of breast cancer through population-based mammographic screening in Asian women: A comparison study between screen-detected and symptomatic breast cancers. Breast J 2009; 15(2): 133–139.
29. Miller AB. Practical applications for clinical breast examination (CBE) and breast self-examination (BSE) in screening and early detection of breast cancer. Breast Care (Basel) 2008; 3(1): 17–20.
30. Chu PC, Hwang JS, Wang JD, et al. Estimation of the financial burden to the National Health Insurance for patients with major cancers in Taiwan. J Formos Med Assoc 2008; 107(1): 54–63.
31. Kaufman PA, Awada A, Twelves C, et al. Phase III open-label randomized study of eribulin mesylate versus capecitabine in patients with locally advanced or metastatic breast cancer previously treated with an anthracycline and a taxane. J Clin Oncol 2015; 33(6): 594–601.
32. Halim A, Wahba H. Second-line neoadjuvant vinorelbine and gemcitabine combination in locally advanced breast cancer showing no early response to TAC. Med Oncol 2012; 29(2): 454–458.
33. Li H, Huang Y, Huang R, et al. Standard treatment cost of female breast cancer at different TNM stages. Chin J Oncol 2013; 35(12): 946–950.

doi: 10.18282/amor.v1.i2.50

Advances in Modern Oncology Research

doi: 10.18282/amor.v1.i2.27

REVIEW ARTICLE

The role of *P2X7R* purinoreceptor in osteosarcoma

Manish Yadav, Ajai Singh, Nazia Rizvi, Sabir Ali, Salma S, Vineet Kumar, Syed Rizwan Hussain*

Department of Orthopaedic Surgery, King George's Medical University, Lucknow, Uttar Pradesh, India.

***Abstract*:** Osteosarcoma is the most common type of bone cancer, which appears mainly in the metaphysis of long bones, especially in males between the age of 0–14 years. Malignancy usually emerges with the abnormal growth of tumor-forming bone cells. These tumor cells act like new bones that are responsible for the spread of sarcoma throughout the bone matrix. In this review, we focused on the expression and function of the P2X7 receptor (*P2X7R*) as a therapeutic target in osteosarcoma malignancy. Two known human *P2X7R* functional splice variants in osteosarcoma cell growth are the full length *P2X7RA* and the truncated *P2X7RB*. The stimulation of growth is attributed to an increase (i) in the mobilization of Ca^{2+} ions, and (ii) in the nuclear factor of activated T-cells, cytoplasmic 1 (NFATc1) activity. Furthermore, Te85 *P2X7RA+B* cells caused membrane depolarization and spontaneous release of extracellular adenosine triphosphate (ATP). The *P2X7R* agonist, benzoyl adenosine triphosphate (BzATP), may increase the liberation of ATP and this may be regulated by *P2X7R*. As a result, cell proliferation occurs with the spread of osteosarcoma throughout the bone matrix. BzATP also increases cell growth and activates NFATc1 to make it cancerous. In this review, we have highlighted the crucial role of the *P2X7R* purinoreceptor in osteosarcoma pathogenesis. It is an upstream regulator of all paths that may inhibit the receptor activator of nuclear factor kappa-B ligand (RANKL) and a mechanistic target of rapamycin (mTOR) blockers. This review suggests that *P2X7R* is an attractive therapeutic target for osteosarcoma.

***Keywords*:** osteosarcoma; purinergic receptor; osteoprotegerin; bone tumor; metastasis; osteoblast; osteoclast

***Citation*:** Yadav M, Singh A, Rizvi N, et al. Role of *P2X7R* purinoreceptor in osteosarcoma. Adv Mod Oncol Res 2015; 1(2): 88–96; http://dx.doi.org/10.18282/amor.v1.i2.27.

*Correspondence to: Syed Rizwan Hussain, Department of Orthopaedic Surgery, King George's Medical University, Chowk, Lucknow, Uttar Pradesh, 226018, India, rizwan59elmc@gmail.com

Received: 14th August 2015; **Accepted:** 27th September 2015; **Published Online:** 3rd December 2015

Osteosarcoma is the most common type of cancer that arises in bones. This type of cancer occurs in bone-forming cells and the cancer-filled bone is weak compared to normal bones. The disease predominantly affects children and teenagers but it may also occur at any age. Osteosarcoma usually arises in the metaphysis of long bones (*Figure 1*)[1], such as the distal end of femur, proximal end of tibia, and proximal humerus during the second decade of one's life[2]. Individuals with this kind of malignancy generally complained about deep-seated pain, and teenagers who are active in sports tend to experience pain in the distal end of their femur. Sudden bone fracture is an initial symptom as the affected bone becomes relatively weak and fractures may occur as a result of minor trauma. A previous study reported that the frequency of pain may be intermittent with varying intensities[3]. In osteosarcoma, swelling is typically not visible unless the disease develops closer to the surface of the body (e.g., pelvis). In addition, pain, swelling, and redness start at the site of the tumor and the feeling of pain increases with physical activities such as lifting or limping.

Osteosarcoma is an aggressive malignant neoplasm that originates from previously transformed cells of me-

senchymal origin and produces malignant osteoid bone tissues as a result of osteoblastic differentiation[4]. The characteristic feature of osteosarcoma is the presence of non-mineralized bone tissue (immature bone) within the tumor. The tumor cells are pleomorphic (variable in shape, size, and their nuclei), with several giant cells. These cells produce irregular trabeculae with or without central calcification of the tumor-filled bone. These tumor cells are incorporated in the osteoid matrix[5,6].

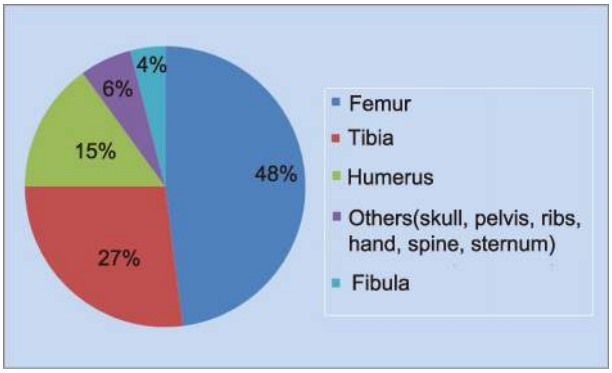

Figure 1 Prevalence of skeletal osteosarcoma malignancy (adapted from Thompson 2013[1])

The incidence of osteosarcoma for all races and both sexes are 4.0 and 5.0 per year per million people in the age range of 0–14 and 0–19 years old, respectively (*Figure 2*)[6]. It should be noted that bone sarcoma is more prevalent in males than females in the age range of 0–14 years old.

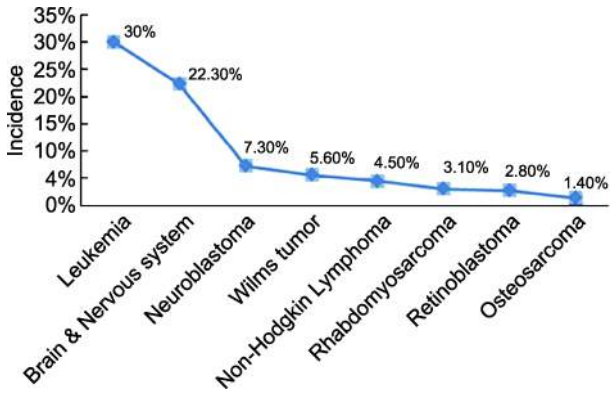

Figure 2 Incidence in relation to different cancers worldwide

Risk factors and pathogenesis

In the older population, around one-third of malignancy cases are due to Paget's disease of bone, followed by osteosarcoma[7]. The precursor conditions for osteosarcoma may be Paget's disease and other benign bony lesions[8], with chemotherapy, irradiation, as well as inherited conditions (i.e., Li-Fraumeni, Rothmund-Thomson, and Bloom and Werner syndromes)[9] being listed as potential causes.

Osteosarcoma occurs at the sites of bone growth and its proliferation creates a tendency for the osteoblastic cells of the cancer to acquire mutations, which could lead to the transformation of cells (*Rb* and *p53* genes are commonly involved). The tumors are solid, hard, and irregular owing to the tumor spicules of calcified bone radiating in triangles. These triangles are known as the Codman's triangle, which is characteristic of osteosarcoma.

Microscopically, the presence of osteoid (bone formation) is the characteristic feature of osteosarcoma within the tumor. A previous study by Smida et al. showed the amplification of chromosomes 6p21, 8q24, and 12q14, as well as the loss of heterozygosity of chromosome 10q21.1, which are the most common genomic alterations in osteosarcoma[10].

When human cells are exposed to a molecular level attack, the DNA of somatic cells may get damaged. Nonetheless, this type of DNA damage may not necessarily lead to malignancy as there are a number of tumor suppressor mechanisms in place. These mechanisms involve either the repair of DNA damage or inducing the apoptosis of these cells. The *p53* and retinoblastoma (*Rb*) genes are well-known tumor suppressor genes. However, tumor suppressor genes may themselves become mutated resulting in the loss of their protective function. Mutations in the *p53* and *Rb* genes have been proven to be involved in osteosarcoma pathogenesis[11]. The molecular pathogenesis (*Table 1*) of this malignant disease is due to abnormalities like the dysfunction of the tumor suppression gene (*p53*), transcriptional factors (*c-fos* and *c-jun* proto-oncogenes), connective tissue growth factors (CTGF), and secretion of cytokines (PTHrP, interleukin 6, and 11).

P2X7R gene

P2X7R is a human protein encoded by the *P2X7R* gene that is located on chromosome 12. The product of this gene belongs to the purinoreceptors of the ATP family[17,18]. The P2X7R is a ligand-gated cation channel, which opens in response to ATP binding and leads to cell depolarization. The P2X7R receptors require higher levels of ATP than other P2X receptors, though this could be due to a reduction in the concentration of divalent cations such as calcium or magnesium. The continuous binding results in increased permeability to *N*-methyl-D-gluca-

doi: 10.18282/amor.v1.i2.27

mine (NMDG)[20].

P2X7R is not readily desensitized and a continuous signaling leads to increased permeability and an increase in current amplitude. The activation of P2X7R by ATP helps to recruit pannexin pores[21], which allow small molecules such as ATP to leak out of the cells. This permits the activation of purinergic receptors and physiological responses such as the spread of cytoplasmic calcium waves[19]. P2X7R has been implicated in ATP-mediated cell death, regulating receptor trafficking and inflammation[22].

There are two types of purinergic receptors, P1 and P2. Adenosine acts on the P1 receptors while ATP and its breakdown products (adenosine diphosphate, ADP and adenosine monophosphate, AMP), act on the P2 receptors[23]. A previous study has proposed the subclassification of the P2 receptors, i.e., P2X (seven subtypes) and P2Y (eight subtypes) receptors, and P2X7R consists of two types: P2X7RA and P2X7RB[24].

Although the growth-promoting function of *P2X7R* seems at odd with its established role in apoptosis, this receptor is highly expressed in some malignancies, seemingly consistent with its growth-promoting role. The apparent anti-apoptotic property of *P2X7R* is based on studies using ATP and KN-93. The initial activation of *P2X7R* (via autocrine/paracrine release of extracellular ATP) promotes cell growth[25]. *P2X7R*-transfected human embryonic kidney (HEK293) cells have a huge amount of intracellular ATP, higher mitochondrial resting potential, and increased basal mitochondrial Ca^{2+} ions compared to HEK293 mock-transfected cells. This growth-promoting function of *P2X7R* is dependent on pore formation since it does not take place in cells transfected with a truncated form of *P2X7R*, which cannot form a pore. *P2X7R*-transfected Henrietta Lacks (HeLa) cells are ATP-challenged, resulting in mitochondrial fragmentation and subsequent cell death (*Figure 3*).

The role of the *P2X7R* gene in osteosarcoma

The *P2X7R* gene is attracting attention for its involvement in cancer. Recent studies have reported the crucial role of *P2X7R* in tumor cell growth, angiogenesis, and invasiveness. Two variants of *P2X7R*, the full length *P2X7RA* and truncated *P2X7RB*, are found in osteosar-

Table 1 Molecular pathogenesis of osteosarcoma

No.	Process	Mechanism	References
1.	Chromosomal abnormalities	Amplification of chromosome 6p21, 8q24, and 12q14 causes genomic alteration in osteosarcoma.	Ta et al., 2009[12]
2.	Tumor suppression gene dysfunction	*p53* is a well-known tumor suppressor gene. It undergoes mutations occasionally, giving rise to cells that cause osteosarcoma.	Chandar et al., 1992[13]
		When exposed to molecular level assaults (e.g., radiation), somatic DNA may get damaged or apoptosis takes place.	
3.	Transcription factor	*AP-1* comprised of *fos* and *jun* protein products of *c-fos* and *c-jun* proto-oncogenes. *C-fos* and *c-jun* are responsible for benign osteoblastic lesions and low-grade osteosarcoma.	Franchi et al., 1998[14]
		The activator protein-1 complex (AP-1) is a regulator of transcription that controls cell proliferation, differentiation, and bone metabolism.	
4.	Osteosarcoma cell proliferation, apoptosis, anchored independent growth	Cancer cells are resistant to apoptosis/proliferation without restriction.	Broadhead et al., 2009[15]
		Apoptosis consists of initiation and execution phases. During initiation, the caspase enzyme (responsible for cleaving cellular proteins) is activated.	
		The execution phase refers to the hydrolysis process performed by an activated caspase.	
		Anoikis is a form of apoptosis involving osteosarcoma cells that are resistant to regular cell death and continue to proliferate despite of deranged cell-cell and cell-matrix attachment. This resistance to anoikis is termed as anchored independent growth (AIG).	
5.	Tumor angiogenesis	Tumor angiogenesis is essential for sustained osteosarcoma growth and metastasis without vasculature.	Hicklin et al., 2005[16]
		Osteosarcoma cells would be unable to obtain nutrients and oxygen for proliferation.	
6.	Osteoclast function	Osteosarcoma invasion of bone relies on bone matrix, osteosarcoma cells, osteoblast, and osteoclast.	Guise et al., 2003[17]
		During the initial stage of osteosarcoma invasion, growth factor such as TGF-β is released from degraded bone matrix and acts on osteosarcoma cells, stimulating the release of PTHrP and interleukins (IL-6,11). These cytokines stimulate osteoclast resorption. As a result, the bone remodels itself from cancerous cell.	

doi: 10.18282/amor.v1.i2.27

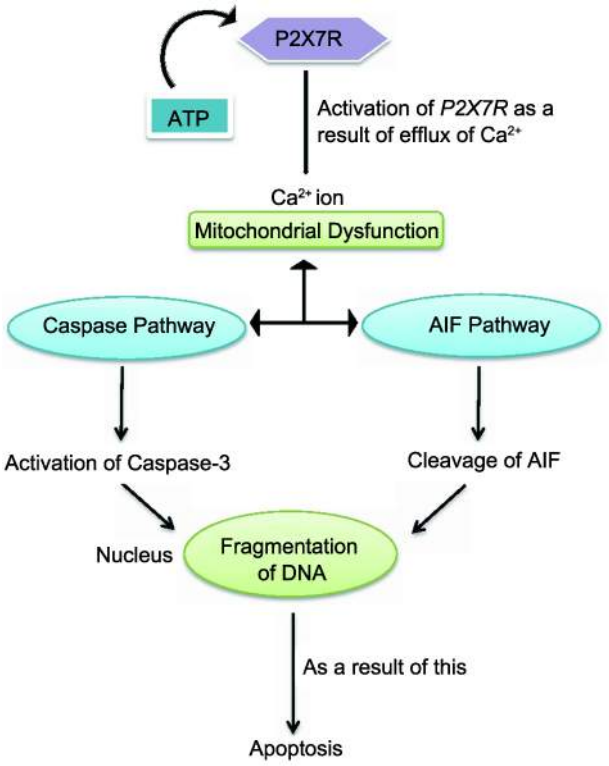

Figure 3 Activation of *P2X7R* causes a Ca^{2+} ion influx via the ion channels of *P2X7R*. An increase in Ca^{2+} ions causes mitochondrial dysfunction, leading to the initiation of caspase and apoptosis inducing factor-flavoproteins (AIF) pathways, thus independently induces neuronal apoptosis.

coma's cell growth[25]. The human osteosarcoma cell line Te85[26], which lacks an endogenous *P2X7R* expression, can be transfected with either *P2X7RA* or *P2X7RB*, or both genes. The expression of receptor shows a powerful stimulus for cell growth, in which *P2X7RB* is the most effective growth-promoting isoform. Growth stimulation is matched by an increased Ca^{2+} ion mobilization and enhanced nuclear factor of activated T-cells cytoplasmic 1 (NFATc1) activity. The Te85 *P2X7RA+B* cells facilitate pore formation as well as spontaneous extracellular ATP release. The release of ATP is then sustained in all clones by the *P2X7R* agonist (BzATP) and reduces the *P2X7R* antagonist (A740003) activity. BzATP also remarkably increases cell growth and activates the NFATc1 levels[27]. On the other hand, cyclosporine-A (CSA) affects both NFATc1 activation and cell growth, exclusively linking *P2X7R* stimulation to NFATc1 and cell proliferation. Moreover, all transfected clones also have reduced nuclear factor kappa B-ligand (*RANKL*) expression. Mineralization rises in Te85 *P2X7RA+B* cells while being significantly diminished in Te85 *P2X7RB* clones.

Recently, *in vitro* and *in vivo* evidence show that *P2X7R* has a main role in carcinogenesis, enhancing tumor cell growth[28,29], tumor-associated angiogenesis, and cancer invasiveness[30]. These data further support previous *in vitro* reports, demonstrating that *P2X7R* expression increases cell proliferation[31,32], mitochondria and endoplasmic reticulum Ca^{2+} levels[33], vascular endothelial growth factor (VEGF) secretion[34], and agarose infiltration[35].

P2X7R is expressed in both osteoblasts[36] and osteoclasts[37-39], and may play a vital role in osteoblasts-osteoclasts cross-talk through calcium oscillations[40] and other signaling pathways[41]. *P2X7R* promotes osteogenesis by stimulating osteoblast proliferation as well as osteodeposition[42], through a series of different pathways, including *c-fos*[43], extracellular signal-regulated kinases (*ERK*)[44], phosphoinositide 3-kinase (*PI3K*)[45], and cyclooxygenase (COX)[46]. Finally, it is likely that *P2X7R* mediates osteoblast ATP release as *P2X7R* blockers inhibit ATP secretion.

For Te85 cells that are transfected either with *P2X7RA*, *P2X7RB*, or co-transfected with both (*P2X7RA+B*) genes, the expression of plasma membrane *P2X7RA* is higher than *P2X7RB*. Nonetheless, the highest level of cell surface expression has been achieved in Te85 cells transfected with both *P2X7RA* and *P2X7RB*. The stimulation of BzATP (corresponding to the EC_{50} for *P2X7RB*, which has a lower affinity for ATP than the full length *P2X7RA*) triggers a rise in Ca^{2+} level in all transfected clones[40]. The Ca^{2+} increments occur in the following order: Te85-*P2X7RB*<Te85-*P2X7RA*<Te85-*P2X7RA+B*. This response may be dependent on the different plasma membrane expression levels of the diverse isoforms (*P2X7RB* being the lowest whereas *P2X7RA+B* is the highest), or on the activation of the receptor-associated large conductance pore. In order to reproduce the typical *P2X7R* signature in the Te85 osteosarcoma cells, the expression of both *P2X7RA* and *B* isoforms is required. Among all cell lines tested, only Te85 cells transfected with both *P2X7RA* and *B* show a significantly higher value than the Te85 wild-type (wt) cells. Hence, the pore formation found in Te85 *P2X7RA+B* cells appears to be related to the extracellular ATP release. Giuliani et al.[25], who used *P2X7R*-transfected Te85 clones, found that a majority of human osteosarcomas express both *P2X7RA* and *B*; however, the expression of either isoform is differently coupled to cell growth/activity. Intracellular calcium mobilization is one of the main stimuli leading to the activation of NFATc1, which has been associated with *P2X7R* dependent proliferation[47], and is well-known in osteoblast biology[48]. Analysis of NFATc1 nuclear translocation also showed

doi: 10.18282/amor.v1.i2.27

that all *P2X7R*-transfected Te85 clones had significantly higher nuclear NFATc1 levels[25]. Combined evidence from various laboratory testing shows that both *P2X7RA* and *B* provided a strong growth-promoting activity[49-52], and in particular *P2X7RA* is over-expressed in many human malignant tumors[53-56]. The *P2X7R* expression is indeed a powerful stimulus for cell growth, in which *P2X7RB* is the most efficient growth-promoting isoform. Treatment with either apyrase or A740003 significantly reduces the proliferative capability of all transfectants, whilst increasing BzATP stimulation. This strongly suggests an ATP-mediated loop controlling and sustaining of cell proliferation.

The function of *P2X7R* in osteosarcoma biology has also been investigated by scrutinizing the expression of two vital molecules for bone homeostasis, the receptor activator of RANKL and osteoprotegerin (OPG)[25]. The OPG mRNA is significantly increased only in *P2X7RB*-transfected cells. However, the RANKL/OPG ratio is decreased in all *P2X7R* clones. The expression of *P2X7R*, which affects mineralization, is another evidence of osteoblastic activity, with the transfection of the two gene isoforms producing different effects. *P2X7RA* alone does not significantly modify mineralization as compared to Te85 wt cells. However, the expression of *P2X7RB* causes a striking reduction in mineralization, with respect to Te85 wt and Te85-*P2X7RA*; whereas a marked increase is observed in cells transfected with both *P2X7RA* and *B* variants[25].

The interaction between tumor cells and ligand molecules present in the tumor microenvironment is crucial in cancer growth and progression. ATP recently emerged as an extracellular messenger that is present at high levels in the tumor microenvironment[57-59], but its effect on carcinogenesis is not completely understood. In a recent article, it has been demonstrated that *P2X7R* is involved in tumor growth and *in vivo* neo-vascularization[54]. *P2X7R* supports the proliferation of lymphocytes[60], osteoblasts[61], and osteosarcoma cells[62]. Human osteosarcomas express a high level of full length *P2X7RA* and truncated *P2X7RB* isoforms. As most osteosarcomas express both *P2X7RA* and *P2X7RB*, there is a possibility that other isoforms (i.e., different from *P2X7RA* or *P2X7RB*) are recognized by the anti-*P2X7R*-ec antibody. On the other hand, if expressed, the non-functional *P2X7RC*, *P2X7RD*, *P2X7RF*, and *P2X7RH* isoforms would be recognized by anti-*P2X7R*-*C*ter as they carry the same C-terminal tail as *P2X7RA*[63]. However, based on a 27.7% positive detection of anti-*P2X7R*-ec from known osteosarcoma cases, this strongly suggests that the only variant expressed by these tumors is *P2X7RB*[63].

Furthermore, the discovery of *P2X7RB*-positive osteosarcomas, which show higher cell density and increased Ki67 expression than those expressing both isoforms, indicates a relationship between *P2X7RB* expression and enhanced cell proliferation. *P2X7R* might autonomously sustain osteosarcoma growth owing to the autocrine/paracrine ATP release. Furthermore, it might also modulate osteosarcoma cell interaction with other bone cells by regulating the release of key molecules such as RANKL and OPG, or by affecting osteodeposition[64]. All *P2X7R*-transfected Te85 osteosarcoma clones display increased proliferation compared to Te85 wt or Te85 mock cells, therefore confirming P2X7R's trophic activity in the tumor. The receptor stimulation by BzATP significantly increases the proliferative activity of all transfected clones, with Te85 *P2X7RB* cells giving the highest growth ability.

Giuliani et al.[25] previously compared tumors cells that are positive for both *P2X7RA* and *P2X7RB*. They found that *P2X7RB* and *P2X7RA+B* have opposing roles on osteosarcoma cell growth and mineralization: the *P2X7R* anion channel is predominantly involved in cell proliferation (*Tables 2 and 3*), while the activation of the *P2X7R*-associated large conductance pore might be chiefly responsible for the differentiation-associated effects[25].

Table 2 Opposing effects of *P2X7RB* and *P2X7RA+B* on osteosarcoma cell growth and mineralization

P2X7RB	*P2X7RA+P2X7RB*
Data observation	
Tumor cell number Cell growth NFATc1 OPG	Tumor matrix Cell growth NFATC-1 ATP release Mineralization
RANKL Mineralization	RANKL
Deduction	
Osteosarcoma with undifferentiated phenotype	Osteosarcoma with differentiated phenotype

Recent reviews[80-83] have mostly focused on the role, as well as therapeutic potential, of *P2X7R* in osteosarcoma. However, most of the evidence is based on *in vitro* studies, with limited studies on *in vivo* experiments and clinical studies. Therefore, further efforts must be invested

doi: 10.18282/amor.v1.i2.27

Table 3 Supporting roles of the *P2X7R* gene as reported in other diseases

Process	Mechanism	References
Inflammation	Nucleotides (such as ATP) are normally retained within the cytoplasm of cell and their presence during the process of cytolysis is thought to provide danger signals, inducing antigen-presenting cells to initiate the innate immune system. The innate immunity can be initiated by a variety of cytokines such as IL1β, IL-18, IL-16, and tumor necrosis factor-α, all of which can be produced by *P2X7R* activation.	Di Virgillo et al. 1995[65]
	The P2X-mediated regulation of IL-1β had been demonstrated within the central nervous system where microglia are the resident monocyte cells. The ATP-induced IL-β production in cultured microglial cells occurs through the activation of the *P2X7R*.	La Sala et al. 2003[66]
	Neutrophil apoptosis is an important part of inflammatory regulation. The role of *P2X7R* is less established in neutrophils. *P2X7R* may have an additional and indirect role in the mediation of inflammatory arthritis via anti-apoptotic signaling in neutrophils. Serum amyloid (SSA) protein is an acute phase reactant that is often correlated with active joint inflammation and is elevated in many patients.	Savill et al. 2002[67]
	P2X7R regulates the production of the pro-inflammatory cytokines IL-1β and IL-18 and potentially, the innate immune response. *P2X7R* is an activator of the inflammasome, an important complex of cytosolic proteins that are known to regulate caspase-1 processing of IL-1β and IL-18. With inflammasome dysregulation known to produce inflammatory disorders such as Muckle-Wells syndrome and neonatal onset multisystem inflammatory disease (NOMID), inhibiting inflammasome activation with *P2X7R* antagonists could affect the outcome of a range of inflammatory disorders.	Mariathasan et al. 2006[68]
Neuropathic pain	The role of extracellular ATP and purinoceptors in cytokine regulation and neurological disorders has been discussed. *P2X7R* represents a critical communication link between the nervous and immune system.	Volonte et al. 2012[69]
	The systematic administration of A740003 and A 4438079 (selective inhibitors of *P2X7R*) reduced tactile allodynia in three different rat models, thus supporting the association between P2X7R and neuropathic pain.	Honore et al. 2006[70]
	The *P2X7R* expression in the spinal cord is increased after a nerve injury. The predominant type of cells expressing these receptors is microgilia, and the intrathecal administration of A430879 attenuates the development of mechanical hyper-sensitivity.	Ferrari et al. 1997[71]
	P2X7R is one of the key players in the release of pro-inflammatory cytokines such as IL-1β, IL-6, and tumor necrosis factor-*α* (TNFα) from activated microglia. IL-1β is released from lipopolysaccharide (LPS)-primed microglia, following ATP stimulation in a manner that depends on *P2X7R*s.	Shigemoto-Mogami et al. 2001[72]
Cancer	*P2X7R* is involved in many tumor-promoting and immune-modulatory effects of extracellular ATP. Like other members from the *P2X7R* family, *P2X7R* mediates cation fluxes across the plasma membrane but it also gates a large non-selective pore owing to its peculiar C terminal tail.	Adinolfi et al. 2012[73]
	Proliferation and other tumor transformation hallmarks seem dependent on channel activity since they are retained by cells expressing the C terminal-truncated *P2X7* splice variants, which lack pore forming activity. Several reports have suggested an association between *P2X7R* and cancer.	
	The participation of *P2X7R* in tumor progression was demonstrated in a recent *in vivo* study. It showed that *P2X7* inhibition by either pharmacological tools or RNA interference caused a dramatic reduction of tumor masses and vice versa. Interestingly, *P2X7* showed a higher vascular endothelial growth factor (VEGF).	
	P2X7-dependent AP-1/Fos–B activation is responsible for the cyclooxygenase-2 (*COX-2*) expression[50], whereas mechanism stimulation triggers arsenic trioxide (ATO) release and *P2X7*-dependent activation of several kinases, including *ERK* and *PI3*.	Liu et al. 2008[41]
	The enhanced plasma tumor necrosis factor (*TNF-α*) has been associated with an increased incidence of prostate cancer, while a polymorphism increasing IL-1β production conferred a greater susceptibility to gastric cancer. Given the importance of *P2X7R* in regulating cell death and cytokine production, it is perhaps unsurprising that it may play a role in cancer. Therefore, the development of either *P2X7R* agonists or antagonists may result in useful anti-cancer agents (i.e., agonists could kill cells whereas antagonists would perhaps stop proliferation).	Oh et al. 2000[74]
Fever	P2 receptors in *P2X7R* are coupled to the release of different autocoid and P2 receptor inhibition to reduce the fever induced by LPS.	El-Omar et al. 2001[75]
	ATP is released into the extra cellular space and activates *P2X7R.* This finding supports the view that the extracellular ATP is a bona fide, or prototypic, danger signal. *P2X7R* is widely expressed in many immune cells, where it controls key signaling pathways. In particular, *P2X7R* is the most potent plasma membrane receptor responsible for inflammasome activation and the release of pro-inflammatory cytokines of the IL-1 family.	La Sala et al. 2003[76]
	P2X7R activation also increases the generation of reactive oxygen species, induces the release of cathepsins, promotes the antigen-driven T-lymphocyte proliferation, and facilitates intracellular pathogen killing.	Yip et al. 2009[77]
Musculoskeletal	Human lung alveolar macrophage releases sufficient amounts of lysosome cathepsins into the extracellular medium within minutes to degrade extracellular collagen matrix *in vitro*. The mechanism of lysosomal release does not require initial pathogen-associated molecular pattern PAMP-induced signaling and therefore, is independent of IL-1β and is abolished by specific *P2X7R* antagonist, but not anti-IL-1, anti-IL-6, or anti-TNF-α approaches or other drugs used in the treatment of rheumatoid arthritis (RA) and osteoarthritis (OA).	Vasiljeva et al. 2007[78]
	Cathepsins are a family of lysosomal protease known to play important roles in the development of both inflammatory and rheumatoid arthritis joint destruction. It is thought that their site of action is intracellular in acidic lysosome, where they could break down phagocytosed extracellular matrix protein at low pH level.	
Miscellaneous	*P2X7R* antagonist may be used for the treatment of several disorders including stroke, traumatic brain, injury (TBI), multiple sclerosis, and Alzheimer's disease.	Collo et al. 1997[79]

doi: 10.18282/amor.v1.i2.27

in exploring therapeutic potential of purinoceptor in cancer diseases, especially osteosarcoma.

Future prospect

Osteosarcoma is the primary form of malignant bone tumor but owing to its rarity, it is difficult to identify, classify, and treat. This disease has a major impact on the patient's life. Currently, there is insufficient knowledge on the proper treatment of osteosarcoma. Studies on this molecular target may lead to future discoveries of effective diagnosis methods, as well as improved treatments, for osteosarcoma. In addition, a better understanding of *P2X7R* will also facilitate the management of various other diseases that are related to the expression of the *P2X7R* genes (i.e., other cancers, neuropathic pain, autoimmune hepatitis, tuberculosis, and inflammation).

The factors regulating the over-expression of *P2X7RA* and *B* in osteosarcoma can be controlled with various drugs. Drugs that can suppress the effect of *P2X7R* and decrease the size of bone tumor will be safe for humans. Since *P2X7R* is an upstream regulator of all cancer pathways, it can be inhibited to increase the secretion of RANKL and mTOR blockers. This is an attractive therapeutic target for osteosarcoma.

Conflict of interests

The authors declared no potential conflict of interest with respect to the research, authorship, and/or publication of this article.

References

1. Thompson H. What is osteosarcoma? Bone Cancer Research Trust 2013; [Last updated January 2015, Assessed on May 2015.] http://www.bonecancerresearch.org.uk/bci_what_is_osteosarcoma.php
2. Meyers PA, Gorlick R. Osteosarcoma. Pediatr Clin North Am 1997; 44(4): 973–989.
3. Stiller CA. International patterns of cancer incidence in adolescents. Cancer Treat Rev 2007; 33(7): 631–645.
4. Luetke A, Meyers PA, Lewis A, et al. Osteosarcoma treatment – where do we stand? A state of the art review. Cancer Treat Rev 2014; 40(4): 523–532.
5. Papalas JA, Balmer NN, Wallace C, et al. Ossifying dermatofibroma with osteoclast-like giant cells: report of a case and literature review. Am J Dermatopathol 2009; 31(4): 379–383.
6. Ottaviani G, Jaffe N. The etiology of osteosarcoma. Cancer Treat Res 2009; 152: 15–32.
7. Mirabello L, Troisi RJ, Savage SA. Osteosarcoma incidence and survival rates from 1973 to 2004: data from the Surveillance, Epidemiology, and End Results Program. Cancer 2009; 115(7): 1531–1543.
8. Grimer RJ, Cannon SR, Taminiau AM, et al. Osteosarcoma over the age of forty. Eur J Cancer 2003; 39(2): 157–163.
9. Hauben EI, Arends J, Vandenbroucke JP, et al. Multiple primary malignancies in osteosarcoma patients. Incidence and predictive value of osteosarcoma subtype for cancer syndromes related with osteosarcoma. Eur J Hum Genet 2003; 11(8): 611–618.
10. Smida J, Baumhoer D, Rosemann M, et al. Genomic alterations and allelic imbalances are strong prognostic predictors in osteosarcoma. Clin Cancer Res 2010; 16(16): 4256–4267.
11. Chandar N, Billig B, McMaster J, et al. Inactivation of *p53* gene in human and murine osteosarcoma cells. Br J Cancer 1992; 65(2): 208–214.
12. Ta HT, Dass CR, Choong PFM, et al. Osteosarcoma treatment: state of the art. Cancer Metastasis Rev 2009; 28(1-2): 247–263.
13. Chandar N, Billig B, McMaster J, et al. Inactivation of *p53* gene in human and murine osteosarcoma cells. Br J Cancer 1992; 65(2): 208–214.
14. Franchi A, Calzolari A, Zampi G. Immunohistochemical detection of *c-fos* and *c-jun* expression in osseous and cartilaginous tumours of the skeleton. Virchows Archiv 1998; 432(6): 515–519.
15. Broadhead ML, Dass CR, Choong PFM. Cancer cell apoptotic pathways mediated by PEDF: prospects for therapy. Trends Mol Med 2009; 15(10): 461–467.
16. Hicklin DJ, Ellis LM. Role of the vascular endothelial growth factor pathway in tumor growth and angiogenesis. J Clin Onco 2005; 23(5): 1011–1027.
17. Guise TA, Chirgwin JM. Transforming growth factor-beta in osteolytic breast cancer bone metastases. Clin Orthop Relat Res 2003; 415(suppl): S32–S38.
18. Rassendren F, Buell GN, Virginio C, et al. The permeabilizing ATP receptor, P2X7. Cloning and expression of a human cDNA. Bio Chem 1997; 272(9): 5482–5486.
19. Deuchars SA, Atkinson L, Brooke RE, et al. Neuronal P2X7 receptors are targeted to presynaptic terminals in the central and peripheral nervous systems. J Neurosci 2001; 21(18): 7143–7152.
20. North RA. Molecular physiology of P2X receptors. Physiol Rev 2013; 82(4): 1013–1067.
21. Iglesias R, Locovei S, Roque A, et al. P2X7 receptor-pannexin1 complex: pharmacology and signaling. Am J Physiol Cell Physiol 2008; 295(3): C752–C760.
22. Boison D, Chen JF, Fredholm BB. Adenosine signaling and function in glial cells. Cell Death Differ 2010; 17(7): 1071–1082.
23. Kawano A, Tsukimoto M, Noguchi T, et al. Involvement

doi: 10.18282/amor.v1.i2.27

of P2X4 receptor in P2X7 receptor-dependent cell death of mouse macrophages. Biochem Biophys Res Commun 2012; 419(2): 374–380.
24. Burnstock G. Pathophysiology and therapeutic potential of purinergic signaling. Pharmacol Rev 2006; 58(1): 58–86.
25. Giuliani AL, Colognesi D, Ricco T, et al. Trophic activity of human P2X7 receptor isoforms A and B in osteosarcoma. PLoS ONE 2014; 9(9): e107224.
26. Adinolfi E, Melchiorri L, Falzoni S, et al. P2X7 receptor expression in evolutive and indolent forms of chronic B lymphocytic leukemia. Blood 2002; 99(2): 706–708.
27. Rhim JS, Putman DL, Arnstein P, et al. Characterization of human cells transformed *in vitro* by N-methyl-N'-nitro-N nitrosoguanidine. Int J Cancer 1977; 19(4): 505–510.
28. Salinas-Souza C, De Oliveira R, Alves MT, et al. The metastatic behavior of osteosarcoma by gene expression and cytogenetic analyses. Hum Pathol 2013; 44(10): 2188–2198.
29. Adinolfi E, Raffaghello L, Giuliani AL, et al. Expression of P2X7 receptor increases *in vivo* tumor growth. Cancer Res 2012; 72(12): 2957–2969.
30. Hattori F, Ohshima Y, Seki S, et al. Feasibility study of B16 melanoma therapy using oxidized ATP to target purinergic receptor P2X7. Eur J Pharmacol 2012; 695(1-3): 20–26.
31. Alqallaf SM, Evans BA, Kidd EJ. Atypical P2X receptor pharmacology in two human osteoblast-like cell lines. Br J Pharmacol 2009; 156(7): 1124–1135.
32. Ke HZ, Qi H, Weidema AF, et al. Deletion of the P2X7 nucleotide receptor reveals its regulatory roles in bone formation and resorption. Mol Endocrinol 2003; 7(7): 1356–1367.
33. Li J, Liu D, Ke HZ, et al. The P2X7 nucleotide receptor mediates skeletal mechanotransduction. J Biol Chem 2005; 280(52): 42952–42959.
34. Wesselius A, Bours MJ, Agrawal A, et al. Role of purinergic receptor polymorphisms in human bone. Front Bio Sci 2011; 16: 2572–2585.
35. Ohlendorff SD, Tofteng CL, Jensen JE, et al. Single nucleotide polymorphisms in the *P2X7* gene are associated to fracture risk and to effect of estrogen treatment. Pharmacogenet Genomics 2007; 17(7): 555–567.
36. Gartland A, Hipskind RA, Gallagher JA, et al. Expression of a P2X7 receptor by a subpopulation of human osteoblasts. J Bone Miner Res 2001; 16(5): 846–856.
37. Buckley KA, Hipskind RA, Gartland A, et al. Adenosine triphosphate stimulates human osteoclast activity via up-regulation of osteoblast-expressed receptor activator of nuclear factor-kappa B ligand. Bone 2002; 31(5): 582–590.
38. Gartland A, Buckley KA, Hipskind RA, et al. P2 receptors in bone-modulation of osteoclast formation and activity via P2X7 activation. Crit Rev Eukaryot Gene Expr 2003; 13(2-4): 237–242.
39. Gartland A, Buckley KA, Bowler WB, et al. Blockade of the pore-forming P2X7 receptor inhibits formation of multinucleated human osteoclasts *in vitro*. Calcif Tissue Int 2003; 73(4): 361–369.
40. Grol MW, Panupinthu N, Korcok J, et al. Expression, signaling, and function of P2X7 receptors in bone. Purinergic Signal 2009; 5(2): 205–221.
41. Okumura H, Shiba D, Kubo T, et al. P2X7 receptor as sensitive flow sensor for ERK activation in osteoblasts. Biochem Biophys Res Commun 2008; 372(3): 486–490.
42. Liu D, Genetos DC, Shao Y, et al. Activation of extracellular-signal regulated kinase (ERK1/2) by fluid shear is Ca^{2+}- and ATP-dependent in MC3T3-E1 osteoblasts. Bone 2008; 42(4): 644–652.
43. Grol MW, Zelner I, Dixon SJ. $P2X_7$-mediated calcium influx triggers a sustained, PI3K-dependent increase in metabolic acid production by osteoblast-like cells. Am J Physiol Endocrinol Metab 2012; 302(5): E561–575.
44. Panupinthu N, Rogers JT, Zhao L, et al. P2X7 receptors on osteoblasts couple to production of lysophosphatidic acid: a signaling axis promoting osteogenesis. J Cell Biol 2008; 181(5): 859–871.
45. Rumney RM, Sunters A, Reilly GC, et al. Application of multiple forms of mechanical loading to human osteoblasts reveals increased ATP release in response to fluid flow in 3D cultures and differential regulation of immediate early genes. J Biomech 2012; 45(3): 549–554.
46. Adinolfi E, Cirillo M, Woltersdorf R, et al. Trophic activity of a naturally occurring truncated isoform of the P2X7 receptor. FASEB J 2010; 24(9): 3393–3404.
47. Adinolfi E, Callegari MG, Cirillo M, et al. Expression of the P2X7 receptor increases the Ca^{2+} content of the endoplasmic reticulum, activates NFATc1, and protects from apoptosis. J Biol Chem 2009; 284(15): 10120– 10128.
48. Stern PH. The calcineurin-NFAT pathway and bone: intriguing new findings. Mol Interv 2006; 6(4): 193–196.
49. Adinolfi E, Callegari MG, Ferrari D, et al. Basal activation of the P2X7 ATP receptor elevates mitochondrial calcium and potential, increases cellular ATP levels, and promotes serum-independent growth. Mol Biol Cell 2005; 16(7): 3260–3272.
50. Franceschini A, Adinolfi E. P2X receptors: new players in cancer pain. World J Biol Chem 2014; 5(4): 429–436.
51. Monif M, Reid CA, Powell KL, et al. The P2X7 receptor drives microglial activation and proliferation: a trophic role for P2X7R pore. J Neurosci 2009; 29(12): 3781–3791.
52. Bianco F, Ceruti S, Colombo A, et al. A role for P2X7 in microglial proliferation. J Neurochem 2006; 99(3): 745–758.
53. Slater M, Danieletto S, Gidley-Baird A, et al. Early pros-

doi: 10.18282/amor.v1.i2.27

tate cancer detected using expression of non-functional cytolytic P2X7 receptors. Histopathology 2004; 44(3): 206–215.
54. Solini A, Cuccato S, Ferrari D, et al. Increased P2X7 receptor expression and function in thyroid papillary cancer: a new potential marker of the disease. Endocrinology 2008; 149(1): 389–396.
55. Chong JH, Zheng GG, Zhu XF, et al. Abnormal expression of P2X family receptors in Chinese pediatric acute leukemias. Biochem Biophys Res Commun 2010; 391(1): 498–504.
56. Pellegatti P, Raffaghello L, Bianchi G, et al. Increased level of extracellular ATP at tumor sites: *in vivo* imaging with plasma membrane luciferase. PLoS ONE 2008; 3(7): e2599.
57. Michaud M, Martins I, Sukkurwala AQ, et al. Autophagy-dependent anticancer immune responses induced by chemotherapeutic agents in mice. Science 2011; 334(6062): 1573–1577.
58. Schumacher D, Strilic B, Sivaraj KK, et al. Platelet-derived nucleotides promote tumor-cell transendothelial migration and metastasis via P2Y2 receptor. Cancer Cell 2013; 24(1): 130–137.
59. Adinolfi E, Raffaghello L, Giuliani AL, et al. Expression of P2X7 receptor increases *in vivo* tumor growth. Cancer Res 2012; 72(12): 2957–2969.
60. Baricordi OR, Melchiorri L, Adinolfi E, et al. Increased proliferation rate of lymphoid cells transfected with the P2X(7) ATP receptor. J Biol Chem 1999; 274(47): 33206–33208.
61. Panupinthu N, Rogers JT, Zhao L, et al. P2X7 receptors on osteoblasts couple to production of lysophosphatidic acid: a signaling axis promoting osteogenesis. J Cell Biol 2008; 181(5): 859–871.
62. Liu PS, Chen CY. Butyl benzyl phthalate suppresses the ATP-induced cell proliferation in human osteosarcoma HOS cells. Toxicol Appl Pharmacol 2010; 244(3): 308–314.
63. Buell G, Chessell IP, Michel AD, et al. Blockade of human P2X7 receptor function with a monoclonal antibody. Blood 1998; 92(10): 3521–3528.
64. Gorlick R, Janeway K, Lessnick S, et al. Children's Oncology Group's 2013 blueprint for research: bone tumors. Pediatr Blood Cancer 2013; 60(6): 1009–1015.
65. Di Virgilio F. The P2Z purinoceptor: an intriguing role in immunity, inflammation and cell death. Immunol Today 1995; 16(11): 524–528.
66. La Sala A, Ferrari D, Di Virgilio F, et al. Alerting and tuning the immune response by extracellular nucleotides. J Leukoc Biol 2003; 73(3): 339–343.
67. Savill J, Dransfield I, Gregory C, et al. A blast from the past: clearance of apoptotic cells regulates immune responses. Nat Rev Immunol 2002; 2(12): 965–975.
68. Mariathasan S, Weiss DS, Newton K, et al. Cryopyrin activates the inflammasome in response to toxins and ATP. Nature 2006; 440(7081): 228–232.
69. Volonte C, Apolloni S, Skaper SD, et al. P2X7 receptors: channels, pores and more. CNS Neurol Disord Drug Targets 2012; 11(6): 705–721.
70. Honore P, Donnelly-Roberts D, Namovic MT, et al. A-740003 [N-(1-{[(cyanoimino)(5-quinolinylamino)methyl]amino}-2,2-dimethylpropyl)-2-(3,4-dimethoxyphenyl) acetamide], a novel and selective P2X7 receptor antagonist, dose dependently reduces neuropathic pain in the rat. J Pharmacol Exp Ther 2006; 319(3): 1376–1385.
71. Ferrari D, Chiozzi P, Falzoni S, et al. Purinergic modulation of interleukin-1 β release from microglial cells stimulated with bacterial endotoxin. J Exp Med 1997; 185(3): 579–582.
72. Shigemoto-Mogami Y, Koizumi S, Tsuda M, et al. Mechanisms underlying extracellular ATP-evoked interleukin-6 release in mouse microglial cell line, MG-5. J Neurochem 2001; 78(6): 1339–1349.
73. Adinolfi E, Raffaghello L, Giuliani AL, et al. Expression of P2X7 receptor increases *in vivo* tumor growth. Cancer Res 2012; 72(12): 2957–2969.
74. Oh BR, Sasaki M, Perinchery G, et al. Frequent genotype changes at -308, and 488 regions of the tumor necrosis factor-alpha (TNF-alpha) gene in patients with prostate cancer. J Urol 2000; 163(5): 1584–1587.
75. El-Omar EM, Charrington M, Chow WH, et al. The role of interleukin-1 polymorphisms in the pathogenesis of gastric cancer. Nature 2001; 412(6842): 99.
76. La Sala A, Ferrari D, Di Virgilio F, et al. Alerting and tuning the immune response by extracellular nucleotides. J Leukoc Biol 2003; 73(3): 339–343.
77. Yip L, Woehrle T, Corriden R, et al. Autocrine regulation of T-cell activation by ATP release and P2X7 receptors. FASEB J 2009; 23(6): 1685–1693.
78. Vasiljeva O, Reinheckel T, Peters C, et al. Emerging roles of cysteine cathepsins in disease and their potential as drug targets. Curr Pharm Des 2007; 13(4): 387–403.
79. Collo G, Neidhart S, Kawashima E, et al. Tissue distribution of the P2X7 receptor. Neuropharmacology 1997; 36(9): 1277–1283.
80. Agrawal A, Gartland A. P2X7 receptors: role in bone cell formation and function. J Mol Endocrinol 2015; 54(2): R75–R88.
81. Adinolfi E, Capece M, Amoroso F, et al. Emerging roles of P2X receptors in cancer. Curr Med Chem 2015; 22(7): 878–890.
82. Burnstock G, Di Virgilio F. Purinergic signalling and cancer. Purinergic Signal 2013; 9(4): 491–540.
83. Franceschini A, Adinolfi E. P2X receptors: new players in cancer pain. World J Biol Chem 2014; 5(4): 429–436.

doi: 10.18282/amor.v1.i2.27

Advances in Modern Oncology Research

doi: 10.18282/amor.v1.i2.42

REVIEW ARTICLE

Paraneoplastic pemphigus: A *trait d'union* between dermatology and oncology

Dario Didona[1], Biagio Didona[1], Antonio G Richetta[2], Carmen Cantisani[2], Elisa Moliterni[2], Stefano Calvieri[2], Giovanni Paolino[2*]

[1] Hospitalization and Health Care, (IRCCS) Istituto Dermopatico dell'Immacolata, Via Monti di Creta, Rome, Italy
[2] Clinica Dermatologica, La Sapienza University of Rome, Viale del Policlinico 15, Rome, Italy

***Abstract*:** Paraneoplastic pemphigus is a rare autoimmune disease of the skin associated with neoplasm. Nowadays, the pathogenesis of paraneoplastic pemphigus is not fully understood. Due to its rarity, various criteria have been proposed for the diagnosis. For this reason, several diagnostic methods have been considered useful for the diagnosis of paraneoplastic pemphigus including indirect immunofluorescence, direct immune of fluorescence, immunoprecipitation, immunoblotting, and enzyme-linked immunosorbent assay (ELISA). However, the polymorphic clinical features and the various results of laboratory tests and pathological evaluation present a challenge for the clinicians.

Keywords: paraneoplastic pemphigus; oncology; cancer; therapy

***Citation*:** Didona D, Didona B, Richetta AG, et al. Paraneoplastic pemphigus: A *trait d'union* between dermatology and oncology. Adv Mod Oncol Res 2015; 1(2): 97–103; http://dx.doi.org/10.18282/amor.v1.i2.42

*Correspondence to: Giovanni Paolino, Clinica Dermatologica, La Sapienza University of Rome, Viale del Policlinico 15, 00186, Rome, Italy, gio8519@libero.it.

Received: 14th September 2015; **Accepted:** 16th October 2015; **Published Online:** 3rd December 2015

Paraneoplastic pemphigus (PNP) is a rare autoimmune blistering disease of the skin, which was first described by Anhalt et al. in 1990[1]. PNP is always associated with neoplasm, among which B-cell lymphomas and other hematological malignant diseases are most common[2]. In 2001, Nguyen et al. suggested the term "paraneoplastic autoimmune multiorgan syndrome" (PAMS) as several organs are affected and autoantibodies bind several tissues[3]. Due to its high mortality rate, PNP must be detected quickly[4].

Epidemiology

PNP is a rare disease. Presently, there is limited data on the prevalence of PNP. Over 450 cases are described in the literature to date[5,6]. PNP usually affects patients aged between 45 and 70 years. Ogawa et al. reported that the mean age of onset in his series was 64.7[7]. However, PNP can affect every age group, including children and adolescents[8-10]. PNP appears to affect males and females equally[2].

Etiology

PNP is mostly associated with lymphoproliferative disorders[2]. Nearly 84% of all PNP are found in association with hematologic neoplasms or disorders[2,6]. Among these, non-Hodgkin's lymphoma accounts for 38.6%, chronic lymphocytic leukemia for 18.4%, Castleman's disease for 18.4%, thymoma for 5.5%, Waldenstrom's macroglobulinemia for 1.2%, Hodgkin's lymphoma for 0.6%, and monoclonal gammopathy for 0.6%[2,5,6,11]. In addition, carcinomas developed from epithelial cells (8.6%)[12-14], sarcomas derived from mesenchymal lines (6.2%)[9,15,16], and melanoma (0.6%)[17] also are reported in association with PNP. There are also cases of PNP triggered by cytotoxic drugs[18,19] and radiotherapy[20] described in the literature.

Genetics

HLA-DRB1*03 and HLA-Cw*14 are associated with PNP in Caucasian[21] and in Chinese patients[22] respectively. The HLA-DRB1*03 and the HLA-Cw*14 alleles were found more frequently, respectively in a series of 13 Caucasian French patients[21] and of 19 Han Chinese patients[22] than in the control populations. The Chinese patients with PNP did not show HLA-DRB1*03 allele[22].

Pathogenesis

The pathogenesis of PNP is not completely known. On one hand, several autoantibodies could play a pivotal role in PNP. Autoantibodies directed against the plakin family are typically found in PNP, including antibodies against the 210 kDa envoplakin, the 190 kDa periplakin, the 250 and 210 kDa desmoplakins I and II, the 500 kDa plectin, and the 230 kDa bullous pemphigoid antigen[23-26]. Furthermore, antibodies against plakophilin 3 and desmocollins (DSC) 1–3 have also been detected in some studies[27,28]. In addition, autoantibodies against desmoglein-1 (DSG-1) and desmoglein-3 (DSG-3) may also have pathogenic activity[29,30]. However, Amagai et al. reported a positivity of 100% only for anti-DSG-3 autoantibodies[29]. Recently, the protease inhibitor α2-macroglobulin-like-1 (A2ML1) has been considered as the possible pathogenic in PNP[31,32].

On the other hand, the cell-mediated immunity could have a role in PNP[2,33]. Another study reported the presence of selective epidermal activated CD8+ T-cells in PNP[34]. There are also four PNP patients without any detectable autoantibodies described by Cummins et al[35]. Furthermore, another study showed that MHC-restricted CD8+ cytotoxic T lymphocytes, non-MHC-restricted CD56+, and CD68+ natural killer cells are at the dermo-epidermal junction of PNP lesions[36].

Clinical features

PNP is identified by polymorphous lesions involving the skin and different mucosae. The variety of lesions could be explained by the presence of different autoantibodies in different patients[2]. Mucosal lesions are often the earliest features in PNP[37-39]. Oral mucosa is always affected in PNP (*Figure 1*)[37-40], although one PNP case without oral involvement is reported in the literature[41]. Usually severe erosions and crusting are found on the vermilion of the lips, showing an erythema multiforme-like or a Stevens-Johnson-like appearance. Erosions also affect the oropharynx, causing a painful stomatitis. In addition, mucosal lesion can also involve the nasopharynx, conjunctivae, anogenital region, and esophagus[6,42,43]. Cutaneous lesions usually rise after the onset of mucosal lesions[2,40]. The most involved sites are the trunk, head, neck, and proximal extremities, although most patients show a widespread cutaneous involvement (*Figure 2*)[4,40,44]. Different kind of lesions may coexist and evolve from one type to another[3,40]. Cutaneous lesions could be similar to those seen in pemphigus, pemphigoid, erythema multiforme or graft versus host disease[11,38,40]. Pustular and psoriasis form presentation have also been described[3]. The different clinical features could be linked to the predominance of the cell-mediated or humoral-mediated cytotoxicity[36,38]. It is well known that if the principal mechanism is humoral-mediated cytotoxicity, a usual pemphigus appearance might be prominent[3,6]. In contrast, if cell-mediated cytotoxicity is the leading mechanism, lichenoid lesions might be easily seen[33,35,36]. Lichenoid lesions are commonly detected in children, especially on the trunk and limbs[9,10]. Lesions resembling those of pemphigoid are usually present on the extremities[45]. Sapadin et al. reported a singular case of pemphigus vegetans-like

Figure 1 Painful erosions of the lips

Figure 2 Extensive areas of denudation

doi: 10.18282/amor.v1.i2.42

PNP[46]. PNP can also involve the respiratory epithelium in 59.1%–92.8% of cases[8,36], causing dyspnea, obstructive lung disease and bronchiolitis obliterans, which may be fatal[6,47]. However, the pulmonary involvement affects mainly children and Chinese patients with Castleman's disease[40,47]. Usually, a neoplasm is detected before the onset of PNP[4,38–40]. However, in about 30% of cases PNP, the clinical manifestation leads to the detection of an occult tumor[36,38].

Histological features

The pathological findings vary with the clinical features[4,30]. On one hand, suprabasal acantholysis with scattered inflammatory infiltrates could be detected in presence of blisters (*Figure 3*)[30]. Furthermore, the presence of dyskeratosis with suprabasal acantholysis is a clue to paraneoplastic pemphigus. On the other hand, interface and lichenoid dermatitis are more easily detected in erythematous inflammatory maculopapular lesions[30,35]. Lesions with a mixed clinical feature might show concomitant acantholysis occurring with lichenoid interface dermatitis[30,38,40].

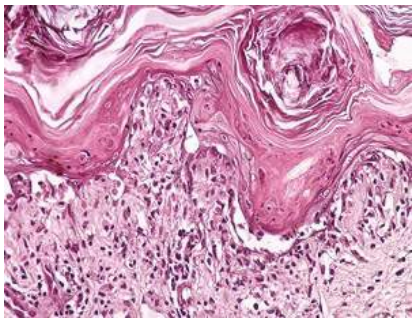

Figure 3 Histology of a skin biopsy shows suprabasal acantholysis. (H&E, magnification 200×)

Immunological studies

Direct immunofluorescence (DIF) usually shows IgG and/or C3 deposition in the epidermal intercellular spaces (EIS) alone[48]. The deposition of IgG and/or C3 in EIS and in the basement membrane zone is reported to be less than 50% of cases[48]. In addition, linear deposits of IgG or C3 in the basement membrane zone could be detected[30]. This pattern could be a clue to differentiate PNP from other forms of pemphigus, in which Ig deposits are detected only between keratinocytes[3]. However, DIF is found to be negative in approximately 50% of the cases[48]. False negatives are commonly due to necrotic tissue (especially in mucosal biopsies) and the lichenoid clinical pattern of some lesions[35,48].

Indirect immunofluorescence (IIF) could be performed on different substrates, including normal human skin, rat bladder (*Figure 4*), rat myocardium, rat lung, and monkey esophagus[48]. IIF detects autoantibodies to plakins; among them, autoantibodies to envoplakin and periplakin are the most specific[30]. IIF on normal human skin has been shown to be positive in up to 50% of the cases, whereas IIF on rat bladder urothelium has been found positive in 75% of the cases, showing a better sensitivity[38,49]. Furthermore, IIF on rat bladder has shown a high specificity (83%)[1,49]. For these reasons, IIF on rat bladder is now considered a useful screening test for PNP. However, autoantibodies directed against members of plakin family have been also detected in other conditions including pemphigus vulgaris, pemphigus foliaceus and Lyell's syndrome[49-51].

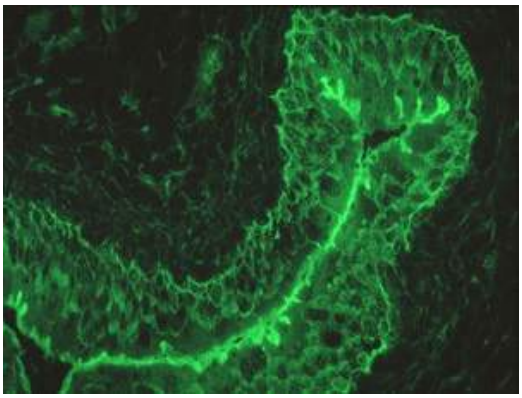

Figure 4 Positive indirect immunofluorescence on rat urinary bladder epithelium

Enzyme-linked immunosorbent assay (ELISA) can be used to detect anti-DSG-3 and anti-DSG-1 autoantibodies in PNP, although most PNP patients have been shown only with anti-DSG-3 IgG[52]. However, there were also PNP patients without anti-DSG autoantibodies described in the literature[52]. In 2009, Probst et al. developed a new ELISA using a recombinant 56 kDa N-terminal fragment of envoplakin which shows a sensitivity of 82% and a specificity of ≥ 98%[53]. Recently, Ishii et al. detected IgG autoantibodies to DSC-1, DSC-2 and DSC-3 in 16.5%, 36.7% and 59.5% of PNP sera respectively, using a novel mammalian ELISA[54].

Immunoprecipitation (IP) has been considered as the gold standard for the diagnosis of PNP[55]. IP can show antibodies against several epidermal antigens, including plakin family and A2ML1[31]. In addition, a positive IP test is a major criterion for the diagnosis of PNP[56].

Immunoblotting (IB) has been used to detect antibodies against desmoplakin I and II, periplakin, and envoplakin on normal human keratinocytes extracts[30,48].

doi: 10.18282/amor.v1.i2.42

Diagnosis

According to Anhalt et al., the diagnostic criteria includes five different points (*Table 1*)[1]. However, Camisa et al. proposed different criteria, including major and minor criteria (*Table 2*)[56]. According to Camisa et al., three major criteria or two major and two minor criteria are needed to diagnose PNP[56]. Furthermore, Mimouni et al.[9] revised the original criteria proposed by Anhalt et al.[1] (*Table 3*). Nowadays, DIF is considered non-essential for diagnosing PNP due to its low sensibility[48,49]. IIF on rat bladder urothelium and monkey esophagus are thought to be useful as a screening for PNP[36,38,48]. In addition, the detection of anti-DSG-3, anti-DSG-1, anti-DSC-1, anti-DSC-2 and anti-DSC-3 antibodies by ELISA is useful to formulate a correct diagnosis[57]. Furthermore, the link between anti-DSG-3 antibodies and bronchiolitis obliterans (BO)[58] has been reported as one of the most important complications of PNP patients. The detection of antibodies against A2ML1 using IP and IB is also useful for the diagnosis of PNP[31,57]. Indeed, Ohzono et al. reported that 60.4% of the patients showed positivity for anti-A2ML1 antibodies that was higher than the positivity for anti-DSG-1 antibodies[57].

In conclusion, as PNP is primarily associated with antibodies against the plakin family, IP is considered as the laboratory gold standard for the diagnosis of PNP[55,56]. However, rat bladder IIF in combination with IB offers an easier and more accurate alternative to IP[59]. Furthermore, the laboratory data should be related to the clinical features[38-40]. In addition, it is mandatory to detect the underlying malignancy[38-40].

Table 1 Diagnostic criteria originally proposed by Anhalt et al.[1]

Parameter	Criterion
Clinical features	Painful erosions involving mucosae with or without a multiform skin eruption producing blisters and erosions, occurring in association with an occult or evident neoplasm
Histopathology	Suprabasal intraepithelial acantholysis, vacuolar interface changes and necrosis of individual keratinocytes
Direct immunofluorescence	Combined presence of IgG and complement (C3) granular-linear deposition within the epidermal intercellular spaces and along the basement-membrane zone
Indirect immunofluorescence	Presence of circulating antibodies that target the intercellular zone of stratified squamous or transitional epithelia
Immunoprecipitation	Typical complex of proteins including desmoplakin I (250 kD), bullous pemphigoid antigen (230 kD), envoplakin (210 kD), desmoplakin II (210 kD), periplakin (190 kD) and α-2-macroglobulin-like-1 (170kD)

Table 2 Diagnostic criteria proposed by Camisa et al.[55]

Relevance	Description
Major	Polymorphic clinical features involving the skin and mucosae
	Presence of an underlying neoplasia
	Characteristic immunoprecipitation pattern of auto-antibodies
Minor	Clear acantholysis on skin biopsy
	Direct immunofluorescence highlighting intercellular and basement membrane staining
	Positive indirect immunofluorescence on rat-bladder epithelium

Table 3 Diagnostic criteria proposed by Mimouni et al.[9]

Criterion
Detection of auto-antibodies against desmoglein 1 and 3, envoplakin, periplakin, and plectin
Exclusion of other disease positive to anti-desmoglein 1 and 3 autoantibodies
Respiratory tract affected by the disease
Lichenoid clinical features on skin

Treatment options

High-dose corticosteroids are used as the first line therapy[60,61]. However, corticosteroids are usually combined with other immunosuppressive drugs. Only two papers reported an improvement of the lesions using only corticosteroids[60,61]. Prednisolone in association with other immunosuppressive drugs including azathioprine[1], cyclosporine[62], mycophenolate mofetil[63] and cyclophosphamide[64,65] have been shown efficient. In addition, the combination of prednisolone and intravenous immunoglobulins[38-40] or plasmapheresis[66,67] have been reported effective in selected number of patients. However, mucosal lesions are usually resistant to most of the therapeutic schedules.

Rituximab, the anti-CD20 monoclonal antibody, has improved the clinical picture in PNP patients with underlying B-cell lymphoma[11,68,69]. Alemtuzumab, a humanized monoclonal antibody which binds CD52, has induced a long-term remission in a patient with B-cell chronic lymphocytic leukemia[70]. Daclizumab, a humanized monoclonal antibody directed against the alpha subunit of the IL-2 receptor of T-cells, is found to be a promising drug in treating PNP[38].

doi: 10.18282/amor.v1.i2.42

On the other hand, whenever feasible, a complete excision of the benign tumor should be performed. This may cause an important improvement of the clinical picture due to a dramatic reduction of autoantibodies[11,38-40]. It has also been suggested to use perioperative intravenous immunoglobulins to block the release of autoantibodies during excision[11]. On the contrary, there is no consensus regarding the management of a malignant tumor as, in some cases, PNP continues to develop despite surgery and chemotherapy[11,38-40].

Early antimicrobial therapy is recommended to reduce the risk of sepsis due to loss of skin integrity and immunosuppressive therapy[11]. Antalgic therapy is thought to be useful in reducing the pain linked to extensive mucosal erosions[11].

Prognosis

The prognosis of PNP is generally poor, with a staggering 90% mortality rate[4-6,11]. The death is usually caused by severe complications including sepsis, gastrointestinal bleedings and BO[4-6,11]. At this regard, a link between anti-DSG-3 antibodies and BO has been reported[58]. Thus, it is important to evaluate accurately the respiratory symptoms in patients with a positivity to anti-DSG-3 antibodies.

PNP and underlying malignancy do not have a parallel evolution[4-6]. In fact, PNP lesions generally progress even if malignancy is removed or under controlled[8-11]. However, it has been highlighted that the outcome is better in PNP patients with concurrent Castleman's disease or benign thymomas upon removal of the tumor[71]. Nevertheless, Dong et al. emphasized that PNP was an independent detrimental prognostic factor in Castleman's disease patients which affects the survival rate of these patients[72].

Conclusion

Due to its polymorphus clinical appearance, PNP presents a challenge for the clinicians. Although several immunological makers have been discovered, the pathogenesis remains largely unknown. Different therapies have been developed to treat this severe condition as the management of the underlying tumor is vital.

Conflict of interest

The authors declared no potential conflict of interest with respect to the research, authorship, and/or publication of this article.

References

1. Anhalt GJ, Kim SC, Stanley JR, et al. Paraneoplastic pemphigus. An autoimmune mucocutaneous disease associated with neoplasia. N Engl J Med 1990; 323(25): 1729–1735.
2. Sehgal VN, Srivastava G. Paraneoplastic pemphigus/ paraneoplastic autoimmune multiorgan syndrome. Int J Dermatol 2009; 48(2): 162–169.
3. Nguyen VT, Ndoye A, Bassler KD, et al. Classification, clinical manifestations, and immunopathological mechanisms of the epithelial variant of paraneoplastic autoimmune multiorgan syndrome: a reappraisal of paraneoplastic pemphigus. Arch Dermatol 2001; 137(2): 193–206.
4. Anhalt GJ. Paraneoplastic pemphigus. J Invest Dermatol Symp Proc 2004; 9(1): 29–33.
5. Vassileva S, Drenovska K, Manuelyan K. Autoimmune blistering dermatoses as systemic diseases. Clin Dermatol 2014; 32(3): 364–375.
6. Czernik A, Camilleri M, Pittelkow MR, et al. Paraneoplastic autoimmune multiorgan syndrome: 20 years after. Int J Dermatol 2011; 50(8): 905–914.
7. Ogawa H, Sakuma M, Morioka S, et al. The incidence of external malignancies in pemphigus and bullous pemphigoid in Japan. J Dermatol Sci 1995; 9(2): 135–141.
8. Cervini AB, Tosi V, Kim SH, et al. Paraneoplastic pemphigus or paraneoplastic autoimmune multiorgan syndrome. Report of 2 cases in children and a review of the literature. Actas Dermosifiliogr 2010; 101(10): 879–886.
9. Mimouni D, Anhalt GJ, Lazarova Z, et al. Paraneoplastic pemphigus in children and adolescents. Br J Dermatol 2002; 147(4): 725–732.
10. Lane JE, Woody C, Davis LS, et al. Paraneoplastic autoimmune multiorgan syndrome (paraneoplastic pemphigus) in a child: case report and review of the literature. Pediatrics 2004; 114(4): 513–516.
11. Yong AA, Tey HL. Paraneoplastic pemphigus. Australas J Dermatol 2013; 54(4): 241–250.
12. Bowen GM, Peters NT, Fivenson DP, et al. Lichenoid dermatitis in paraneoplastic pemphigus: a pathogenic trigger of epitope spreading? Arch Dermatol 2000; 136(5): 652–656.
13. Matz H, Milner Y, Frusic-Zlotkin M, et al. Paraneoplastic pemphigus associated with pancreatic carcinoma. Acta Derm Venereol 1997; 77(4): 289–291.
14. Wong KC, Ho KK. Pemphigus with pemphigoid-like presentation, associated with squamous cell carcinoma of the tongue. Australas J Dermatol 2000; 41(3): 178–180.
15. Lee IJ, Kim SC, Kim HS, et al. Paraneoplastic pemphigus associated with follicular dendritic cell sarcoma arising

doi: 10.18282/amor.v1.i2.42

from Castleman's tumor. J Am Acad Dermatol 1999; 40(2 Pt 2): 294–297.
16. VanderWaal RI, Pas HH, Anhalt GJ, et al. PNP as the presenting symptom of lymphoma of the tongue. Oral Oncol 1998; 34(6): 567–570.
17. Schaeppi H, Bauer JW, Hametner R, et al. Localized variant of paraneoplastic pemphigus: acantholysis associated with malignant melanoma. Br J Dermatol 2001; 144(6): 1249–1254.
18. Bazarbachi A, Bachelez H, Dehen L, et al. Lethal paraneoplastic pemphigus following treatment of chronic lymphocytic leukaemia with fludarabine. Ann Oncol 1995; 6(7): 730–731.
19. Anhalt GJ. Paraneoplastic pemphigus: the role of tumours and drugs. Br J Dermatol 2001; 144(6): 1102–1104.
20. Lee MS, Kossard S, Ho KK, et al. Paraneoplastic pemphigus triggered by radiotherapy. Australas J Dermatol 1995; 36(4): 206–210.
21. Martel P, Loiseau P, Joly P, et al. Paraneoplastic pemphigus is associated with the DRB1*03 allele. J Autoimmun 2003; 20(1): 91–95.
22. Liu Q, Bu DF, Li D, et al. Genotyping of HLA-I and HLA-II alleles in Chinese patients with paraneoplastic pemphigus. Br J Dermatol 2008; 158(3): 587–591.
23. Kiyokawa C, Ruhrberg C, Nie Z, et al. Envoplakin and periplakin are components of the paraneoplastic pemphigus antigen complex. J Invest Dermatol 1998; 111(6): 1236–1238.
24. Kim SC, Kwon YD, Lee IJ, et al. cDNA cloning of the 210-kDa paraneoplastic pemphigus antigen reveals that envoplakin is a component of the antigen complex. J Invest Dermatol 1997; 109(3): 365–369.
25. Oursler JR, Labib RS, Ariss-Abdo L, et al. Human autoantibodies against desmoplakins in paraneoplastic pemphigus. J Clin Invest 1992; 89(6): 1775–1782.
26. Borradori L, Trueb RM, Jaunin F, et al. Autoantibodies from a patient with paraneoplastic pemphigus bind periplakin, a novel member of the plakin family. J Invest Dermatol 1998; 111(2): 338–340.
27. Lambert J, Bracke S, van Roy F, et al. Serum plakophilin-3 autoreactivity in paraneoplastic pemphigus. Br J Dermatol 2010; 163(3): 630–632.
28. Brandt O, Rafei D, Podstawa E, et al. Differential IgG recognition of desmoglein 3 by paraneoplastic pemphigus and pemphigus vulgaris sera. J Invest Dermatol 2012; 132(6): 1738–1741.
29. Amagai M, Nishikawa T, Nousari HC, et al. Antibodies against desmoglein 3 (pemphigus vulgaris antigen) are present in sera from patients with paraneoplastic pemphigus and cause acantholysis *in vivo* in neonatal mice. J Clin Invest 1998; 102(4): 775–782.
30. Zimmermann J, Bahmer F, Rose C, et al. Clinical and immunopathological spectrum of paraneoplastic pemphigus. J Dtsch Dermatol Ges 2010; 8(8): 598–606.
31. Numata S, Teye K, Tsuruta D, et al. Anti-alpha-2-macroglobulin-like-1 autoantibodies are detected frequently and may be pathogenic in paraneoplastic pemphigus. J Invest Dermatol 2013; 133(7): 1785–1793.
32. Schepens I, Jaunin F, Begre N, et al. The protease inhibitor alpha-2-macroglobulin-like-1 is the p170 antigen recognized by paraneoplastic pemphigus autoantibodies in human. PLoS One 2010; 5(8): e12250.
33. Billet SE, Grando SA, Pittelkow MR. Paraneoplastic autoimmune multiorgan syndrome: review of the literature and support for a cytotoxic role in pathogenesis. Autoimmunity 2006; 39(7): 617–630.
34. Reich K, Brinck U, Letschert M, et al. Graft-versus-host disease-like immunophenotype and apoptotic keratinocyte death in paraneoplastic pemphigus. Br J Dermatol 1999; 141(4): 739–746.
35. Cummins DL, Mimouni D, Tzu J, et al. Lichenoid paraneoplastic pemphigus in the absence of detectable antibodies. J Am Acad Dermatol 2007; 56(1): 153–159.
36. Wade MS, Black MM. Paraneoplastic pemphigus: a brief update. Australas J Dermatol 2005; 46: 1–8.
37. Bialy-Golan A, Brenner S, Anhalt GJ. Paraneoplastic pemphigus: oral involvement as the sole manifestation. Acta Derm Venereol 1996; 76(3): 253–254.
38. Lee SE, Kim SC. Paraneoplastic pemphigus. Dermatol Sin 2010; 28(1): 1–14.
39. Vassileva S, Drenovska K, Manuelyan K. Autoimmune blistering dermatoses as systemic diseases. Clin Dermatol 2014; 32(3): 364–375.
40. Zhu X, Zhang B. Paraneoplastic pemphigus. J Dermatol 2007; 34(8): 503–511.
41. Lee SE, Hashimoto T, Kim SC. No mucosal involvement in a patient with paraneoplastic pemphigus associated with thymoma and myasthenia gravis. Br J Dermatol 2008; 159(4): 986–988.
42. Meyers SJ, Varley GA, Meisler DM, et al. Conjunctival involvement in paraneoplastic pemphigus. Am J Ophthalmol 1992; 114(5): 621–624.
43. Ng PP, Rencic A, Nousari HC. Paraneoplastic pemphigus: a refractory autoimmune mucocutaneous disease. J Cutan Med Surg 2002; 6(5): 434–437.
44. Mutasim DF, Pelc NJ, Anhalt GJ. Paraneoplastic pemphigus. DermatolClin 1993; 11(3): 473–481.
45. Tankel M, Tannenbaum S, Parekh S. Paraneoplastic pemphigus presenting as an unusual bullous eruption. J Am Acad Dermatol 1993; 29(5 Pt 2): 825–858.
46. Sapadin AN, Anhalt GJ. Paraneoplastic pemphigus with a pemphigus vegetans-like plaque as the only cutaneous

doi: 10.18282/amor.v1.i2.42

manifestation. J Am Acad Dermatol 1998; 39(5 Pt 2): 867–871.
47. Maldonado F, Pittelkow MR, Ryu JH. Constrictive bronchiolitis associated with paraneoplastic autoimmune multi-organ syndrome. Respirology 2009; 14(1): 129–133.
48. Joly P, Richard C, Gilbert D, et al. Sensitivity and specificity of clinical, histologic, and immunologic features in the diagnosis of paraneoplastic pemphigus. J Am Acad Dermatol 2000; 43(4): 619–626.
49. Helou J, Allbritton J, Anhalt G. Accuracy of indirect immunofluorescence in the diagnosis of paraneoplastic pemphigus. J Am Acad Dermatol 1995; 32(3): 441–447.
50. Cozzani E, Dal Bello MG, Mastrogiacomo A, et al. Antidesmoplakin antibodies in pemphigus vulgaris. Br J Dermatol 2006; 154(4): 624–628.
51. Kazerounian S, Mahoney MG, Uitto J, et al. Envoplakin and periplakin, the paraneoplastic pemphigus antigens, are also recognized by pemphigus foliaceus autoantibodies. J Invest Dermatol 2000; 115(3): 505–507.
52. Ishii N, Maeyama Y, Karashima T, et al. Immunoserological analyses of 55 patients with pemphigus at the Dermatological Department of Kurume University Hospital: an 11-year retrospective study (1996–2006). Int J Dermatol 2008; 47(12): 1321–1322.
53. Probst C, Schlumberger W, Stöcker W, et al. Development of ELISA for the specific determination of autoantibodies against envoplakin and periplakin in paraneoplastic pemphigus. Clin Chim Acta 2009; 410(1-2): 13–18.
54. Ishii N, Teye K, Fukuda S et al. Anti-desmocollin autoantibodies in nonclassical pemphigus. Br J Dermatol 2015 Jul; 3(1): 59–68.
55. Hashimoto T, Amagai M, Watanabe K, et al. Characterization of paraneoplastic pemphigus autoantigens by immunoblot analysis. J Invest Dermatol 1995; 104(5): 829–834.
56. Camisa C, Helm TN. Paraneoplastic pemphigus is a distinct neoplasia-induced autoimmune disease. Arch Dermatol 1993; 129(7): 883–886.
57. Ohzono A, Sogame R, Li X, et al. Clinical and immunological findings in 104 cases of paraneoplastic pemphigus. Br J Dermatol 2015 Sep 10. doi: 10.1111/bjd.14162. [Epub ahead of print]
58. Hata T, Nishimoto S, Nagao K, et al. Ectopic expression of epidermal antigens renders the lung a target organ in paraneoplastic pemphigus. J Immunol 2013; 191(1): 83–90.
59. Poot AM, Diercks GF, Kramer D, et al. Laboratory diagnosis of paraneoplastic pemphigus. Br J Dermatol 2013; 169(5): 1016–1024.
60. Dega H, Laporte JL, Joly P, et al. Paraneoplastic pemphigus associated with Hodgkin's disease. Br J Dermatol 1998; 138(1): 196–198.
61. Martínez De Pablo MI, Iranzo P, et al. Paraneoplastic pemphigus associated with non-Hodgkin B-cell lymphoma and good response to prednisone. Acta Derm Venereol 2005; 85(3): 233–235.
62. Gergely L, Váróczy L, Vadász G, et al. Successful treatment of B cell chronic lymphocytic leukemia-associated severe paraneoplastic pemphigus with cyclosporin A. Acta Haematol 2003; 109(4): 202–205.
63. Williams JV, Marks JG, Billingsley EM. Use of mycophenolate mofetil in the treatment of paraneoplastic pemphigus. Br J Dermatol 2000; 142(3): 506–508.
64. Hertzberg MS, Schifter M, Sullivan J, et al. Paraneoplastic pemphigus in two patients with B-cell non-Hodgkin's lymphoma: significant responses to cyclophosphamide and prednisolone. Am J Hematol 2000; 63(2): 105–106.
65. Hayag MV, Cohen JA, Kerdel FA. Immunoablative high-dose cyclophosphamide without stem cell rescue in a patient with pemphigus vulgaris. J Am Acad Dermatol 2000; 43(6): 1065–1069.
66. Tan-Lim R, Bystryn JC. Effect of plasmapheresis therapy on circulating levels of pemphigus antibodies. J Am Acad Dermatol 1990; 22(1): 35–40.
67. Izaki S, Yoshizawa Y, Kitamura K, et al. Paraneoplastic pemphigus: potential therapeutic effect of plasmapheresis. Br J Dermatol 1996; 134(5): 987–989.
68. Hertl M, Zillikens D, Borradori L, et al. Recommendations for the use of rituximab (anti-CD20 antibody) in the treatment of autoimmune bullous skin diseases. J Dtsch Dermatol Ges 2008; 6(5): 366–373.
69. Hainsworth JD, Burris HA, Morrissey LH, et al. Rituximab monoclonal antibody as initial systemic therapy for patients with low-grade non-Hodgkin's lymphoma. Blood 2000; 95(10): 3052–3056.
70. Hohwy T, Bang K, Steiniche T, et al. Alemtuzumab-induced remission of both severe paraneoplastic pemphigus and leukaemic bone marrow infiltration in a case of treatment-resistant B-cell chronic lymphocytic leukaemia. Eur J Haematol 2004; 73(3): 206–209.
71. Wang J, Zhu X, Li R, et al. Paraneoplastic pemphigus associated with Castleman tumor: a commonly reported subtype of paraneoplastic pemphigus in China. Arch Dermatol 2005; 141(10): 1285–1293.
72. Dong Y, Wang M, Nong L, et al. Clinical and laboratory characterization of 114 cases of Castleman disease patients from a single centre: paraneoplastic pemphigus is an unfavourable prognostic factor. Br J Haematol 2015; 169(6): 834–842.

doi: 10.18282/amor.v1.i2.42

Advances in Modern Oncology Research

doi: 10.18282/amor.v1.i2.4

ORIGINAL RESEARCH ARTICLE

Synthesis and antiproliferative activity of various novel indole Mannich bases

Mardia T El Sayed[1*], Hoda AR Hussein[2], Khadiga M Ahmed[3], Nehal A Hamdy[1]

[1]Applied Organic Chemistry Department, National Research Centre, Dokki, Cairo, Egypt
[2]Photochemistry Department, National Research Center, Dokki, Cairo, Egypt
[3]Natural Compounds Department, Pharmaceutical Industries Division, National Research Centre, El Behous Street, Dokki, Cairo, Egypt

***Abstract*:** Various secondary and primary amines were converted into bis-indolyl Mannich bases with good to excellent yields via double condensation reactions with indole and glutaraldehyde. The expected bis-indolyl Mannich bases (2, 3 and 4) were formed by using piperazine hexahydrate and 4,4′-trimethylenedipiperidine. Meanwhile, the use of primary amines, phenylhydrazine, amino acids and primary diamine produced the corresponding bis-indolyl-1,2,6-trisubstituted piperidines (5a-e) and indolyl-quinolizine (6) and dibis-indolyl-1,2,6-trisubstituted piperidines (7). All analytical and spectral data of these bis-indolyl Mannich bases have been determined. Six of the synthesized bis-indolyl Mannich bases have been subjected to antiproliferative activity screening at National Cancer Institute (NCI), Egypt, towards three human tumor cell lines representing different tumor types: breast adenocarcinoma cell (MCF-7), non-small lung cancer cell (NCI-H460), and central nervous system (CNS) cancer cell (SF-268). Compound (4) indicated the best and highest inhibitory effect against all three tested tumor cell lines with inhibition of 50% concentration (IC_{50}) for MCF-7 (0.08 μmol/L), NCI-H460 (0.05 μmol/L) and SF-268 (0.01 μmol/L).

***Keywords*:** bis-indolyl Mannich bases; double condensation reaction; cytostatic activity

***Citation*:** El Sayed MT, Hussein HAR, Ahmed KM, et al. Synthesis and antiproliferative activity of some novel indole Mannich bases. Adv Mod Oncol Res 2015; 1(2): 104–111; http://dx.doi.org/10.18282/amor.v1.i2.4.

*Correspondence to: Mardia T. El Sayed, Applied Organic Chemistry Department, National Research Centre, 12311 Dokki, Cairo, Egypt, mardia_elsayed2009@aol.com.

Received: 18th July 2015; **Accepted:** 21st September 2015; **Online Published:** 25th November 2015

Indole Mannich bases possess a great synthetic potential and are capable of participating in a variety of transformations leading to interesting and important types of compounds. The use of indole Mannich bases in organic synthesis has already led to important practical and basic results, contributing to the development of promising directions in the chemistry of indoles. The indole Mannich bases are well known indole derivatives in organic synthesis; it is of relevance both for obtaining a large group of endogenous substances, and for the synthesis of natural compounds and indole derivatives which possessing high biological activity[1-5]. Mannich reaction of indole and formaldehyde or acetaldehyde with several types of secondary and primary amines was published in 1937[6]. N-(1H-indol-3-ylmethyl)-N, N-dimethylamine (gramine) is the very important indole Mannich base which synthesized by Kuhn and Stein[6] from the aminomethylation reaction of indole and formaldehyde with dimethylamine. Gramine is a widely used initial compound in the synthesis of a large variety of substituted indoles, including agents playing important roles in living organisms[7,8]. In particular, gramine is most frequently used among the substances in the synthesis of L-tryptophan and substituted derivatives of this essential amino acid. The role of L-tryptophan is not restricted to being a component of protein molecules. This amino acid is a precursor of a number of biologically significant endogenous compounds such as nicotinic acid and 5-hydroxytryptamine (5-HT, serotonin), a compound whose meditor function is of basic significance in neu-

ropharmacology[8,9]. Another indole derivative, N-(1H-indol-3-ylmethyl)acetic acid (Heteroauxin), is a plant growth hormone, which is also synthesized in the human organism and can be prepared from gramine[10]. The condensation of glutaraldehyde with methylamine and acetonedicarboxylic acid was reported by Menzies and Robinson[12] and by Schopf and Lehmann[13] for preparing of pseudopelletierine. A number of alkaloids were prepared by the condensation of dialdehydes or reactions somewhat analogous to those used for the synthesis of pseudopelletierine and tropinone[14]. The cyclization of glutaraldehyde and β-phenylglutaraldehyde, with nitroalkanes to give the nitrodiol which react with two moles of secondary or primary amines afforded the nitro bis-Mannich bases, was reported[15]. 1-alkyl-, 1-aryl-, 1-(alkylamino)-, or 1-amido-substituted and of 1,2,6-trisubstituted piperidines were synthesized by Katritzky and Fan[16], from the condensation reaction of glutaraldehyde and primary amines or monosubstituted hydrazines with benzotriazole[17,18]. Many N-substituted piperidines and their 2,6-dialkyl derivatives are pharmacologically active and form an essential part of the molecular structure for important drugs[19]. For example, the 1-piperidino group is a feature of the antihistaminic agent and the spasmolytic benhexol[20], of narcotic analgesics[21], of postganglionic parasympathetic agonists[22] and of oral anesthetics. Many 1,2,6-trialkylpiperdine alkaloids have been isolated from both animal and plant species[23,24].

Materials and method

Materials

Fetal bovine serum (FBS) and L-glutamine were purchased from Gibco Invitrogen Co. (Scotland, UK). RPMI-1640 medium was purchased from Cambrex (New Jersey, USA). Dimethyl sulfoxide (DMSO), doxorubicin, penicillin, streptomycin and sulforhodamine B (SRB) were from Sigma Chemical Co. (Saint Louis, USA).

Cell cultures

Three human tumor cell lines, MCF-7 (breast adenocarcinoma), NCI-H460 (non-small cell lung cancer), and SF-268 (CNS cancer) were used. MCF-7 was obtained from the European Collection of Cell Cultures (ECACC, Salisbury, UK). NCI-H460, SF-268 and normal fibroblast cells (WI 38) were kindly provided by the National Cancer Institute (NCI, Cairo, Egypt). They were grown as a monolayer and routinely maintained in a RPMI-1640 medium supplemented with 5% heat inactivated FBS, 2 mmol/L glutamine and antibiotics (penicillin 100 U/mL, streptomycin 100 µg/mL), at 37°C in a humidified atmosphere containing 5% CO_2. Exponentially growing cells were obtained by plating 1.5×10^5 cells/mL for MCF-7 and SF-268 and 0.75×10^4 cells/mL for NCI-H460, followed by 24 h of incubation. The effect of the vehicle solvent DMSO on the growth of these cell lines was evaluated in all the experiments by exposing untreated control cells to the maximum concentration (0.5%) of DMSO used in each assay.

Tumor cell growth assay

The effects of six selected target compounds (2, 3, 4, 5a, 5c and 5d) on the *in vitro* growth of human tumor cell lines were evaluated according to the procedure adopted from the National Cancer Institute (NCI, USA) in the '*In vitro* Anticancer Drug Discovery Screen' that uses the protein-binding dye sulforhodamine B to assess cell growth[16]. Exponentially growing cells in 96 well plates were exposed for 48 h to five serial concentrations of each compound, starting from a maximum concentration of 150 µmol/L. Following this exposure period, the adherent cells were fixed, washed, and stained. The bound stain was solubilized and the absorbance was measured at 492 nm in a plate reader (Bio-Tek Instruments Inc., Powerwave XS, Winooski, USA). A dose-response curve and the inhibition of 50% concentration (IC_{50}), corresponding to the minimum inhibitory concentration was obtained for each test compound and cell line. Doxorubicin was used as a positive control and tested in the same manner.

Structure-activity relationship of the newly synthesized products

The effect of the selected synthesized bis-indole Mannich bases (2, 3, 4, 5a, 5c and 5d) was evaluated on the *in vitro* growth of three human tumor cell lines representing different tumor types: breast adenocarcinoma (MCF-7), non-small lung cancer cell (NCI-H460), and CNS cancer (SF-268) after continuous exposure for 48 h (*Table 1*).

Table 1 Effect of compounds (2, 3, 4, 5a, 5c and 5d) on the growth of three human tumor cell lines

Compound No.	IC_{50} (µmol/L)			
	MCF-7	NCI-H460	SF-268	WI 38
(5c)	20.4 ± 2.8	16.2 ± 3.2	18.6 ±2.6	16.2 ± 8.6
(3)	33.6 ± 8.5	40.3 ± 12.3	30.4 ± 2.8	62.2 ± 2.0
(2)	0.4 ± 0.09	0.2 ± 0.08	0.2 ± 0.06	80.8 ± 26.8
(5d)	22.6 ± 8.0	22.6 ± 8.6	12.4 ± 3.6	40.4 ± 11.3
(5a)	4.8 ± 1.0	6.8 ± 0.3	12.8 ± 4.2	26.8 ± 4.0
(4)	0.08 ± 1.4	0.05 ± 0.4	0.01 ± 0.6	>100

doi: 10.18282/amor.v1.i2.4

All of the tested compounds were able to inhibit the growth of the tested human tumor cell lines in a dose-dependent manner. Compound (4) showed the highest inhibitory effect against all three tumor cell lines with IC_{50} for MCF-7 (0.08 µmol/L), NCI-H460 (0.05 µmol/L) and SF-268 (0.01 µmol/L). Compound (2) proceeded to compound (4) in its activity against the tested cancer cell lines with IC_{50} for MCF-7 (0.4 µmol/L), NCI-H460 (0.2 µmol/L) and SF-268 (0.2 µmol/L). Both Mannich bases (2) and (4) showed activity towards normal fibroblast cells (WI 38). Compounds (3, 5c and 5d) showed the minimum inhibitory effect among the tested compounds with overall IC_{50} ranged from 12.4 to 62.2 µmol/L. Whereas compound (5a) showed moderate growth inhibitory effect against two of the tested cancer cells MCF-7 (IC_{50} = 4.8 µmol/L), NCI-H460 (IC_{50} = 6.8 µmol/L) and minimum inhibitory effect towards the cancer cell line SF-268 (IC_{50} = 12.8 µmol/L). From the overall results, we can conclude that compound (4) is the most active compound.

Results and discussion

The present work describes a novel synthesis of a variety of bis-indolyl Mannich bases by double condensations of indole and glutaraldehyde with secondary or primary amines or phenylhydrazine or chiral primary amine or amino acid. The preparation of condensation products from aldehydes (formaldehyde, acetaldehyde), indole and secondary or primary amines is usually carried out in glacial acetic acid[1-5]. We have now found that the same procedure can be easily applied to glutaraldehyde instead of formaldehyde. Indole reacts overnight after refluxing for 1 h with glutaraldehyde and secondary or primary amines as shown in *Figure 1*. We expect a wide range of possibilities for the use of these compounds for the synthesis of various biologically active indole-containing substances.

The expected condensation product 2,6-di(1H-indol-2-yl)-1,7-diaza-bicyclo[5.2.2]undecane (2), was prepared by using piperazine hexahydrate (98%) with glutaralde-

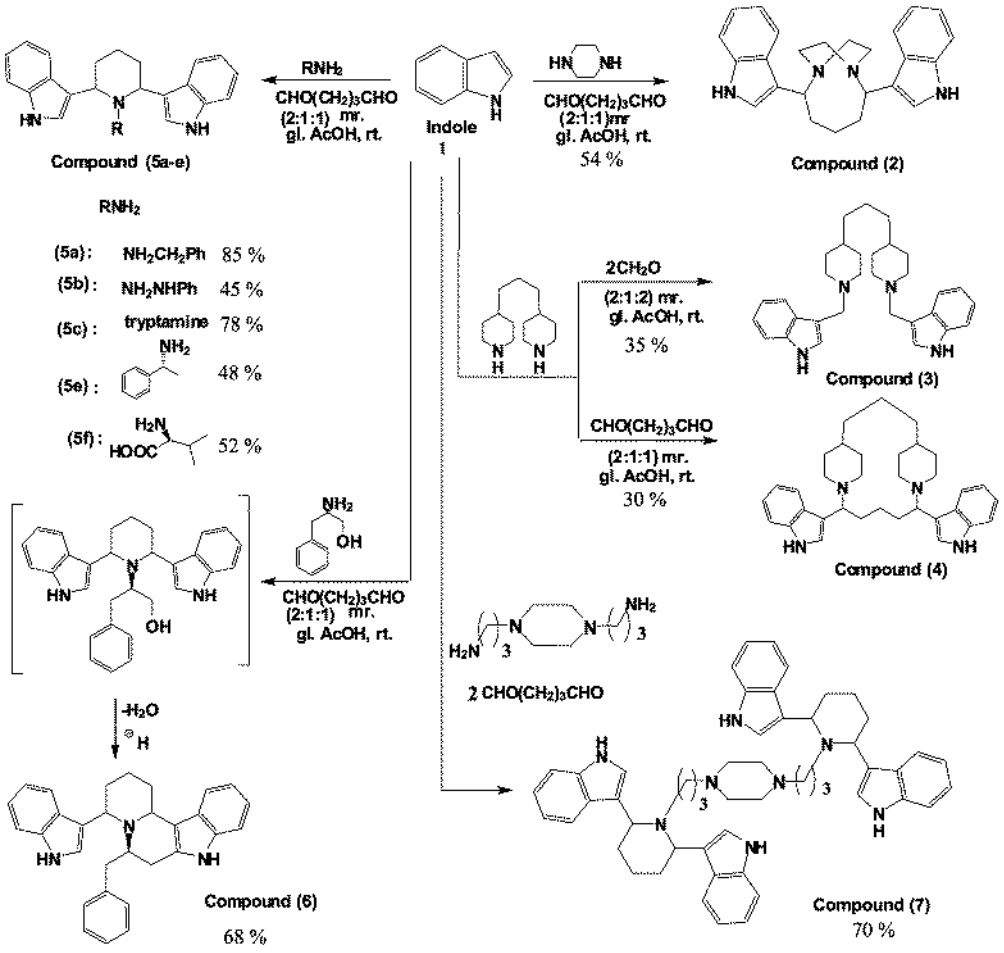

Figure 1 Reactions of indole with secondary and primary amines leading to the formation of bis-indolyl Mannich bases

doi: 10.18282/amor.v1.i2.4

hyde and indole in a molar ratio (2:1:1) in a 54% yield. Bis-indolyl-diazobicycloundecane derivative (2), is a novel compound, has not been reported in the literature before and cannot be prepared by other methods. The structure of compound (2) was identified based on its spectral data. The expected bis-indolyl Mannich base (3) (obtained in 45% yield) is likely the product of a condensation reaction between 4,4′-trimethylenedipiperidine and two mole equivalents of formaldehyde. This low yield can be explained by the lower basicity of the piperidine ring in 4,4′-trimethylenedipiperidine. Whereas, using one equivalent mole of glutaraldehyde leads to the formation of the new macro heterocyclic ring system (4) in a low yield of 30%, which can be attributed to the lower basicity, the stearic hindrance in the macro structure (4). Thus, the reaction time was long and the product formed in a low yield of 30%.

Many N-substituted piperidines and their 2,6-dialkyl derivatives are pharmacologically active and form an essential part of the molecular structure for important drugs[19]. There are many alternative methods available for the synthesis of the N-substituted piperidines. Cyclization with the formation of a bond between a carbon atom and a heteroatom is the usual heterocyclization that forms a six-membered heterocyclic ring system. Thus, the most familiar approach to piperidines is from a 1-pentanamine derivative with a leaving group on carbon 5[25]. Such methods utilize various 1,5-disubstituted pentanes as the starting materials. The preparation of a suitable starting material is often a major problem that restricts application, particularly in the preparation of 1,2,6-trisubstituted piperidines. Double reductive Mannich condensation of a dicarbonyl compound with an amine provided an alternative route for the preparation of N-substituted heterocycles with five and six-membered rings[26]. Watanabe et al.[27] reported the synthesis of N-substituted piperidines from the reductive amination of glutaraldehyde and primary amines with tetracarbonylhydridoferrate as a reducing agent. However, this method is inapplicable to 1,2,6-trisubstituted piperidines. The reaction of glutaraldehyde with primary amines, followed by potassium cyanide produced N-alkyl-2, 6- dicyanopiperidines[26]. In our recent work, we described a novel synthesis of a variety of N-alkyl, N-aryl, N-heteroaryl piperidine derivatives, containing two indole units in positions 2,6, in which it cannot be synthesized by any other approaches. The derivatives were synthesized by double condensations of indole and glutaraldehyde with primary amines in glacial acetic acid in a molar ratio (2:1:1). An example of aliphatic primary amines benzylamine was employed to afford, 1,2,6-trisubstituted piperidines (5a) in an excellent yield of 85%. When monosubstituted hydrazine (phenylhydrazine) was used as the amine component, the expected N-(alkylamino) piperidine derivative (5b) was obtained. The double condensation reaction by using a bio interesting amine (tryptamine) has been carried out for the preparation of 1,2,6-trisubstituted piperidine derivative (5c) in 78% yield. This reaction will open doors for the synthesis of trisubstituted piperidine derivative containing three indole units in each molecule in positions 1, 2 and 6 and by one step reaction. In view of the continuous interest in this new reaction, primary amines, double amino methylation reaction by using chiral primary amines such as (R)-1-phenylethaneamine and (R)-2-amino-2-phenylethanol have been carried out as a possible way to obtain the expected 3-(6-(1H-indol-3-yl)-1-((R)-1-phenylethyl)piperidin-2-yl)-1H-indole (5d) in a 48% yield by using (R)-1-phenylethaneamine. Meanwhile, in the case of (R)-2-amino-2-phenylethanol as amine component, the reaction proceeds with cyclization by elimination of one mole of water, which is activated by the acid medium to afford the final product (6) as an end product. Compound (6) is identified based on its spectral data as 6-benzyl-1,2,3,4,6,7,8,12c-octahydro-4-(1H-indol-3-yl)indolo[3,2-a]quinolizine. The indolyl-quinolizine derivative has never been published, and cannot be prepared by other synthetical methods. However, the present study has successfully obtained in a good yield of 68% in this study. An attempt with double condensation reaction with indole and glutaraldehyde, the (S)-2-amino-3- methylbutanoic acid has been studied as an approach using the bioactive amino acid as amine component. The reaction produced (R)-2-(2,6-di(1H-indol-3-yl)piperidin-1-yl)-3-methylbutanoic acid (5e), in a 52% yield. The expected product (7) formed by four Mannich condensation reactions by using 3,3′-(piperazine-1,4-diyl) dipropan-1-amine as primary diamine with four equivalent indoles and two equivalent glutaraldehydes. Compound (7) was determined as 1,4-bis ((2,6-di (1H-indol-3-yl) piperidin-1-yl)methyl) piperazine based on its analytical and spectral data as presented in the experimental section. The novel bis-indolyl Mannich bases including compounds (2-4), bis-indolyl trisubstituted piperidine (5a-e), the quinolizine derivative 6 and 1, 4-bis ((2,6-di(1H-indol-3-yl) piperidin-1-yl) methyl) piperazine (7), were not reported in the literature yet and fully characterized by spectral data (^{1}H and ^{13}C NMR), in addition to their mass and IR spectra.

Experimental section

^{1}H-NMR spectra (300 MHz) and (400 MHz) and ^{13}C-NMR spectra (75 MHz) and (100 MHz) were measured and expressed in ppm (d) using residual $CHCl_3$

doi: 10.18282/amor.v1.i2.4

(d: 7.26) and $CDCl_3$ (d: 77.0), respectively, as the internal standards. Infrared spectra (IR) were recorded on a Nicolet Model 205 spectrophotometer. High-resolution mass spectra (HRMS) (EI, unless otherwise stated) were taken for most of the key liquid products. Melting points (mp.) were checked using a Yanagimoto micro melting point determination apparatus and are uncorrected. Flush column chromatography was performed using silica gel (Merck silica gel).

2,6-di(1H-indol-2-yl)-1,7-diazobicyclo[5.2.2]undecane (2): 15 mL glacial acetic acid, (0.01 mol) of piperazine-hexahydrate (98%) was cooled in an ice bath. Then, (0.01 mol, 2.0 mL of glutaraldehyde solution (50%) was added, and the mixture was shaken well. The mixture was poured into a flask containing (0.02 mol, 2.4 g) indole, and the mixture was stirred until the indole dissolved to give a clear solution. Then, the mixture was left overnight. The product was detected by thin layer chromatography (TLC) (1% methanol/CH_2Cl_2), after that, the reaction mixture was added dropwise into a solution of 14 g NaOH in 1 L cold water with cooling and stirring. Then, the whole mixture was left to cool with stirring over 2 h. The product was filtered and washed with cold water and dried, then collected from column chromatography eluted with (30% ethylacetate/cyclohexane), to give a pale brown powder with mp. 221°C, in a 54% yield, **^{1}H NMR (400 MHz, DMSO-d_6) δ (ppm):** 1.15–1.23 (m, 2H, CH_2); 1.62–1.92 (m, 4H, $2CH_2$); 2.28–2.30 (m, 8H, $4CH_{2\ piperazine}$); 4.35 (t, *J* = 7.1 Hz, 2H, 2CH); 6.85 (t, *J* = 7.41 Hz, 2H, ArH); 6.99 (t, *J* = 7.41 Hz, 2H, ArH); 7.01 (s, 2H, ArH); 7.15 (d, *J* = 7.87 Hz, 2H, ArH); 7.28 (d, *J* = 7.86 Hz, 2H, ArH); 10.69 (br., 2H, NH). **^{13}C NMR (100 MHz, DMSO-d_6) δ (ppm):** 26.63, 38.87, 39.92, 40.12, 101.12, 111.42, 117.97, 119.01, 119.51, 120.67, 121.95, 126.76 and 136.57. **ESI-MS:** 385.2 (M+H), 405.5 (M+H_2O+3H). **GC-MS:** 384.63 (M), 385.7 (M+H), 386.9 (M+2H), 298.36 (M-piperazine), 117 (indolyl unit) base peak. **IR (KBr, cm^{-1}):** 3405.82 (NH), 2855.81, 2926.01 ($CH_{2\ aliphatic\ stretching}$), 1455.24 ($CH_{2\ aliphatic\ bending}$), 3267.53 (broad for hydrate) and 1338.11 (C–N).

3-((4-(3-(1-((1H-indol-3-yl)methyl)piperidin-4-yl)propyl)piperidin-1-yl)methyl)-1H-indole (3): 15 mL glacial acetic acid and 2.6 g (0.0125 mol) of 4,4′-trimethylenedipiperidine was cooled in an ice bath. Then, 2.2 mL (0.025 mol) of formalin solution (37%) was added, and the mixture was shaken well. The mixture was poured into a flask containing 3 g (0.025 mol) indole, and was stirred until the indole dissolved to give a clear solution then the mixture was left overnight. The product was detected by TLC. (0.5% methanol/CH_2Cl_2). After that, the reaction mixture was added drop wise to a solution of 14 g NaOH in 1 L cold water with cooling and stirring. Then, the whole mixture was left to cool with stirring over 2 h. The solution extracted with dichloromethane (CH_2Cl_2) was dried over anhydrous sodium sulfate. The product was purified by using a column (0.5% methanol/CH_2Cl_2) to give brown crystals with mp. 107°C, in 35% yield, **^{1}H NMR (400 MHz, $CDCl_3$) δ (ppm):** 1.22–1.24 (m, 2H, CH_2); 1.63–1.83 (m, 14H, CH, $CH_{2\ piperidine}$); 2.10–2.16 (m, 8H, $CH_2NCH_{2\ piperidine}$); 3.47 (s, 4H, CH_2); 6.97 (s, 2H, ArH); 7.19–7.24 (m, 8H, ArH); 9.20 (br., 2H, NH); **^{13}C NMR (75 MHz, $CDCl_3$) δ (ppm):** 14.15, 20.40, 21.01, 29.18, 31.67, 53.40, 53.66, 55.66, 109.77, 113.39, 115.30, 119.38, 122.13, 128.60 and 136.66. **ESI-MS:** 472.3 (M+4H), 495.2 (M+Na+4H), 963.0 (2M+Na+3H). **IR (KBr, cm^{-1}):** 3403.79 (NH), 2823.88, 2969.82 ($CH_{2\ aliphatic\ stretching}$), 1458.85 ($CH_{2\ aliphatic\ bending}$), 1330.07 (C–N).

Tricyclo[11.2.2.2^{5,8}]nonadecane system (4): 15 mL glacial acetic acid and 2.6 g (0.0125 mol) of 4,4′-trimethylenedipiperidine was cooled in an ice bath. Then, 2.5 mL (0.0125 mol) of glutaraldehyde solution (50%) was added and the mixture was shaken well. The mixture was poured in a flask containing (0.025 mol, 3 g) indole, and the mixture was stirred until the indole dissolved to give a clear solution, then the mixture was left for some days. The product was detected by TLC (1% methanol/ CH_2Cl_2), and after that the reaction mixture was added drop wise to a solution of 14 g NaOH in 1 L cold water with cooling and stirring. Then, the mixture was stirred under cooling over 2 h, then the product was filtered and recrystallized twice with acetone/methanol to give white powder with mp. 199°C, in 30% yield, **^{1}H NMR (400 MHz,$CDCl_3$) δ (ppm):** 0.64–1.25 (m, 4H, $2CH_2$); 1.80–2.04 (m, 8H, $8CH_2$, 2CH); 2.06–2.25 (m, 4H, CH_2); 2.63–2.90 (m, 8H, CH_2, $CH_{\ piperidine}$); 3.07–3.14 (m, 8H, $2CH_2NCH_{2\ piperidine}$); 4.25 (t, *J* = 1.52 Hz, 2H, 2CH); 6.587 (d, *J* = 10.17 Hz, 2H, ArH); 7.03–7.16 (m, 4H, ArH); 7.33–7.57 (m, 4H, ArH); 10.60 (br., 2H, NH). **^{13}C NMR (75 MHz, DMSO-d_6) δ (ppm):** 14.50, 21.02, 26.50, 32.50, 34.00, 39.47, 40.73, 54.45, 111.79, 112.30, 118.00, 119.32, 120.97, 122.05, 126.52, 126.63 and 136.93. **ESI-MS:** 509.6 (M+H), 530.5 (M+Na), 1041.9 (2M+Na+2H). **IR (KBr, cm^{-1}):** 3413.19 (NH), 2857.36, 2930.47($CH_{2\ aliphatic\ stretching}$), 1457.13($CH_{2\ aliphatic\ bending}$) and 1338.05 (C–N).

General procedure for compounds (5, 6): 15 mL glacial acetic acid, (0.005 mol) of the primary amine was cooled in an ice bath. Then, (0.005 mol, 1 mL) of glu-

doi: 10.18282/amor.v1.i2.4

taraldehyde solution (50%) was added and the mixture was shaken well. The mixture was poured into a flask containing (0.01 mol, 1.2 g) indole, and was stirred until the indole dissolved to give a clear solution, then was left overnight. The product was detected by TLC (0.5% methanol/CH_2Cl_2). After that, the reaction mixture was added drop wise into a solution of 14 g NaOH in 1 L cold water with cooling and stirring. The whole mixture was left to cool with stirring over 2 h, then, the solution was extracted with CH_2Cl_2 and dried over anhydrous sodium sulfate. The product was purified using a column chromatography.

3-(1-benzyl-6-(1H-indol-3-yl)piperidin-2-yl)-1H-indole (5a): Column chromatography with 1% methanol/ CH_2Cl_2, produced brown powder with mp. 150°C, in a 85% yield, **^{1}H NMR (400 MHz, $CDCl_3$) δ (ppm):** 1.50–1.57 (m, 2H, CH_2); 2.05–2.18 (m, 2H, CH_2); 2.24–2.28 (m, 2H, CH_2); 3.48 (s, 2H, $CH_{2\ benzyl}$); 4.41 (t, *J* = 7.32 Hz, 2H, 2CH); 6.79 (d, *J* = 2.02 Hz, 2H, ArH); 6.98 (t, *J* = 7.05 Hz, 2H, ArH); 7.09 (t, *J* = 7.13Hz, 2H, ArH); 7.27 (d, *J* = 8.1Hz, 2H, ArH); 7.53 (d, *J* = 7.9Hz, 2H, ArH); 11.02 (br., 2H, NH). **^{13}C NMR (100 MHz, $CDCl_3$) δ (ppm):** 26.46, 33.73, 35.50, 72.50, 110.31, 110.98, 118.87, 118.88, 119.03, 119.67, 120.17, 120.67, 121.53, 121.56, 122.46, 127.08, 136.50, and 136.51. **ESI-MS:** 404.2 (M-H), 430.2 (M+Na+2H), 446.2 (M+K+2H). **IR (KBr, cm^{-1}):** 3408.71 (NH), 2858.24, 2928.73 ($CH_{2\ aliphatic\ stretching}$), 1455.14 ($CH_{2\ aliphatic\ bending}$), 1337.64 (C—N).

N-(2,6-di(1H-indol-3-yl)piperidin-1-yl)benzenamine (5b): Column chromatography with 30% ethyl acetate /hexane, produced brown powder with mp. 125°C, in a 45% yield, **^{1}H NMR (400 MHz, CD_3OD) δ (ppm):** 1.61–1.76 (m, 2H, CH_2); 1.99–2.03 (m, 4H, $2CH_2$); 4.45–4.52 (m, 2H, 2CH); 6.67 (dd, *J* = 1.01, 3.21 Hz, 2H, ArH); 6.73–6.94 (m, 4H, ArH); 7.06–7.11 (m, 9H, ArH); 7.79 (br., 1H, NH $_{phenyl}$); 11.98 (br., 2H, NH). **^{13}C NMR (75 MHz, CD_3OD) δ (ppm):** 20.88, 32.74, 60.41, 111.18, 114.69, 117.19, 118.55, 119.44, 120.51, 121.37, 122.46, 123.62, 126.60, 129.19, 133.67, 137.01 and 171.39. **ESI-MS:** 406.4 (M), 404.2 (M-2H), 443.3 (M+K-2H) 428.2 (M+Na-H). **IR (KBr, cm^{-1}):** 3405.22 (NH), 2861.55, 2928.77 ($CH_{2\ aliphatic\ stretching}$), 1456.52 ($CH_{2\ aliphatic\ bending}$), 1337.23 (C–N).

3-(2-(2,6-di(1H-indol-3-yl)piperidin-1-yl)ethyl)-1H-indole (5c): Column chromatography with 30% ethyl acetate/hexane, produced brown powder with mp. 174°C, in a 78% yield, **^{1}H NMR (400 MHz, DMSO) δ (ppm):** 1.19–1.36 (m, 2H, CH_2); 1.37–1.48 (m, 2H, CH_2); 1.59–1.69 (m, 2H, CH_2); 1.89 (t, *J* = 7.1 Hz, 2H, CH_2); 2.46 (t, *J* = 1.9 Hz, 2H, CH_2); 4.27 (t, *J* = 8.3 Hz, 2H, 2CH); 6.81 (t, *J* = 7.5 Hz, 3H, ArH); 6.94 (t, *J* =7.5 Hz, 4H, ArH); 7.03–7.10 (m, 4H, ArH); 7.22 (d, *J* = 8.1 Hz, 2H, ArH); 7.42 (d, *J* = 7.9 Hz, 2H, ArH); 10.73 (br., 3H, NH). **^{13}C NMR (75 MHz, CD_3OD) δ (ppm):** 23.30, 29.25, 33.46, 40.77, 77.20, 110.67, 111.06, 117.83, 118.45, 119.36, 120.59, 121.22, 122.62, 126.71, and 136.48. **EI-MS:** 459.5 (M+H), 342.3 (M-indolyl), 223.3 (M-2indolyl). **IR (KBr, cm^{-1}):** 3409.33 (NH), 2857.24, 2928.11 ($CH_{2\ aliphatic\ stretching}$), 1455.92 ($CH_{2\ aliphatic\ bending}$), 1338.14 (C–N).

3-(6-(1H-Indol-3-yl)-1-(*R*-1-phenylethyl)piperidin-2-yl)-1H-indole (5d): Column chromatography with 30% ethyl acetate/hexane, produced brown crystals with mp.158°C, in a 48% yield, **^{1}H NMR (400 MHz, $CDCl_3$) δ (ppm):** 1.75–1.78 (m, 2H, Me); 2.02 (d, *J* = 4.94Hz, 3H, Me); 2.05–2.23 (m, 2H, CH_2); 2.67–2.72 (m, 2H, CH_2); 4.08 (q, *J* = 7.13 Hz, 1H, CH); 4.54 (t, *J* = 3.11 Hz, 1H, CH); 5.03 (t, *J* = 3.66 Hz, 1H, CH); 6.39 (d, *J* = 1.28 Hz, 1H, ArH); 6.88 (d, *J* = 1.83 Hz, 4H, ArH); 7.12–7.16 (m, 4H, ArH); 7.26 (d, *J* = 8.1 Hz, 1H, ArH); 7.42 (dd, *J* = 7.31, 17.56 Hz, 2H, ArH); 7.63 (d, *J* = 6.23 Hz, 1H, ArH); 7.78 (d, *J* = 2.01 Hz, 2H, ArH); 8.50 (br., 2H, NH). **^{13}C NMR (75 MHz, CD_3OD) δ (ppm):** 14.15, 18.07, 20.69, 21.04, 32.84, 48.48, 60.45, 110.97, 118.84, 119.65, 120.15, 121.53, 121.61, 123.64, 127.07, 129.27, 136.50, 137.12 and 138.74. **EI-MS:** 419.1 (M), 417.9 (M-2H), 458.6 (M+K), 444.9 (M+Na+2H), 864.5 (2M+Na+3H). **IR (KBr, cm^{-1}):** 3380.59 (NH), 2843.54, 2922.08 ($CH_{2\ aliphatic\ stretching}$), 1458.36 ($CH_{2\ aliphatic\ bending}$), 1339.71 (C–N).

(*R*)-2-(2,6-di(1H-indol-3-yl)piperidin-1-yl)-3-methyl butanoic acid (5e): Column chromatography with 30% methylbutanoic/hexane, produced dark brown oil, with a 52% yield; **^{1}H NMR (400 MHz, $CDCl_3$) δ (ppm):** 0.97 (d, *J* = 6.59 Hz, 6H, CH_3); 1.22–1.25 (m, 2H, CH_2); 1.89–1.94 (m, 2H, CH_2); 2.03–2.13 (m, 2H, CH_2); 2.57–2.62 (m, 1H, CH); 4.09–4.23 (m, 2H, CH); 5.23 (d, *J* = 6.77 Hz, 1H, CH); 6.95 (d, *J* = 2.36 Hz, 2H, ArH); 7.17–7.22 (m, 4H, ArH); 7.19 (d, *J* = 7.7 Hz, 2H, ArH); 7.64 (d, *J* = 3.3 Hz, 2H, ArH); 11.02 (br., 1H, NH); 12.23 (br., 1H, COOH). **^{13}C NMR (75 MHz, $CDCl_3$) δ (ppm):** 17.18, 18.96, 21.75, 29.56, 31.48, 32.79, 65.10, 69.37, 110.96, 119.56, 121.81, 122.22, 124.15, 127.59, 136.11, and 176.29. **EI-MS:** 418.3 **(**M+3H), 419.4 (M+4H), 441.6 (M+Na+3H). **IR (KBr, cm^{-1}):** 3409.63 (NH), 2867.41, 2955.48 ($CH_{2\ aliphatic\ stretching}$), 1455.11 ($CH_{2\ aliphatic\ bending}$), 1724 (C=O), 1336.81 (C–N).

6-benzyl-1,2,3,4,6,7,8,12c-octahydro-4-(1H-indol-3-yl) indolo[3,2-a]quinolizine (6): Column chromatography

doi: 10.18282/amor.v1.i2.4

methanol MeOH/CH_2Cl_2, produced brown oil, in a 68% yield; **^{1}H NMR (400 MHz, DMSO-d_6) δ (ppm):** 1.13–1.23 **(**m, 2H, CH_2); 1.42–1.44 (m, 4H, $2CH_2$); 2.28 (d, *J* = 7.14 Hz, 4H, $2CH_2$); 3.42–3.49 (m, 1H, CH); 4.01–4.14 (m, 1H, CH); 4.35 (t, *J* = 7.5Hz, 1H, CH); 6.84 (t, *J* = 7.05 Hz, 3H, ArH); 6.98 (t, *J* = 7.32 Hz, 3H, ArH); 7.15 (d, *J* = 2.2Hz, 2H, ArH); 7.28 (d, *J* = 8.05Hz, 3H, ArH); 7.46 (d, *J* = 7.9 Hz, 3H, ArH); 10.68 (br., 2H, NH). **^{13}C NMR (75 MHz, DMSO-d_6) δ (ppm):** 26.57, 33.51, 35.01, 38.67, 38.94, 40.33, 48.68, 54.94, 101.02, 111.32, 111.41, 117.86, 118.31, 118.80, 118.94, 119.08, 120.04, 120.56, 120.91, 121.88, 125.21, 126.70, 127.65, 135.89, 136.51. **ESI-MS:** 431.7 (M), 432.2 (M+H), 457.5 (M+Na+3H). **IR (KBr, cm^{-1}):** 3408.05 (NH), 2854.61, 2925.26 (CH_2 aliphatic stretching), 1455.40 (CH_2 aliphatic binding), 1337.05 (C–N).

Procedure for the preparation of compound (7): 15 mL glacial acetic acid, (0.005 mol, 1 g) of the primary diamine, 3,3'-(piperazine-1,4-diyl)dipropan-1-amine was added under cooling in an ice bath. Then, (0.01 mol, 2 mL) of glutaraldehyde solution (50%) was added, and the mixture was shaken well. The mixture was poured into a flask containing (0.02 mol, 2.4 g) indole, and was stirred until the indole dissolved to give a clear solution, the mixture was left standing overnight. The product was detected by TLC (0.5% methanol/CH_2Cl_2), after that the reaction mixture was added drop wise into a solution of 14 g NaOH in 1 L cold water with cooling and stirring. The whole mixture was left to cool with stirring over 2 h, then, the solution extracted with CH_2Cl_2 was dried over anhydrous sodium sulfate. The product was purified by using a column chromatography.

1,4-bis((2,6-di(1H-indol-3-yl)piperidin-1-yl)methyl)piperazine (7): Column chromatography with 1% methanol/hexane, produced a pale brown powder with mp. 174°C, in a 70% yield, **^{1}H NMR (400 MHz, DMSO-d_6) δ (ppm):** 1.17 (t, 2H, *J* = 2.7Hz, CH_2); 1.38 (t, 2H, *J* = 2.4Hz, CH_2); 1.75–1.79 (m, 2H, CH_2); 1.98 (t, 2H, *J* = 2.6 Hz, CH_2); 2.25–2.46 (m, 4H, $2CH_2$); 4.30 (t, *J* = 8.3 Hz, 2H, 2CH); 6.82 (t, *J* = 7.5 Hz, 4H, ArH); 6.95 (t, *J* = 7.5 Hz, 4H, ArH); 7.11 (d, *J* = 7.2 Hz, 4H, ArH); 7.24 (d, *J* = 8.1Hz, 4H, ArH); 7.43 (dd, *J* = 2.3,7.9Hz, 4H, ArH); 10.65 (s, 4H, 4NH). **^{13}C NMR (75 MHz, DMSO-d_6) δ (ppm):** 23.30 (CH), 29.25 (CH_2), 33.46 (CH), 35.01 (CH_2), 39.48 (CH_2), 39.75 (CH_2), 40.77 (CH_2), 54.97 (CH_2), 69.25 (CH_2), 77.20 (CH_2), 110.67, 111.06, 111.36, 117.88, 118.45, 119.09, 119.36, 119.69, 120.58, 120.93, 121.92, 120.59, 121.22, 122.62, 126.71 and 136.53. **EI-MS:** 806.23 (M+H), **Elemental analysis:** calculated**,** C, 77.57; H, 8.51; N, 13.92, found, C, 77.72; H, 8.80; N, 14.02, **IR (KBr, cm^{-1}):** 3459.32 (NH), 2887.24, 2988.11 (CH_2 aliphatic stretching), 1475.92 (CH_2 aliphatic bending), 1348.14 (C–N).

Conclusion

The current bis-indolyl Mannich bases have been synthesized in a good to excellent yields via double or multiple condensation reactions of indole with glutaraldehyde and various primary or secondary amines. The expected bis-indolyl Mannich bases (2, 3 and 4) were formed by using piperazine hexahydrate and 4,4′-trimethylenedipiperidine. Whereas, the use of primary amines, phenylhydrazine, amino acids and primary diamine afforded the corresponding bis-indolyl-1,2,6-trisubstituted piperidines (5a-e) and indolyl-quinolizine (6) and di-bis-indolyl-1,2,6-trisubstituted piperidines (7). All these bis-indolyl Mannich bases are fully characterized based on its analytical and spectral data. This new indole Mannich bases will explore several aspects involved in the preparation of numerous indole derivatives by investigating their chemistry. Six of the synthesized bis-indolyl Mannich bases have been selected for antiproliferative activity at NCI, Egypt, towards three human tumor cell lines representing different tumor types: breast adenocarcinoma cell (MCF-7), non-small lung cancer cell (NCI-H460), and CNS cancer cell (SF-268). Compound (4) showed the best and highest inhibitory effect against all three tumor cell lines with IC_{50} for MCF-7 (0.08 µmol/L), NCI-H460 (0.05 µmol/L) and SF-268 (0.01 µmol/L).

Acknowledgments

Authors are grateful to the National Cancer Institute, Egypt for performing the antiproliferative screening for the synthesized Mannich bases.

Conflict of interest

The authors declared no potential conflict of interest with respect to the research, authorship, and/or publication of this article.

References

1. El Sayed MT, Mahmoud K, Hilgeroth A. Glacial acetic acid as an efficient catalyst for simple synthesis of dindolylmethanes. Curr Chem Lett 2014; 3(1): 7–14.
2. El Sayed MT, Ahmed KM, Mahmoud K, et al. Synthesis, cytostatic evaluation and structure activity relationships of novel bis-indolylmethanes and their corresponding

doi: 10.18282/amor.v1.i2.4

tetrahydroindolocarbazoles. Eur J Med Chem 2015; 90: 845–859.
3. El Sayed MT, Mahmoud K, Ahmed KM, et al. First oxidized tetraindoles with antimicrobial evaluation and structure activity relationship. J Harmo Res Pharm 2014; 3(4): 167–176.
4. El Sayed MT, Ahmed KM, Mahmoud K, et al. Novel aspects of domino reaction of indoles with homophthalaldehyde and tere-phthalaldehyde. Glob J Sci Frontier Res 2014; 14(6): 14–22.
5. El-Sayed MT, Mahmoud K, Hilgeroth A, et al. Synthesis of novel indolo-spirocyclic compounds. J Heterocyclic Chem 2015; doi: 10.1002/jhet.2402
6. Kuhn H, Stein O. Over condensations from indoles with aldehydes and secondary amines: a new gramine synthesis [in German]. Eur J Inorg Chem 1937; 70(3): 567–569.
7. Mashkovskii MD. Drugs of the 20th century [in Russian], Moscow: Novaya Volna; 1998.
8. Granik VG. Drugs: Pharmacological, biochemical, and chemical aspects [in Russian]. Moskow; Vuzovskaya Kniga; 2001.
9. Lehninger AL. Principles of biochemistry. New York: Worth Publishers; 1982.
10. Cru J. Biochemistry: Medical and biological aspects [in Russian]. Moscow: Medicina; 1979.
11. Tramontini M. Advances in the chemistry of Mannich bases. Synthesis 1973; 1973(12): 703–775.
12. Menzies RC, Robinson R. Synthesis of ψ-Pelletierine. J Chem Soc 1924; 125: 2163–2168.
13. Schopf C, Lehmann G. The synthesis of troponons, Pseudopelletierine, Lobelanins and related alkaloids under physiological conditions [in German]. Justus Liebigs Ann Chem 1935; 518(1): 1–37.
14. Henry TA. The plant alkaloids. 4th ed. London: Churchill Ltd; 1949.
15. Lichtenthaler FW, Leinert H, Scheidegger U. Nitromethane condensation with aldehydes, XIII. For Styrian of the cyclization of aliphatic 1,5-dialdehydes with nitromethylene compounds [in German]. Chem Ber 1968; 101: 1819–1836.
16. Katritzky AR, Fan W. The chemistry of benzotriazole. A novel and versatile synthesis of 1-alkyl-, 1-aryl-, 1-(alkylamino)-, or 1-amido-substituted and of 1,2,6-trisubstituted piperidines from glutaraldehyde and primary amines or monosubstituted hydrazines. J Org chem 1990; 55(10): 3205–3209.
17. Katritzky AR, Urogdi L, Mayence A. Benzotriazole-assisted synthesis of monoacyl α-aminoglycines J Chem Soc Chem Commun 1989; 337–338.
18. Coutts RT, Casy AF. Pyridines and reduced pyridines of pharmacological interest. In: Abramovitch R, ed. by. Chemistry of heterocyclic compounds: pyridine and its derivatives, supplement, Pt. 4, Vol. 14. New York: John Wiley & Sons; 1974. p. 445–524.
19. Ison RR, Franks FM, Soh KS. The binding of conformationally restricted antihistamines to histamine receptors. J Pharm Pharmacol 1973; 25(11): 887–894.
20. Reynolds AK, Randall LO. Morphine and allied drugs. Toronto: University of Toronto Press; 1957. p. 269.
21. Hermans B, van Daele P, van de Westeringh, C, et al. 4-substituted piperidines. IV. The synthesis of 4-[(2,6-dioxo-3-phenyl)-3-piperidyl]piperidines. J Med Chem 1968; 11(4): 797–800.
22. McElvain SM. 2,6-Dimethylpyridine. Org Synthesis J Am Chem Soc 1927; 49: 2835–2840.
23. MacConnell JG, Blum MS, Fales HM. The chemistry of fire ant venom. Tetrahedron 1971; 27(6): 1129–1139.
24. Jones G. Pyridines and their benzo derivatives (v) synthesis. In: Katritzky AR, Rees C, ed. by. Comprehensive heterocyclic chemistry. Oxford [Oxfordshire]: Pergamon Press; 1984. Vol. 2, p. 395–510.
25. Lane CF. Sodium cyanoborohydride – a highly selective reducing agent for organic functional groups. Synthesis 1975; 1975(3): 135–146.
26. Takahashi K, Mikajiri T, Kurita H, et al. Stereoselective synthesis of 1-substituted 2,6-dicyanopiperidines and transformation of 2,6-dialkylated products of l-phenyl-2, 6-dicyanopiperidine to delta-diketones and cyclohexenones. J Org Chem 1985; 50(22): 4372–4375.
27. Watanabe Y, Shim SC, Mitsudo T, et al. Takegami reaction of toluidine with glutaraldehyde in the presence of a stoichiometric quantity of potassium hydridoferrate. Bull Chem Soc Jap 1976; 49(8): 2302–2305.

doi: 10.18282/amor.v1.i2.4

Advances in Modern Oncology Research

doi: 10.18282/amor.v1.i2.15

ORIGINAL RESEARCH ARTICLE

The correlation between aldehyde deydrogenase-1A1 level and tumor shrinkage after preoperative chemoradiation in locally advanced rectal cancer

Rhandyka Rafli[1*], Soehartati A Gondhowiardjo[1], Adang Bachtiar Kantaatmadja[2], Sahat Matondang[3], Ening Krisnuhoni[4]

[1]Department of Radiotherapy, University of Indonesia, Jakarta, Indonesia
[2]Department of Public Health, University of Indonesia, Jakarta, Indonesia
[3]Department of Radiology, University of Indonesia, Jakarta, Indonesia
[4]Department of Anatomical Pathology, Cipto Mangunkusumo Hospital, Jakarta, Indonesia

***Abstract*:** This study was performed to determine the correlation between aldehyde dehydrogenase-1A1 (ALDH1A1) level and tumor shrinkage after chemoradiation in locally advanced rectal cancer. This is a retrospective study of 14 locally advanced rectal cancer patients with long course neoadjuvant chemoradiation. The ALDH1A1 level was measured using ELISA from paraffin embedded tissue. Tumor shrinkage was measured from computed tomography (CT) scan or magnetic resonance imaging (MRI) based on Response Evaluation Criteria in Solid Tumor v1.1 (RECIST v1.1). The mean of ALDH1A1 level was 9.014 ± 3.3 pg/mL and the mean of tumor shrinkage was 7.89 ± 35.7%. Partial response proportion was 28.6%, stable disease proportion was 50% and progressive disease proportion was 21.4%. There was a significantly strong negative correlation (r = –0.890, p < 0.001) between ALDH1A1 and tumor shrinkage. In conclusion, tumor shrinkage in locally advanced rectal cancer after preoperative chemoradiation was influenced by ALDH1A1 level. Higher level of ALDH1A1 suggests decreased tumor shrinkage after preoperative chemoradiation.

***Keywords*:** ALDH1A1; rectal cancer; chemoradiation; RECIST v1.1

***Citation*:** Rafli R, Gondhowiardjo SA, Kantaatmadja AB, et al. The correlation between aldehyde deydrogenase-1A1 level and tumor shrinkage after preoperative chemoradiation in locally advanced rectal cancer. Adv Mod Oncol Res 2015; 1(2): 112–116; http://dx.doi.org/10.18282/amor.v1.i2.15.

*Correspondence to: Rhandyka Rafli, Department of Radiotherapy, University of Indonesia, Jakarta, 3173030, Indonesia, bubuyrafli@gmail.com

Received: 31st July 2015; **Accepted:** 19th October 2015; **Published Online:** 2nd December 2015

Rectal cancer is the third most common malignancy in the world and also in Indonesia. Worldwide, there are 1.2 million new cases of colorectal cancer diagnosed annually with 600,000 death cases each year[1]. Chemoradiation as neoadjuvant therapy before surgery to shrink tumor size is widely accepted as a treatment for locally advanced rectal cancer.

Radiation exposure to rectal cancer cell will increase reactive oxygen species that can alter membrane bilayer and cause lipid peroxidation. The breakdown products of lipid peroxides are mostly aldehydes, which may serve as "oxidative stress second messengers" with prolonged half-life and the ability to diffuse from their site of formation to nucleus, compared to reactive oxygen species (ROS). Cells possess aldehyde dehydrogenase-1 (ALDH1), a family of polyform enzyme, which detoxifies these aldehydes. ALDH1 is located in cytoplasm, mitochondria or nucleus[2-4].

In addition to its known function to oxidize aldehyde, ALDH1 was also found in cancer stem cell (CSC). In 2007, Ginestieret and co-workers have successfully demonstrated the first isoform of ALDH1 as a marker for

normal and malignant human mammary stem cell and predictor of poor clinical outcome[5]. In the following years, ALDH1 activity would be used successfully as a CSC marker for many cancers including lung, liver, bone, colon, pancreatic, prostate, head and neck, bladder, thyroid, brain, melanoma and cervical[6]. With the exception of one recent study on malignant melanoma, increasing evidence suggests that ALDH1 activity is a universal CSC marker[7].

The role of ALDH1 in rectal cancer is not fully understood. Avoranta et al. have demonstrated the prognostic value of ALDH1 in early rectal cancer that received postoperative adjuvant chemotherapy regimens through immunohistochemistry[8]. This study was in line with other colorectal studies, showing the ALDH1 correlation with 5-FU plus oxaliplatin (FOLFOX) resistance in colorectal cancer[9].

One of the isoforms of ALDH1, such as ALDH1A1, was involved in retinoic acid (RA) cell signaling via RA production by oxidizing all-*trans*-retinal and 9-*cis*-retinal. Depending on cellular context, this may lead to cell proliferation, apoptosis and cell cycle arrest. This function, in particular, has been linked to the "stemness" characteristic of cancer stem cell and through a different mechanism, cancer stem cell inherently became more resistant to chemo and radiotherapy[6,10,11].

These properties are believed to hold an important role in tumor response after chemoradiation. Several qualitative and semi-quantitative studies using immunohistochemistry showed that the expression of ALDH1A1 in cell cytoplasm have no prognostic significance in rectal cancer, but the expression of ALDH1A1 in stromal and the nucleus is associated with shorter survival[12].

In order to provide additional analysis of the biological relevance of ALDH1A1 in locally advanced rectal cancer, we examined the level of ALDH1A1 using the quantitative method with enzyme-linked immunosorbent assay (ELISA) to determine the correlation between ALDH1A1 level in rectal cancer tissue and tumor shrinkage after preoperative chemoradiation.

Materials and methods

Study design

This retrospective study enrolled locally advanced rectal cancer patients (T3–4 N0/+ M0) who underwent radiation therapy in Cipto Mangunkusumo Hospital from January 2009 to January 2014. Out of 144 patients, only 43 patients were able to complete the long course chemoradiation (46–50 Gy in 23–25 fractions) with concurrent Capecitabine or FOLFOX. Also, only 14 from 43 patients who had a decent formalin fixed-paraffin embedded (FFPE) rectal cancer tissue, base and evaluation CT-scan or magnetic resonance imaging (MRI) were found to be eligible for this study. Only three patients underwent surgery after chemoradiation.

Deparaffinization and protein extraction

The study material consisted of FFPE tissue from a biopsy sample. A section with 25 µm thickness and area 40–100 mm^2 were cut from FFPE blocks. Paraffin was removed by washing with xylene 3 times, followed by serial washing with 100%, 70%, and 40% alcohol and aqua dest mixtures. Tissue was rinsed with phosphate buffered saline (PBS), homogenized in 1:1 PBS and stored overnight at –20°C. After two cycles, freeze-thaw cycles were performed to break the cell membranes. The homogenates were centrifuged for 5 min at 5000 × *g*, in 2–8°C. The supernatant was removed and assayed immediately.

Enzyme-linked immunosorbent assay

ALDH1A1 concentration was determined by using Cusabio human retinal dehydrogenase 1 (ALDH1A1). 100 µL of sample supernatant and provided standard were added to each well and incubated for 2 h at 37°C. Subsequently, the liquid layer in each well was removed, and 100 µL biotin antibody were added to each well. The mixture was incubated for 1 h at 37°C. Wells were aspirated and washed 3 times using washing buffer. 100 µL HRP-avidin were added to each well and incubated for 1 h at 37°C. After removing the liquid and 5 times of washings with washing buffer, 90 µL tetramethylbenzidine (TMB) substrate were added to each well and incubated for 15–30 min at 37°C. Then, 50 µL of stop solution were added to each well. Within 5 min, ELISA plates were read in a microplate reader, which was set to 450 nm.

Tumor shrinkage evaluation

Baseline imaging and evaluation after chemoradiation were collected by 5 mm slice CT scan or MRI. The longest tumor diameter from baseline and evaluation were compared and classified using RECIST v1.1 methods[13]. Imaging baseline was done within 4 weeks before chemoradiation, and imaging evaluation was done after 4 weeks upon completion of chemoradiation. The longest diameter of tumor was measured and compared with the baseline and evaluation imaging. Correlation between ALDH1A1 level and tumor shrinkage was analyzed using bivariate (Pearson) correlation with bootstrap.

doi: 10.18282/amor.v1.i2.15

Ethics statement

This study was approved by the ethics committee of Medical Faculty, University of Indonesia.

Results

Patient characteristics and outcome

A total of 14 patients were included in our analysis. After preoperative chemoradiation, 4 patients (28.6%) had partial response, 7 patients (50%) with stable disease and 3 patients with progressive disease (*Table 1*).

Table 1 Characteristics of patients treated with neoadjuvant chemoradiation for rectal cancer

		N	%
Number of patients		14	
Gender	: Male/Female	6/8	43/57
T Stage (before treatment)	: T3	2.0	14.3
	: T4	12.0	85.7
N Stage (before treatment)	: N0	2.0	14.3
	: N1	7.0	50.0
	: N2	5.0	35.7
Age	: Mean (SD)	46.8	12.9
Karnofsky performance status	: ≥80	11.0	78.6
	: <80	3.0	21.4
Pathology	: Adenocarcinoma	12.0	71.4
	: Signet ring cell	2.0	28.6
Chemotherapy	: Capecitabine	10.0	71.4
	: FOLFOX	4.0	28.6
Response after chemoradiation	: Partial response	4.0	28.6
	: Stable disease	7.0	50.0
	: Progressive disease	3.0	21.4

ALDH1A1 and tumor shrinkage

Mean of ALDH1A1 level was 9.014 pg/mL. The mean of the longest tumor diameter before chemoradiation was 4.42 cm and after chemoradiation was 4.09 cm. The mean of tumor shrinkage percentage was 7.89%. There was a significantly strong negative correlation (r = –0.890, p < 0.001) (*Figure 1*) with higher ALDH1A1 indicating a decreased tumor shrinkage response (*Tables 2 and 3*).

Table 2 ALDH1A1 results and tumor size and shrinkage after chemoradiation

	Mean
ALDH1A1	9.014 ± 3.3 pg/mL
Tumor largest diameter before chemoradiation	4.42 ± 1.33 cm
Tumor largest diameter after chemoradiation	4.09 ± 1.99 cm
Tumor shrinkage percentage	7.89 ± 35.7 %

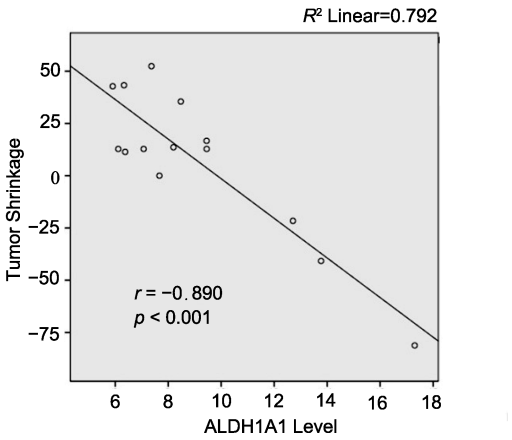

Figure 1 ALDH1A1 level has a significantly strong negative correlation with tumor shrinkage after chemoradiation. r = –0.890 and p < 0.001

Table 3 Tumor shrinkage and ALDH1A1 level in tumor tissue

No	Tumor diameter (cm)		% Shrinkage	RECIST	ALDH1A1 (pg/mL)
	Before chemoradiation	After chemoradiation			
1	7.0	4.0	42.8	PR	5,906
2	4.4	3.8	13.6	SD	8,198
3	3.0	1.7	43.3	PR	6,332
4	4.2	2.0	52.4	PR	7,368
5	2.9	2.9	0.0	SD	7,668
6	3.9	3.4	12.8	SD	7,074
7	4.8	8.7	–81.2	PD	17,306
8	4.9	6.9	–40.8	PD	13,770
9	7.0	6.1	12.8	SD	6,115
10	3.7	4.5	–21.6	PD	12,708
11	3.5	3.1	11.4	SD	6,376
12	3.9	3.4	12.8	SD	9,453
13	5.6	4.7	16.7	SD	9,450
14	3.1	2.0	35.5	PR	8,477

Abbreviations: PR = Partial response; SD = Stable disease; PD = Progressive disease

doi: 10.18282/amor.v1.i2.15

Discussion

This is a quantitative study using ELISA to determine ALDH1A1 level from FFPE rectal cancer tissues. Previous ALDH1 studies on rectal cancer mostly used a semi-quantitative method such as immunohistochemistry. The tumor shrinkage was evaluated using RECIST v1.1, which is widely used as a tool to evaluate solid tumor response. The pathological response was unable to be assessed due to low number of operation after chemoradiation.

ALDH1A1 has been proposed in association with worse prognosis and response to chemotherapy[12]. The expression of ALDH1A1 in normal crypts and colorectal carcinoma tissues has been previously investigated. Researchers have indicated that cells with ALDH1A1 expression were sparse and limited to the bottom of the normal crypts, where the stem cells or the proliferative cells reside[14]. ALDH1A1 is also known for its capability to differentiate stem cell cancer and non-stem cell cancer[15].

Xu et al.[16] stated the different results with heterogeneous pattern of ALDH1A1 staining between rectal cancer cell and adjacent stromal cell. 32.3% of the samples showed a high expression in cancer cell and low expression in adjacent stromal cell. 48.8% of the samples showed a high expression of ALDH1A1 in adjacent stromal cell. Only 16% showed no difference from cancer cell and adjacent stromal[16].

Our present study measured the quantitative level of ALDH1A1 from rectal cancer biopsy tissue that contains both cancer cell and adjacent stromal tissue. It was also shown that there was a strong negative and significant correlation between ALDH1A1 level in FFPE rectal cancer tissue with tumor shrinkage after chemoradiation.

Chemoradiation response is lower (28.6%) compared to the previous study by Lim et al. (40.8%)[17], which may be due to a fewer number of samples in this study. There is a prospect of using ALDH1A1 as a tool to select more suitable locally advanced rectal patients who will undergo preoperative chemoradiation to avoid unnecessary morbidity. A further study with larger sample size is needed to validate it.

Conclusion

ALDH1A1 level in locally advanced rectal cancer tissue is associated with decreased tumor shrinkage response after preoperative chemoradiation.

Conflict of interest

The authors declared no potential conflict of interest with respect to the research, authorship, and/or publication of this article.

References

1. Ferlay J, Soerjomataram I, Ervik M, et al. GLOBOCAN 2012 v1.0, Cancer Incidence and Mortality Worldwide: IARC Cancer Base. No. 11 [Internet]. Lyon, France: International Agency for Research on Cancer. 2013. Available from: http://globocan.iarc.f.
2. Barrera G. Oxidative stress and lipid peroxidation products in cancer progression and therapy. ISRN Oncol 2012; 2012: 137289.
3. Vasiliou V, Nebert DW. Analysis and update of the human aldehyde dehydrogenase (ALDH) gene family. Hum Genomics 2005; 2(2): 138–143.
4. Lindahl R. Aldehyde dehydrogenases and their role in carcinogenesis. Crit Rev Biochem Mol Bio 1992; 27(4-5): 283–335.
5. Ginestier C, Hur MH, Charafe-Jauffret E, et al. ALDH1 is a marker of normal and malignant human mammary stem cells and a predictor of poor clinical outcome. Cell Stem Cell 2007; 1(5): 555–567.
6. Marcato P, Dean CA, Giacomantonio CA, et al. Aldehyde dehydrogenase: its role as a cancer stem cell marker comes down to the specific isoform. Cell Cycle 2011; 10(9): 1378–1384.
7. Prasmickaite L, Engesæter BØ, Skrbo N, et al. Aldehyde dehydrogenase (ALDH) activity does not select for cells with enhanced aggressive properties in malignant melanoma. PLoS One 2010; 5(5): e10731.
8. Avoranta ST, Korkeila EA, Ristamaki RH, et al. ALDH1 expression indicates chemotherapy resistance and poor outcome in node-negative rectal cancer. Hum Pathol 2013; 44(6): 966–974.
9. Oh PS, Patel VB, Sanders MA, et al. Schlafen-3 decreases cancer stem cell marker expression and autocrine/juxtacrine signaling in FOLFOX-resistant colon cancer cells. Am J Physiol Gastrointest Liver Physiol 2011; 301(2): G347–G355.
10. Vogler T, Kriegl L, Horst D, et al. The expression pattern of aldehyde dehydrogenase 1 (ALDH1) is an independent prognostic marker for low survival in colorectal tumors. Exp Mol Pathol 2012; 92(1):111–117.
11. Ishii H, Iwatsuki M, Ieta K, et al. Cancer stem cells and

doi: 10.18282/amor.v1.i2.15

chemoradiation resistance. Cancer Sci 2008; 99(10): 1871–1877.
12. Kahlert C, Gaitzsch E, Steinert G, et al. Expression analysis of aldehyde dehydrogenase 1A1 (ALDH1A1) in colon and rectal cancer in association with prognosis and response to chemotherapy. Ann Surg Oncol 2012; 19(13): 4193–4201.
13. Eisenhauer EA, Therasse P, Bogaerts J, et al. New response evaluation criteria in solid tumours: Revised RECIST guideline (version 1.1). Eur J Cancer 2009; 45(2): 228–247.
14. Hessman CJ, Bubbers EJ, Billingsley KG, et al. Loss of expression of the cancer stem cell marker aldehyde dehydrogenase 1 correlates with advanced-stage colorectal cancer. Am J Surg 2012; 203(5): 649–653.
15. Balicki D. Moving forward in human mammary stem cell biology and breast cancer prognostication using ALDH1. Cell Stem Cell 2007; 1(5): 485–487.
16. Xu SL, Zeng DZ, Dong WG. Distinct patterns of ALDH1A1 expression predict metastasis and poor outcome of colorectal carcinoma. Int J Clin Exp Pathol 2014; 7(6): 2976–2986.
17. Lim JS, Kim D, Baek SE, et al. Perfusion MRI for the prediction of treatment response after preoperative chemoradiotherapy in locally advanced rectal cancer. Eur Radiol 2012; 22(8): 1693–1700.

doi: 10.18282/amor.v1.i2.15

Advances in Modern Oncology Research

doi: 10.18282/amor.v1.i2.5

ORIGINAL RESEARCH ARTICLE

Administration of anti-neoplastic agents to treat malignancies in solid organ transplant recipients

Omar Al Ustwani[1], Neha Gupta[2], Adrienne Groman[1], Hongbin Chen[1*]

[1]Roswell Park Cancer Institute, Elm & Carlton Streets, Buffalo, New York, United States
[2]State University of New York at Buffalo, Buffalo, New York, United States

***Abstract*:** The management of advanced malignancies in solid organ transplant (SOT) recipients is not well-structured as the patients need immunosuppressive agents to avoid graft rejection. Simultaneous administration of chemotherapy and immunosuppressive agents may increase treatment toxicities. The data of SOT recipients treated at Roswell Park Cancer Institute (RPCI) were reviewed for different malignancies to assess their treatment patterns, tolerance and outcomes. Chart review of 40 SOT patients seen at RPCI (2000–2012) for cancer management was conducted. The median age was 61.5 years and 50% were males. The median lag time between SOT and cancer diagnosis was 8.4 years. It was found that 46% of solid tumors were metastatic at diagnosis, 78% received chemotherapy and 22% had hormonal therapy alone. In the chemotherapy group, the patients received an average of 1.8 lines of therapy, where 13% were given definitive chemotherapy and radiotherapy while 26% received chemotherapy in the neoadjuvant/adjuvant setting. Treatment delays were necessary in 32%, and dose omission or reduction in 42%. The most common hematologic adverse events (AEs) were anemia (78%) and thrombocytopenia (59%). Febrile neutropenia occurred in 12.5%. The most common non-hematologic AEs were fatigue (55%) and hepatic dysfunction (45%). The most common grade 3/4 hematologic AEs were neutropenia (33%) and leukopenia (27%) while non-hematologic grade 3/4 AEs was fatigue (12.5%). At the time of analysis, 26% patients were still alive. The median overall survival period of the patients was 28.5 months. In conclusion, SOT patients can tolerate chemotherapy; however AEs, dose reductions and delays occur. Thus, the treating physicians should be cautious on dosing chemotherapy in these cases.

***Keywords*:** anti-neoplastic agents; malignancies; solid organ transplant

***Citation*:** Al Ustwani O, Gupta N, Groman A, et al. Administration of anti-neoplastic agents to treat malignancies in solid organ transplant recipients. Adv Mod Oncol Res 2015; 1(2): 117–121; http://dx.doi.org/10.18282/amor.v1.i2.5.

*Correspondence to: Hongbin Chen, Roswell Park Cancer Institute, Elm & Carlton Streets, Buffalo, New York 14263, United States, hongbin.chen@roswellpark.org.

Received: 20th July 2015; **Accepted:** 30th October 2015; **Published Online:** 2nd December 2015

About 28,000 patients receive solid organ transplantation each year in the United States alone[1]. These patients continue to have improved survival with the advancement of medical care and immunosuppression regimens. However, transplant recipients are noted to have increased the risk of developing malignancies in comparison with general population[2]. This observation is believed to be related in part to the state of immunosuppression, viral infections or, rarely, donor-transmitted cancers[3]. The noted malignancies vary in nature and stages but tend to be more aggressive, leading to poor outcomes[4]. However, the management of advanced malignancies in this patient population is not well-structured. Treatment of these cancers may require administration of chemotherapy or other anti-neoplastic agents that could lead to toxicities such as profound bone marrow suppression or end organ damage. As this field is limited and only few published data are available, the

current paper describes our experience in our institute in the use of chemotherapy and hormonal therapy to treat malignancies developed in solid organ transplant (SOT) recipients.

Materials and methods

Patients

This study is a retrospective chart review to capture the treatment pattern, safety and outcomes in patients who developed post-SOT malignancies. After the approval by the Institutional Review Board, 129 patients were identified for diagnosis of both malignancy and SOT seen between 2000 and 2012 at Roswell Park Cancer Institute (RPCI). Patients who had post-transplant lymphoproliferative disorder (PTLD) or non-metastatic non-melanoma skin cancer, or who did not receive chemotherapy, were excluded. History of previous malignancy was not an exclusion criterion in this study. A total of 40 patients were eligible for the final chart review and were included in the analysis. Patients' demographic and clinical characteristics, including history of SOT, cancer diagnosis, stage, treatments received, and adverse events (AEs) were extracted from the charts. The treatment-related AEs were graded according to the Common Terminology Criteria for Adverse Events (CTCAE), version 4.0[5]. Survival data were obtained from patients' electronic medical charts and tumor registry.

Statistical analysis

Patients' demographic and clinical characteristics, such as history of SOT, cancer diagnosis and stage were summarized. Treatment-related information including immunosuppressive therapy and chemotherapy tolerance were recorded. Common hematologic and non-hematologic treatment-related AEs were presented. Overall survival (OS) was defined as the time interval from the diagnosis of cancer to the date of last visit or death, whichever occurred first. Univariate Cox Proportional Hazard model analysis was performed to assess the effect of different variables of interest on OS. Kaplan-Meier curve and log-rank analysis methods were used to compare OS based on disease stage, the number of chemotherapeutic agents given and the type of SOT. All the analyses used statistical software SAS version 9.3 (SAS Institute, Cary, North Carolina).

Results

Among the 40 patients with a history of SOT, the two most common types of transplanted organs were kidney and liver (42.5% each, as shown in *Table 1*). On average, it took about 8.4 years to develop malignancies after SOT, with gastrointestinal (30%) and lung (15%) cancers as the most common post-SOT malignancies. According to the tumour-node-metastases (TNM) staging system, almost half of the patients presented stage IV cancer at diagnosis. Apart from the well-established PTLD, other hematologic malignancies such as multiple myeloma (1 patient) and acute myeloid leukemia (AML) (3 patients) were also noticed. Two-thirds of these patients were found to have a family history of one or more malignancy in a first-degree relative.

At the time of diagnosis of cancer, 92.5% of the patients still continued on immunosuppressive post-transplant therapy (namely azathioprine, mycophenolic acid, tacrolimus, sirolimus, and cyclosporine), but only 7.5%

Table 1 Patients characteristics (N = 40)

Type of cancer (N)	Gender (male) (%)	Initial age at cancer (mean/median/standard deviation, years)	Type of transplant				Stage IV at diagnosis (%)	Family history of cancer (%)	Lag time to cancer diagnosis (mean/median/standard deviation, years)
			Renal (%)	Liver (%)	Lung (%)	Heart (%)			
Gastrointestinal (12)	83.3	57.7/57/11.9	25.0	75.0	0.0	0.0	66.7	58.3	5.8/2.5/10.7
Lung (6)	50.0	64.3/65.5/9.5	50.0[a]	33.3	0.0	16.7	33.3	60.0	9/8.5/3.7
Breast (9)	0.0	62.9/66/11.8	44.4	33.3	0.0	22.2	11.1	100.0	7.3/8/4.1
Hematologic (4)	75.0	64.5/64/4.2	75.0	0.0	0.0	25.0	N/A[b]	50.0	14.8/12/13.2
Head/Neck (3)	33.3	62/62/3	0.0	66.7	33.3	0.0	100[c]	100.0	3.7/3/2.1
Gynaecological (2)	0.0	40/40/19.8	50.0	0.0	50.0	0.0	0.0	50.0	23/23/15.6
Genitourinary (2)	50.0	78/78/1.4	100.0	0.0	0.0	0.0	50.0	50.0	9.5/9.5/12
Metastatic Skin (2)	100.0	70/70/4.2	50.0	50.0	0.0	0.0	100.0	0.0	6.3/6.3/6.7
Overall (40)	50.0	61.5/63/11.9	42.5	42.5	5.0	10.0	45.9	67.6	8.4/6/9

[a]One lung cancer patient had renal and liver transplant
[b]Hematologic malignancies (4) consist of 3 acute myeloid leukemia and one multiple myeloma patients therefore stage is not applicable
[c]Stage IV head & neck cancer also consists of stage IV-a per tumour-node-metastases staging (locally advanced or N3 disease)

doi: 10.18282/amor.v1.i2.5

of the patients were on corticosteroids. Patients received various anti-neoplastic agents to treat their cancers including standard systemic chemotherapy (78%), hormonal therapy (22%) and targeted agents. In the chemotherapy group, patients received an average of 1.8 lines of therapy where 13% of the patients were given definitive chemotherapy and radiotherapy while 26% received chemotherapy in the neoadjuvant/adjuvant setting. Treatment delays were necessary in 32%, and dose omission or reduction in 42%. Over one-third of the patients were able to receive more than one line of chemotherapy after progression of the cancer (ranging between 1–6 lines). Details of immunosuppressive therapy monitoring and dosing changes were not available for our review of most patients as they were mostly managed by transplant specialists in the community. The most common treatment-related hematologic AE was anemia (78% of patients) and non-hematologic AE was fatigue (55% of patients, as shown in *Table 2*). Neutropenia (33%) and fatigue (12.5%) were the most commonly observed grade 3/4 AEs. The neutropenic fever occurred in 12.5% of patients in addition to renal (30%) and hepatic (45%) dysfunctions.

At the time of analysis, 26% patients were still alive.

Table 2 Treatment-related adverse events (AEs)

AE	All grades, *N* (%)	Grade 3–4, *N* (%)
Hematologic (*N* = 37)[a]		
Anemia	29 (78)	5 (14)
Thrombocytopenia	22 (59)	4 (11)
Leukopenia	19 (51)	10 (27)
Neutropenia	16 (43)	12 (33)
Neutropenic fever	5 (12.5)	5 (12.5)
Non-hematologic (*N* = 40)		
Fatigue	22 (55)	5 (12.5)
Nausea	16 (40)	2 (5)
Diarrhea	14(35)	4(10)
Alkaline phosphatase	14 (35)	2 (5)
Aspartate aminotransferase	13 (32.5)	0
Renal (Cr)	12 (30)	1 (2.5)
Vomiting	11(27.5)	1(2.5)
Neuropathy	11(27.5)	2 (5)
Mucositis	8 (20)	1 (2.5)
Rash	8 (20)	0
Alanine aminotransferase	5 (12.5)	1 (2.5)
Bilirubin	4 (10)	0

[a]Hematologic AEs of treatments for acute myeloid leukemia are not registered as they represent a direct drug effect on the affected bone marrow

The median OS was 28.5 months. In order to assess the correlation between selected covariates of demographic and clinical characteristics and OS, univariate analysis was conducted (*Table 3*). Only male patients and advanced stage at diagnosis were shown to have statistically significant correlation with worse OS. The difference in OS was estimated by Kaplan-Meier curves and log-rank test (*Figure 1*), where median survival was only 7.3 months (95% confidence interval (CI95%): 5.0–24.1) in patients with stage IV cancer at diagnosis in comparison with 91.8 months (CI95%: 45.6–not reached) in patients with stages I, II or III after a median follow-up of 47.5 months (range 3–100.4) for all patients. Four

Table 3 Univariate analysis describing the association between different covariates of interest and overall survival using Cox Proportional Hazards model

Covariate	Hazard ratio estimates (95% Confidence interval)	*p* value	Sample size[a]
Age	1.02 (0.97–1.06)	0.486	38
Positive family history	1.61 (0.59–4.37)	0.354	35
More than one line of chemotherapy	1.12 (0.43–2.91)	0.810	30
More than one immune-suppressive therapy	0.78 (0.30–2.06)	0.619	38
Gender (female)	0.24 (0.10–0.61)	0.0003	38
Advanced stage of disease at diagnosis	6.29 (2.21–17.89)	<0.001	35
Type of solid organ transplant	0.55 (0.23–1.36)	0.197	38

[a]Sample sizes vary due to missing covariate data in some cases

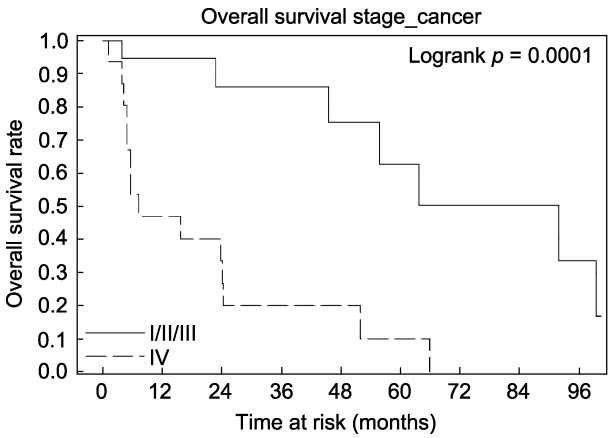

Figure 1 Unadjusted Kaplan Meier estimates of difference in overall survival between patients with stage IV and early stage cancer. Patients with stage IV cancer (*N* = 16) at diagnosis (dashed line), and patients with stage I, II and III cancer (*N* = 19) at diagnosis (solid line). Sample size: *N* = 35 due to missing or inapplicable data

doi: 10.18282/amor.v1.i2.5

patients with hematological malignancies (acute myeloid leukemia and multiple myeloma) were excluded from this analysis. OS did not differ in renal transplant patients when compared with other types of solid organ transplant, or between patients who received one line of chemotherapy compared with those who received more than one line of therapy (data not shown).

Discussion

In the present manuscript, we described the experience of a single institute in treating malignancies that developed in patients with a history of SOT. The increased risk of primary malignancies in patients post-SOT on chronic immunosuppression has been well-documented since 1988[6]. The most common cancers developed in these cases are skin cancer, head and neck cancer, Kaposi sarcoma, gynecologic malignancies and lymphoproliferative disorders[6,7]. We did not find any Kaposi sarcoma patients who received treatment at our institute which may be due to the pattern of referral. Furthermore, we excluded PTLD patients from our study as its biology and treatments are better understood than the disease entities selected in our study. The incidence of malignancies in the post-SOT setting could not be estimated from our study as our patients were identified from a pool of cancer patients rather than transplant patients. Many reports have estimated the incidence to range between 2.6% and 26%[8,9].

Cancer can develop as early as 22 months into post-SOT but may also take up to 10 years to be detected[7]. The mean number of years between date of transplantation and developing cancer was 8.4 years in our study, which is consistent with the published data. While the current literature on post-SOT malignancies mainly focuses on renal transplant patients, our study reviewed a collection of various transplantations including renal, liver and a few lung and heart transplant patients. Our study did not show a difference in OS between renal and non-renal transplant patients with a median survival of 24.2 months among all the patients. A previous study that assessed lung cancer alone in a group of various organ transplantation patients (N = 24) reported a median OS of 1.5 years[10]. Although the number of lung cancer patients (N = 6) in our study is small, the median OS is slightly better (2.1 years) with similar stage distribution (about a third of patients diagnosed with stage IV at diagnosis). We also observed 6 patients with recurrence of malignancies post-SOT in the setting where transplant was indicated for organ dysfunction after resection performed for the same malignancy. One renal transplant patient had recurrence of clear cell renal carcinoma (transplant was indicated for renal failure post-nephrectomy for the same tumor) and 5 liver transplant patients developed recurrence for cholangiocarcinoma or hepatocellular carcinoma (for which the transplant was originally indicated). None of the patients with lung cancer had prior double lung transplant in this study.

Immunosuppression inhibits host defense and surveillance that could play a role in allowing growth of microscopic malignant cells[11]. In addition, some immunosuppressive agents such as azathioprine and cyclosporine have been suggested to promote carcinogenesis[12,13]. However, no effect was noted on OS with additive multiple immunosuppressive agents in our patients. Dose reduction of immunosuppressive agents is common when cancer is diagnosed, but it needs to be balanced with the preservation of graft function[14]. Switching immunosuppression to sirolimus was observed to cause regression of Kaposi sarcoma and PTLD, but no effect evident on solid organ cancers[15]. Thus, the lack of benefit in switching from immunosuppression to sirolimus in post-SOT cancers discouraged it to be attempted in our patient population. Similar to the findings in general cancer population, OS correlated closely with the stage of disease. For solid tumors in our series, stage IV at diagnosis was associated with shorter OS. Although it is not obvious in our patient population, malignancies in the post-transplant setting are associated with poorer survival when compared stage by stage in The Surveillance, Epidemiology, and End Results (SEER) database[14]. The hematologic malignancies observed in our review consisted of one patient with multiple myeloma (alive for 5 years since diagnosis with Durie-Salmon stage III) and three patients with acute myelogenous leukemia (AML) (with extremely short survival as all died at 2, 4 and 6 months, respectively).

Treatments of post-SOT malignancies may require chemotherapy, hormonal therapy or biologic agents similar to cancer patients without the history of SOT. In the past, case reports have described experiences with treatment of non-small cell lung cancer in post-SOT patients, the difficulties associated with administering chemotherapy (cisplatin and vinblastine in one patient and carboplatin and paclitaxel in another patient), and complications including diarrhea, neutropenic fever and sepsis[16,17]. In a previous study which involved 5 children who had liver or heart transplantation for primary malignancies, the children received various chemotherapy agents (adriamycin, cyclophosphamide, ifosfamide, etc.) in the adjuvant setting, and dose modifications due to neutropenia were required in 60% of the courses given in all patients. No sepsis or renal toxicity were reported in that study[18]. Capecitabine has been reported to be well-tolerated in

doi: 10.18282/amor.v1.i2.5

rectal cancer in two patients[19]. Cisplatin was previously used in treating invasive bladder cancer in the adjuvant setting in a small series of SOT patients but without reporting the incidence of AEs[20]. Despite the limitation of the data to anecdotal case reports, it is clear from our data, which is the largest cohort on this topic reported so far, that chemotherapy is tolerable but precaution to AEs is advised. It is noteworthy that none of our patients who received hormonal therapy (for example, androgen deprivation therapy for prostate cancer or tamoxifen for breast cancer) had any documented AEs.

In conclusion, the study provides insight into patterns and safety of cancer-directed treatments in a subset of patients with delicate organ function. Although the present study is a retrospective study accounting for a small number of patients, it shows promising results of feasible yet cautious administration of chemotherapy and hormonal therapy in SOT recipients with relatively good tolerance. Prospective studies are warranted to confirm these findings and further detail the impact and adjustment of immunosuppressive agents during the systemic treatment for post-SOT malignancies.

Acknowledgments

This work was supported by Roswell Park Cancer Institute and National Cancer Institute (NCI) grant #P30 CA016056.

Declaration

The study was presented in part as a poster in the 2013 Annual Meeting of the American Society of Clinical Oncology, Chicago, IL, USA, 2013.

Conflict of interest

The authors declared no potential conflict of interest with respect to the research, authorship, and/or publication of this article.

References

1. United Network for Organ Sharing 2007 Annual Report of the U.S. Organ Procurement and Transplantation Network and the Scientific Registry of Transplant Recipients: Transplant Data 1997–2006. Health Resources and Services Administration, Healthcare Systems Bureau, Rockville MD, Division of Transplantation.
2. Kasiske BL, Snyder JJ, Gilbertson DT, et al. Cancer after kidney transplantation in the United States. Am J Transplant 2004; 4: 905–913.
3. Chen H, Shah AS, Girgis RE, et al. Transmission of glioblastoma multiforme after bilateral lung transplantation. J Clin Oncol 2008; 26: 3284–3285.
4. Watt KD, Pedersen RA, Kremers WK, et al. Long-term probability of and mortality from *de novo* malignancy after liver transplantation. Gastroenterology 2009; 137: 2010–2017.
5. U.S. Department of Health and Human Services, National Institutes of Health, National Cancer Institute. Common Terminology Criteria for Adverse Events (CTCAE) Version 4.0. Published: May 28, 2009 (v4.03: June 14, 2010).
6. Penn I. Secondary neoplasms as a consequence of transplantation and cancer therapy. Cancer Detect Prev 1988; 12: 39–57.
7. Penn I. Incidence and treatment of neoplasia after transplantation. J Heart Lung Transplant 1993; 12: S328–336.
8. Saigal S, Norris S, Muiesan P, et al. Evidence of differential risk for posttransplantation malignancy based on pretransplantation cause in patients undergoing liver transplantation. Liver Transpl 2002; 8: 482–487.
9. Herrero JI, Lorenzo M, Quiroga J, et al. *De novo* neoplasia after liver transplantation: an analysis of risk factors and influence on survival. Liver Transpl 2005; 11: 89–97.
10. Genebes C, Brouchet L, Kamar N, et al. Characteristics of thoracic malignancies that occur after solid-organ transplantation. J Thorac Oncol 2010; 5: 1789–1795.
11. Fung JJ, Jain A, Kwak EJ, et al. *De novo* malignancies after liver transplantation: a major cause of late death. Liver Transpl 2001; 7: S109–118.
12. Guba M, Graeb C, Jauch KW, et al. Pro- and anti-cancer effects of immunosuppressive agents used in organ transplantation. Transplantation 2004; 77: 1777–1782.
13. Hojo M, Morimoto T, Maluccio M, et al. Cyclosporine induces cancer progression by a cell-autonomous mechanism. Nature 1999; 397: 530–534.
14. Buell JF, Gross TG, Woodle ES. Malignancy after transplantation. Transplantation 2005; 80: S254–264.
15. Boratynska M, Watorek E, Smolska D, et al. Anticancer effect of sirolimus in renal allograft recipients with *de novo* malignancies. Transplant Proc 2007; 39: 2736–2739.
16. Stagner LD, Allenspach LL, Hogan KK, et al. Bronchogenic carcinoma in lung transplant recipients. J Heart Lung Transplant 2001; 20: 908–911.
17. De Pas T, Spitaleri G, Pelosi G, et al. Erlotinib combined with cyclosporine in a liver-transplant recipient with epidermal growth factor receptor-mutated non-small cell lung cancer. J Thorac Oncol 2009; 4: 138–139.
18. Horn M, Phebus C, Blatt J. Cancer chemotherapy after solid organ transplantation. Cancer 1990; 66: 1468–1471.
19. Liu HY, Liang XB, Li YP, et al. Treatment of advanced rectal cancer after renal transplantation. World J Gastroenterol 2011; 17: 2058–2060.
20. Tomaszewski JJ, Larson JA, Smaldone MC, et al. Management of bladder cancer following solid organ transplantation. Adv Urol 2011; 2011: 256985.

doi: 10.18282/amor.v1.i2.5

Advances in Modern Oncology Research

doi: 10.18282/amor.v1.i2.35

ORIGINAL RESEARCH ARTICLE

The effect of hydroxybenzoate calcium compounds in inducing cell death in epithelial breast cancer cells

Nada M Merghani[1], Amal Al Hazzaa[2], Eamon JG Mahdi[3], Abigail J Manning[4], Andea GS Buggins[5], Chris Pepper[6], Jassem G Mahdi[6*]

[1]Central Lab and Prince Naif for Health Research Centre, King Saud University, Riyadh, Saudi Arabia
[2]College of Science, King Saud University, Riyadh, Saudi Arabia
[3]Cardiff School of Medicine, Cochrane Medical Education Centre, Heath Park, Cardiff, UK
[4]Cardiff School of Pharmacy, Cardiff University, Cardiff, UK
[5]King's College London, Department of Haematological Medicine, London, UK
[6]Institute of Cancer and Genetics, School of Medicine, Cardiff University, Cardiff, UK

***Abstract*:** Hydroxybenzoate (HB) compounds have shown their significance in inducing apoptosis in primary chronic lymphocytic leukemia (CLL) and cancer cell lines, including HT-1080. The current study focuses on assessing the effects of 2-, 3- and 4-hydroxybenzoate calcium (HBCa) compounds on MCF-10A, MDA-MB231 and MCF-7 epithelial breast cell lines. The HBCa-treated cells were examined using annexin V, to measure apoptosis in the three epithelial breast cell lines, after 48 h of treatment. The results indicated that 0.5 and 2.5 mmol/L of HBCa induced cell death in a dose-dependent manner. The induction of cell death in normal MCF-10A cells was found to be significantly less (p = 0.0003–0.0068), in comparison to the malignant cell lines (MDA-MB231 and MCF-7). HBCa compounds were also found to cause cell cycle arrest in the epithelial breast cells at G1/G0. Furthermore, HBCa compounds induced the upregulation of apoptotic proteins (p53, p21, Bax and caspase-3), as well as the downregulation of the anti-apoptotic protein Bcl-2, which may suggest that apoptosis is induced via the intrinsic pathway.

***Keywords*:** hydroxybenzoate calcium; cell death; breast cancer cells

***Citation*:** Merghani NM, Hazzaa AA, Mahdi EJG, et al. The effect of hydroxybenzoate calcium compounds in inducing cell death in epithelial breast cancer cells. Adv Mod Oncol Res 2015; 1(2); 122–131; http://dx.doi.org/10.18282/amor.v1.i2.35.

*Correspondence to: Jassem G. Mahdi, Institute of Cancer and Genetics, School of Medicine, Cardiff University, Cardiff, UK, jmahdi@su.edu.sa.

Received: 4th September 2015; **Accepted:** 15th September 2015; **Published Online:** 2nd December 2015

Breast cancer is a major global health issue that mainly affects women of all age groups. It is the most common cancer worldwide, with more cases in developing countries than in developed countries[1]. Breast cancer is the second leading cause of cancer death after lung cancer in developed countries (198,000 cases, 15.4%). Incidence rates continue to increase globally except in a few high-income countries. The estimated breast cancer incidents of less developed cases in 2012 were 883,000 (52.8%) and 788,000 more developed cancer cases, with mortality rates of 324,000 (62.1%) and 198,000 (37.9%), respectively[2]. In contrast, more than 60% of breast cancer patients survive in developed countries. Lower survival rates occur in developing countries due to the lack of early detection schemes and diagnosis[3]. Statistics related to breast cancer cases have attracted the attention of various researchers to effectively treat the cancer with chemotherapy.

As part of this effort, a large number of compounds have been assessed for their anticancer potential in dif-

ferent cancer cells[4-7]. The assessed compounds include hydroxybenzoate (HB), 2-acetylbenzoic acid (2-ABA) or aspirin, and its precursor 2-hydroxybenzoic acid (2-HBA). These compounds showed apoptotic effects at high doses (1–10 mmol/L), which highlight concern regarding their side effects[8,9]. Our previous studies have shown the induction of apoptosis at lower doses in different cancer cell lines and primary chronic lymphocytic leukaemia (CLL)[4,10–12]. For instance, the morphological and immunological evidence for apoptosis were obtained when 4-hydroxybenzoate zinc (HBZn) or 4-hydroxybenzoate calcium (HBCa) compounds were evaluated[11–13]. The mechanism of these compounds is to induce apoptosis via the intrinsic pathway involving the upregulation of the expression of p53, Bax and caspase-9[4,10,12]. In parallel, these compounds downregulated Bcl-2, an anti-apoptotic protein that is able to suppress cytochrome c release and subsequently caspase-3. The regulation of apoptosis-related proteins in the intrinsic pathway is an important indicator for assessing anticancer compounds' activities. Similar results were obtained in MCF-7 and MDA-MB231 human breast cancer cells when tamoxifen was used[14].

Hydroxybenzoic acid (HBA) and its metal-bearing analogs are simple compounds with different chemical properties. For example, 2-HBA has a higher acidic content when compared to 3-HBA and 4-HBA. 4HBZn is more potent while 4-HBA is less acidic than the corresponding 2-HBZn and 3-HBZn compounds[12]. The current research examines the cytotoxic effects of three types of HBCa compounds; 2-HBCa, 3-HBCa and 4-HBCa in two epithelial breast cancer cells, MDA-MB231 and MCF-7, and the normal breast cell line MCF-10A, as shown in *Figure 1*.

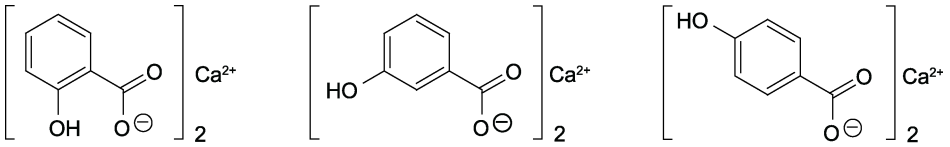

2-HBCa 3-HBCa 4-HBCa

Figure 1 Chemical structures of the three HBCa complexes

Materials and methods

Cell lines: The mammary epithelial cell lines of both normal (MCF-10A) and cancer (MCF-7 and MDA-MB-231) were obtained from the American Type Culture Collection (ATCC), USA.

Chemicals: 2-, 3-, and 4-HBCa were prepared from 2-, 3- and 4-HBA (Sigma-Aldrich, UK) and calcium carbonate (Sigma-Aldrich, UK), respectively through acid-base reaction.

Cell culture

MCF-10A, MDA-MB-231 and MCF-7 cells (ATCC, USA) were cultured in a RPMI-1640 medium. It contained GlutaMAX, 25 mmol/L HEPES buffer (Sigma-Aldrich, UK), 10% fetal bovine serum (FBS) (Sigma-Aldrich, UK) and 1% penicillin (10,000 U/mL; Sigma-Aldrich, UK). For MCF-10A cells, the universal medium (1:1 mixture of Dulbecco's modified Eagle's medium (DMEM) and Ham's F12 medium (Sigma-Aldrich, UK) were used. This medium was supplemented with 10% FBS, 1% antibiotic-antimitotic, 20 ng/mL epidermal growth factor (EGF), 100 ng/mL cholera toxin, 10 µg/mL insulin and 500 ng/mL hydrocortisone. Then, the cells were cultured at 37°C in a humidified atmosphere containing 5% CO_2.

Detection of cell viability by MTT cell proliferation assay

Breast cells were seeded in a 96-well plate at a density of 2×10^5 cell/well in 90 µL optimized medium. The cells were allowed to settle for 24 h before treated with individual dose of HBCa, i.e., 0, 0.1, 0.3, 0.5, 1.0, 2.0 and 5.0 mmol/L. The treated cells were allowed to grow for 48 h. At the end of the incubation period and dose point, 110 µL of 0.22 µm filter-sterilized, 5 mg/mL 3-(4,5-dimethyl thiazol-2-yl)-2,5-diphenyltetrazolium bromide (MTT) (Sigma-Aldrich, UK) was added at a temperature of 37°C. The 96-well plate was kept in the dark for 2 h before the medium containing MTT was removed. 100 µL dimethyl sulphoxide (DMSO) obtained from Ajax Finechem Pty Ltd, Australia, was added to dissolve the formasane crystals. The 96-well plates were shaken for 15 min in the dark to dissolve the formasane crystals. The optical density (OD) of each treatment was measured at 570 nm using LabSystems Multiskan EX Version 3.0 (Thermo

doi: 10.18282/amor.v1.i2.35

Labsystems, Helsinki, Finland). Each experiment was performed in four replicates. The optical densities were normalized according to the control.

Detection of apoptosis by flow cytometry

Vybrant® Apoptosis Assay Kit #2 (Molecular Probes™, Invitrogen™ Life Technologies, USA) was used to detect apoptosis in HBCa-treated breast cells. Breast cells (5×10^5 cell/mL) were cultured to approximately 70% confluence in T-100 tissue culture flasks under optimized media and standard culture conditions. The medium was replaced with medium containing 0.0, 0.5 or 2.5 mmol/L individual HBCa and allowed to culture for 48 h. The cells were then trypsinized, centrifuged and washed in phosphate-buffered saline (PBS). The cells (1×10^6 cells/mL) were suspended in 1 × annexin V binding buffer (10 mmol/L Hepes adjusted to pH 7.4, 140 mmol/L NaCl and 2.5 mmol/L $CaCl_2$). Then, 5 µL of Alexa Fluor® 488 Annexin V and 1 µL of the 100 µg/mL propidium iodide (PI) solution were added to each 100 µL of cell suspension and incubated for 15 min at room temperature. Next, 400 µL of 1 × annexin V binding buffer was added and mixed gently followed by rapid mixing. The stained cells were then analyzed by flow cytometry. The percentage of apoptotic cells was determined using a FACSCalibur flow cytometer and Cell Quest Pro software (Becton Dickinson Biosciences, New Jersey, USA).

Assessment of cell cycle through flow cytometry

Cells (5×10^5 cell/mL) were seeded in T-100 flasks (Nunc, Denmark) in 10 mL of fresh optimal medium and allowed to grow to approximately 60%–70% confluence before the cells were subjected to serum starvation for 24 h. The cells were then cultured in optimal medium containing 0.0, 0.5 or 2.5 mmol/L of individual HBCa compounds and incubated for 48 h prior to harvesting and washing with PBS. The harvested cells were centrifuged (300 × *g* for 5 min) and resuspended in 1 mL of PBS before fixation with 3 mL cold 100% methanol. The fixed cells were then centrifuged (300 × *g* for 10 min), washed with PBS and re-centrifuged (4000 rpm for 10 min). 1 mL of hypotonic DNA staining buffer (Sigma-Aldrich, UK) containing PI at 0.01% (w/v), ribonuclease A (RNase A) at 0.002% (w/v), 0.3% (v/v) Triton X-100 and 0.1% (w/v) sodium citrate (pH 7.8) were added to the pellet. The cells were resuspended and incubated at 4°C for 30 min.

Relative DNA contents was assessed as a function of PI labeling according to the method documented by Crissman and Steinkamp[15] which using the Cell-Quest™ Pro software to acquire and analyze data obtained from the flow cytometer (Becton, Dickinson and Company, San Jose, CA, USA).

Assessment of protein expression by Western blot

Breast cells (5×10^5 cell/mL) were seeded in T-100 flask, cultured and treated with HBCa complexes (0, 0.5, 2.5 mmol/L) for 48 h, as described in the previous section. The medium was removed and the cells were washed with cold PBS to remove the medium. Subsequently, RIPA buffer (150 mmol/L sodium chloride (NaCl), 2 mmol/L ethylenediaminetetraacetic acid (EDTA), 50 mmol/L Tris-HCl, pH 7.5) and lysis buffer (1% deoxycholic acid and 1% NP-40) were added. Protease inhibitor cocktail tablets (Bio-Rad Laboratories, USA) were also added. The cell lysates were then centrifuged at 12,000 × *g* for 15 min. The supernatant was further centrifuged at 4°C at 16,000 × *g* for 5 min to obtain a clear solution of the protein mixture. The protein mixture was used to measure the expression of p53, p21, Bcl-2, Bax and caspase-3 by Western blotting using glyceraldehyde-3-phosphate dehydrogenase (GAPDH) as an internal antibody control. Total cell lysate protein doses were determined by assay dye (Bio-Rad Laboratories, USA) and absorption was measured at 595 nm. 60 µg of the extracted protein and GAPDH internal antibody control on sodium dodecyl sulfate (SDS) were loaded to 4%–12% Bis-tris acrylamide gel in 3-(N-Morpholino) propanesulfonic acid (NuPAGE MOPS) running buffer (Invitrogen™ Life Technologies, Scotland, UK). After running the gel at 75 V for 3 h at room temperature, the resolved proteins were transferred onto a nitrocellulose membrane (Sigma-Aldrich, UK). The membranes were first incubated with an appropriate primary antibody (p53, Bcl-2, Bax, or GAPDH as a loading control and internal standard), followed by peroxidase conjugated anti-mouse IgG antibody (Sigma-Aldrich, UK). The membranes were washed and developed using a chemiluminescent reagent (Amersham, UK) prior to exposure to photographic films. The protein bands' intensities were scanned and quantified using a densitometer.

Statistical analysis

Data obtained in these experiments represented an average of different replicates which were evaluated using equal variance and paired with Student's *t*-test along with other statistical analyses using GraphPad Prism 5.0 software (GraphPad Software Inc., San Diego, CA, USA).

doi: 10.18282/amor.v1.i2.35

Results

Response of breast epithelial cell lines to HBCa treatments

The response of breast cells towards various treatments was studied using MTT assay (*Figure 2*). HBCa compounds showed different effects on cell proliferation after 48 h treatment. However, different doses of HBCa demonstrated that cell proliferation decreased as the dose of HBCa increased in a dose-dependent manner (*Figure 2*). In addition, the apoptotic response of normal MCF-10A cells and cancer cells (MDA-MB231 and MCF-7) to HBCa compounds were assessed *in vitro* after 48 h using annexin V/propidium iodide assay (*Figure 3A*). A clear dose-dependent response was observed for 2-, 3- and 4-HBCa compounds to induce total cell death, particularly in MDA-MB231 and MCF-7 breast epithelial cancer cells (*Figure 3B*). HBCa-treated MCF-10A, MDA-MB231 and MCF-7 cells showed a higher level of late apoptosis and necrosis of cells (60%–84%) than early apoptosis of cells (18%–40%). The highest total cell death (17.03%) occurred when MCF-7 cells were treated with 2.5 mmol/L 2-HBCa for 48 h (*Figure 3B*). The 2.5 mmol/L HBCa treatments inhibited cell growth in other cells in a range between 9.10%–10.64%. In addition, statistical analyses indicated that HBCa-treated normal MCF-10A breast cells did not show significant differences (p = 0.1161–0.7216) compared to the control, except when treated with 2.5 mmol/L 3-HBCa (p = 0.0016). However, the treatment of MDA-MB231 breast cancer cells (p = 0.0003–0.0068) and MCF-7 (p = 0.0001–0.0005) with 0.5 or 2.5 mmol/L HBCa compounds had significantly increased total cell death compared to the control samples (*Figure 3C*). Similar results were also obtained with the treated MCF-7 cells (p = 0.001–0.01), except when cells were treated with 0.5 mmol/L 2-HBCa (p = 0.2174) as shown in *Figure 1*. The HBCa compounds increased cell death significantly in MDA-MB231 (p = 0.0001–0.0459) and MCF-7 (p = 0.0001–0.0051) cancer cells in comparison to the normal MCF-10A treated cells. MCF-10A cells were between 3 to 6 times less sensitive to the apoptotic effects of the HBCa compounds when compared with the cancer cell lines.

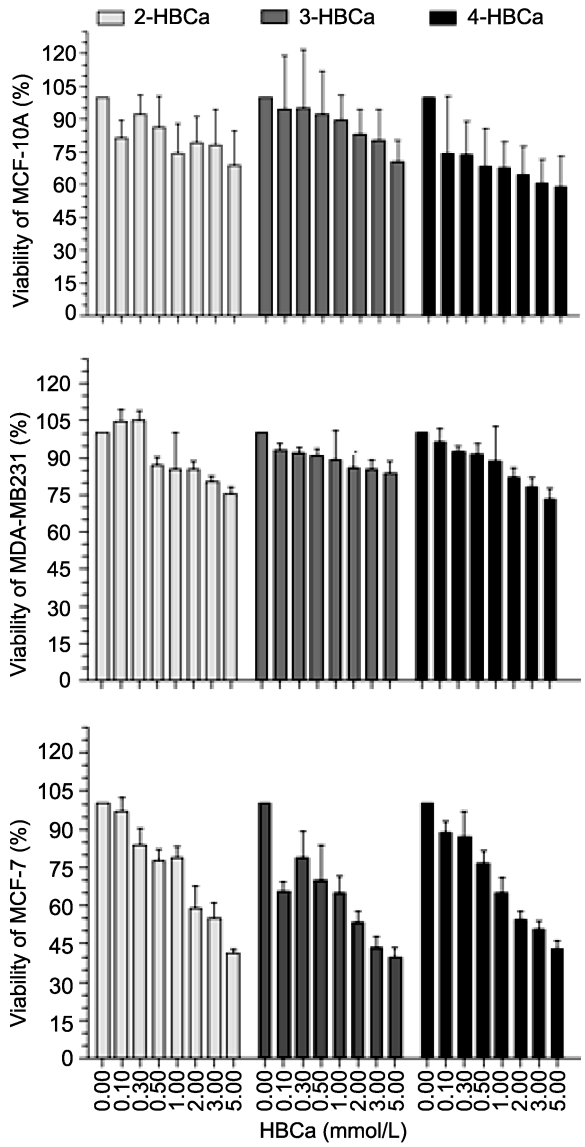

Figure 2 Dose-dependent effects of HBCa on the viability of normal (MCF-10A) and cancer (MDA-MB231 and MCF-7) breast epithelial cells as measured by MTT assay. The cells were treated for 48 h and cultured at standard growth conditions. Data is shown as mean ± standard error of mean (SEM) of four values

The effects of HBCa on cell cycle

The regulation of the cell cycle in the HBCa-treated breast epithelial cells (MCF-10A, MDA-MB231 and MCF-7) was analyzed after 48 h. Flow cytometry was used to quantify the DNA content within the cells which indicated that the distribution of different phases of the cell cycle were dependent on both the breast cell line and the HBCa compounds (*Figure 4A*). The treatment of the normal cell line (MCF-10A) resulted in an accumulation of cells in the G0/G1 phase in a dose-dependent manner compared to the control. The DNA contents increased from 8% to 31.47%. 2-HBCa was more effective in arresting MCF-10A at G0/G1 phase than the 3- and 4-HBCa compounds. However, the effects of different HBCa doses did not show significant differences (p =

doi: 10.18282/amor.v1.i2.35

0.05) in arresting the cell cycle at G0/G1 (*Figure 4B*). The DNA contents in MCF-10A cells decreased in parallel in the S and G2/M phases, in comparison to the corresponding untreated cells. Cell cycle arrests in breast cancer cells (MDA-MB 231 and MCF-7) showed less response to HBCa in comparison to the control sample and normal breast cells (MCF-10A). The cell cycle in MDA-MB231 cells was arrested at G0/G1 by approximately 2.82% to 15.22% and between 0.19% and 12.06% in MCF-7 cells when treated with HBCa compounds.

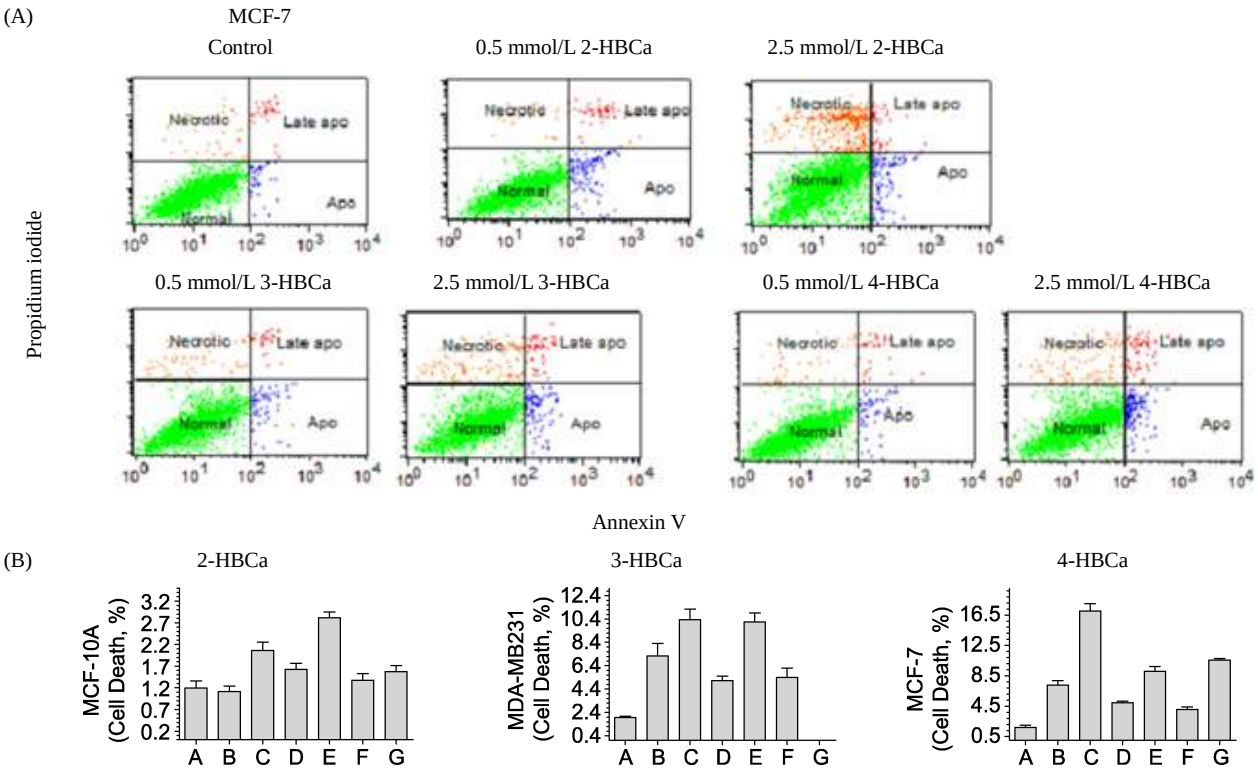

A = Control, B = 0.5 mmol/L 2-HBCa, C = 2.5 mmol/L 2-HBCa, D = 0.5 mmol/L 3-HBCa, E = 2.5 mmol/L 3-HBCa, F = 0.5 mmol/L 3-HBCa, G = 2.5 mmol/L 2-HBCa

(C)

Cell line/treatment		Significance
MCF-10		$p < 0.0016–0.7216$
MDA-MB231	Control vs. 0.5 or 2.5 mmol/L 2-HBC, 3-HBC or 4-HBC	$p < 0.0003–0.0068$
MCF-10		$p < 0.0001–0.0005$
Control vs. 0.5 or 2.5 mmol/L 2HBC, 3HBC or 4HBC	MCF-10A vs. MDA-MB231	$p < 0.0001$
	MCF-10A vs. MCF-7	$p < 0.0001$
	MDA-MB231 vs. MCF-7	$p < 0.0913–0.8634$

Figure 3 The treatment of normal (MCF-10A) and cancer (MDA-MB231) breast epithelial cells with HBCa for 48 h. (A) Examples of annexin V/propidium iodide dot plots illustrating the effect of HBCa compounds in MCF-7 breast cancer cells. (B) The percentage of breast cell death in normal (MCF-10A) and cancer (MDA-MB231 and MCF-7) cells when they were incubated with 0.5 mmol/L and 2.5 mmol/L HBCa for 48 h. (C) Summary of the statistical analysis of different HBCa compounds' treatments

Molecular modulation of apoptosis-related proteins by HBCa compounds

Figure 5 showed the effects of 0.5 mmol/L of 2-, 3- and 4-HBCa compounds on the expression of apoptosis-related proteins on MCF-10A, MDA-MB231 and MCF-7 breast cells. These compounds induced the upregulation of the proapoptotic proteins p53, p21, Bax and caspase-3 in MCF-10A, MDA-MB231 and MCF-7 cells after 48 h.

doi: 10.18282/amor.v1.i2.35

In contrast, the same treatments induced the downregulation of anti-apoptotic Bcl-2. Treatment of normal breast epithelial cells (MCF-10A) with 2-, 3- and 4-HBCa showed downregulated Bcl-2 less than the control by 8%–43%, while the expression of Bax increased in comparison to the control by 42%–92%.

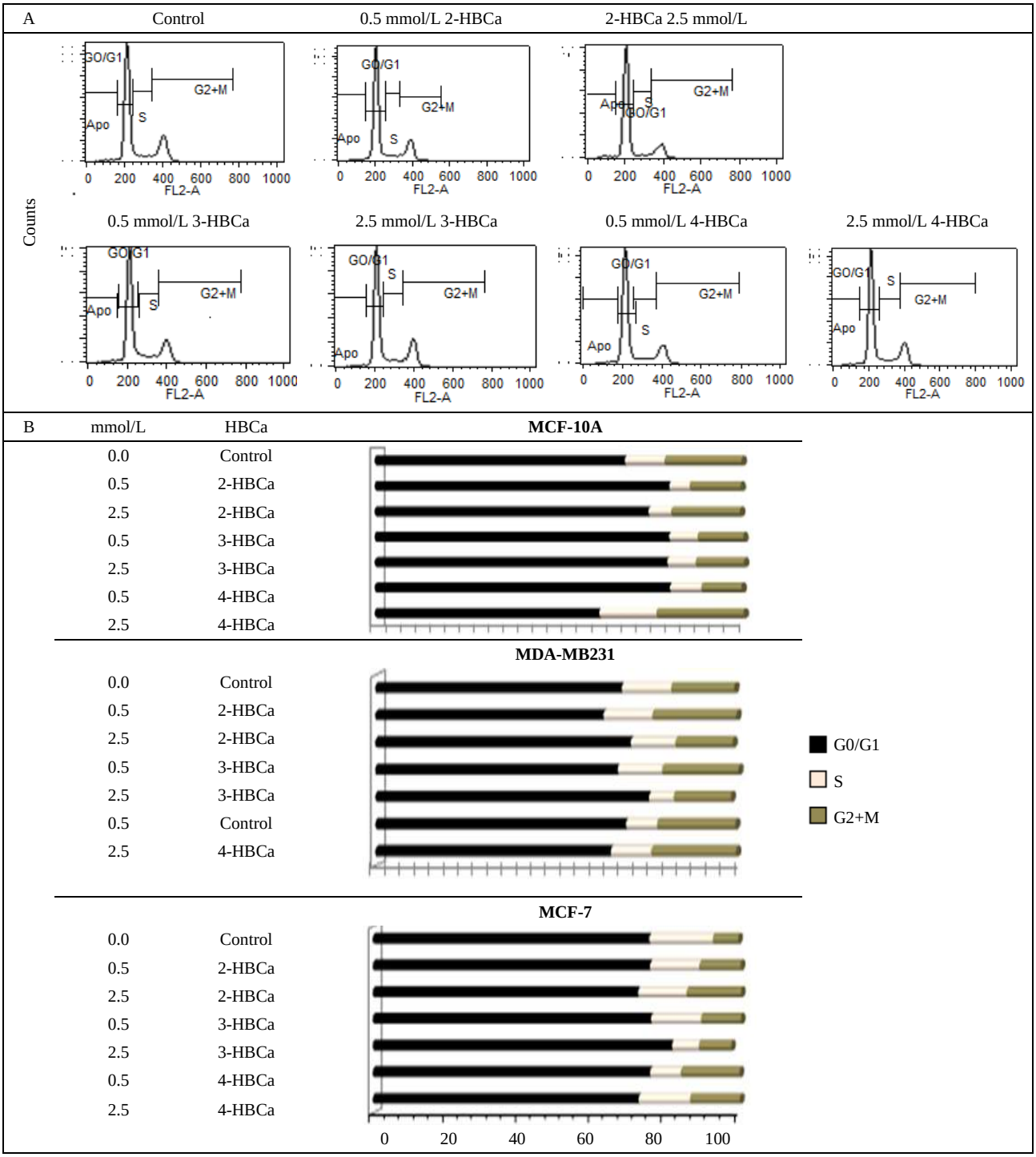

Figure 4 Effects of HBCa compounds on the cell cycle progression in normal (MCF-10A) and cancer (MDA-MB231) breast cells. (A) Examples of cell cycle analyses of MDA-MB231 cells under different treatments with HBCa compounds for 48 h, illustrating the distribution of the DNA levels at different phases. (B) The percentage of DNA modulation due to treatment with the HBCa compound

doi: 10.18282/amor.v1.i2.35

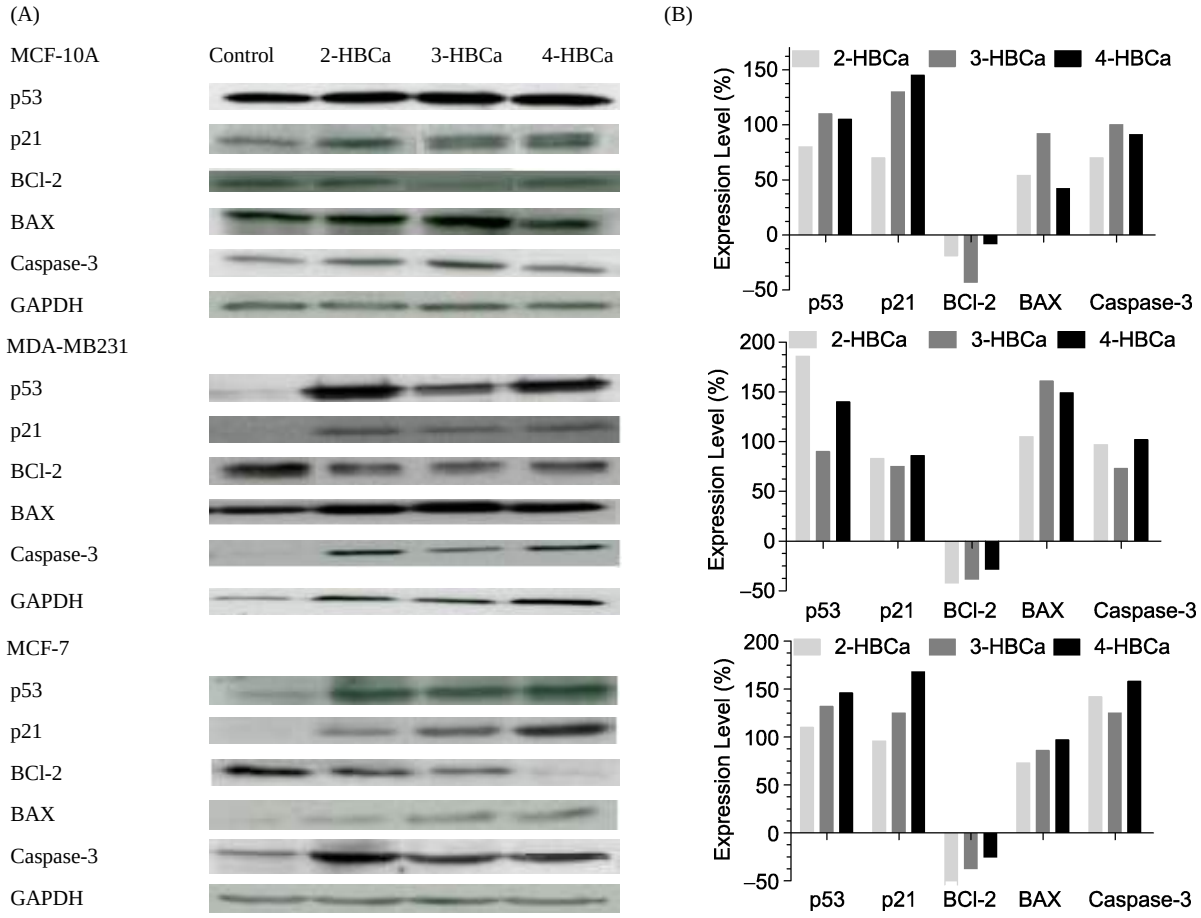

Figure 5 Molecular expressions of pro- and anti-apoptotic proteins in 0.5 mmol/L HBCa-treated MCF-10A, MDA-MB231 and MCF-7 cells. (A) Western blot analyses of p53, p21, BCl-2, Bax and caspase-3 after treatment with different HBCa compounds for 48 h. (B) Percentage of protein expression was expressed in percentage based on the control sample. Expression level of individual protein was calculated by first converting optical density (OD), OD (%) = (OD of treated sample/OD of control sample) × 100. The expression levels of individual protein were calculated using the following equation (% OD of protein in treated cells – % OD of protein in control) to give positive or negative values. Positive values indicate upregulation, while negative values indicate downregulation of protein expression

The 3-HBCa results showed a similar level of Bax and Bcl-2 expressions (*Figure 5A*). Similar results were obtained when the breast cancer cells (MDA-MB231 or MCF-7) were treated with 2.5 mmol/L HBCa (*Figure 5B*). Furthermore, the treatment of MCF-7 cells at 0.5 mmol/L was more effective than 2- and 3-HBCa in manipulating the expression of both Bcl-2 and Bax. The reduction of the expressed Bcl-2 in MCF-7 cells was between 25% and 70%, while the increase in Bax expression was between 73% and 97% (*Figure 5B*).

In addition, the apoptotic effects of HBCa compounds on breast epithelial cells indicated that the level of expressions of p53, p21 and caspase-3 were dependent on the type of cells. 3-HBCa was more effective than 2- and 4-HBCa. 4-HBCa was more effective in the breast cancer cells (MDA-MB231 and MCF-7) (*Figures 5B and C*). In MDA-MB231, the expression of p53, p21 and caspase-3 were 140%, 86% and 102%, respectively. Furthermore, 4-HBCa upregulated apoptosis-related proteins in MCF-7 by 146%, 168% and 158%, respectively. However, when the breast cells were treated with 2.5 mmol/L HBCa compounds, the expressions of the pro- and anti-apoptotic cells were lowered within 60%–100%. In addition, the treatment of breast epithelial cells with 2.5 mmol/L HBCa induced irregular expression of the pro- and anti-apoptotic proteins.

doi: 10.18282/amor.v1.i2.35

Discussion

Breast cancer is one of the most commonly diagnosed malignancies in women. Various strategies have been adopted to combat this disease. Chemotherapy is one of the main therapeutic strategies and it has attracted the interest of many researchers aiming to develop effective anticancer compounds. Various compounds including natural and synthetic have been studied. Among these HB compounds include the most common drugs acetylsalicylic acid (ASA) and its precursor 2-HBA, or also known as salicylic acid. Although ASA and 2-HBA exert some side effects, their derivatives exhibit less acidity and possess more apoptotic potential. For example, earlier work has highlighted the potential for 4-HBZn to induce apoptosis, particularly in primary CLL and other cancer cells[4,16]. HBCa compounds have also shown their apoptotic potential in human fibrosarcoma HT-1080 cells[10]. Metal ions including calcium (Ca^{2+}), zinc (Zn^{2+}) and platinum (Pt^{2+}) showed improved efficacy to various organic compounds against cancer cells. For example, the incorporation of Zn^{2+} or Ca^{2+} ions improved the apoptotic potentials of HBA compounds[4,10,16]. In addition, platinum-based anticancer drugs have proven to exert highly effective therapeutic potentials in various cancer types[17]. Thus, the incorporation of metal ions enhances the anticancer activity of organic compounds and may also be considered as a novel strategy for further development of anticancer drugs[18-20]. Our previous results[12,13,16] have encouraged us to investigate the apoptotic effects of HBCa compound on human's normal (MCF-10A) and breast epithelial cancer cell lines (MDA-MB231 and MCF-7) breast epithelial cells. The current study revealed that the treatment of these epithelial cells with HBCa compounds for 48 h has significantly induced cell death in a dose-dependent manner, as assayed by annexin V. The three HBCa compounds showed variable effectiveness in the normal breast epithelial cells and two breast cancer cell lines. The results may suggest the importance of metal-based compounds in the development of a new anticancer drug. It is clear that HBCa caused a notably higher proportion of cell death in breast cancer cells (MDA-MB231 and MCF-7) than in normal breast cells (MCF-10A). The results may encourage further studies in order to explore the anticancer function and potential of HBCa and its corresponding zinc analogues.

Chemotherapeutically, apoptosis is a novel strategy to kill cancer cells without affecting the neighboring normal cells[21]. Although physiological and drug-induced apoptosis lead to cell death, both are different in regards to initiating and proceeding apoptosis[22]. In both cases, apoptosis inhibits cell growth or proliferation which is associated with modulation of cell cycle check points. Our results showed that HBCa-treated MCF-10A, MDA-MB231 and MCF-7 cells arrested the cell cycle at G1/G0 after 48 h. Normal and cancer cells showed different responses to the increasing doses of HBCa compounds. Lower doses were more effective than higher doses when arresting normal MDA-MB231 cells at the G0/G1 phase. Similar results were obtained when pro- and anti-apoptotic proteins were investigated in HBCa-treated breast cells. The response of cancer cells to different HBCa doses was dependent on the type of cancer cell line and HBCa compound. These results may suggest different cytotoxic mechanisms of the two doses (0.5 and 2.5 mmol/L). Perhaps, 2.5 mmol/L HBCa might cause cytotoxicity to the breast cells, causing cells to undergo cell death. Although, assessing the morphology remains the most significant way to differentiate between apoptosis and necrosis. The results obtained from annexin V and the cell cycle may explain why 2.5 mmol/L HBCa was less effective apoptotically than 0.5 mmol/L HBCa. 2.5 mmol/L HBCa showed a higher level of late apoptosis and necrotic cells. These results may also explain the cytotoxic effect of higher doses of HBCa compounds. This issue highlights the association between the level of doses used and the type of cell death occurring: apoptosis or necrosis. The processes of aponecrosis can occur independently, sequentially and simultaneously, partly depending upon the type and level of stimuli, including anticancer drugs[23-25]. Apoptosis occurs via ligand binding and protein cross-linking with FAS (intrinsic pathway) or tumor necrosis factor (TNF) (extrinsic pathway) receptors. Other cells have a default death pathway that must be blocked by a survival factor such as a hormone or growth factor[25]. However, it should be noted that due to the lack of phagocytic cells in *in vitro* culture conditions, apoptosis fragments lyse and induce secondary necrosis or post-apoptotic necrosis in a process similar to necrosis[26]. It may be possible that the higher level of HBCa compounds contributed to the intracellular Ca^{2+} overload, causing post-apoptotic necrosis. Necrosis or death channel in the cytoplasmic membrane can be a result of colloid osmotic forces and entry of cations that cause swelling and ultimately rupturing[27]. This effect causes the permeability transition pores to open in the mitochondrial inner membrane in response to the stimuli of intracellular Ca^{2+} ions leading to necrosis[28]. This is also partly due to the inhibition of adenosine triphosphate (ATP) production by glycolysis or oxi-

doi: 10.18282/amor.v1.i2.35

dative phosphorylation[27,29]. In addition, the necrotic process is regulated by oxidative stress and p53 when the anticancer compound 2-phenylethynesulfonamide was used[30]. Reactive oxygen species (ROS) is often highly expressed in cancer cells as a by-product of oxidative phosphorylation[31]. The higher doses of HBCa may cause a further increase in the level of ROS, either by increasing the level of the oxidative stress or detoxification, in order to regulate cellular processes including cell survival. In both cases, the increased level of ROS production leads to the diversion of apoptosis into necrosis signaling. In this regard, a previous research reported the lack of antioxidants in the breast cancer cells[32].

Literature has demonstrated cross-links between apoptosis and the cell cycle through the molecular modulation of different proteins, including Cdks, p53, Bax and Bcl-2[33–37]. Thus, the ideal approach to assess the apoptotic effects of HBCa compounds is to measure the expression of both pro- and anti-apoptotic-related proteins. The use of Western blots clearly indicated that 0.5 mmol/L HBCa showed upregulation of p53, p21, Bax and caspase-3, while the expression of the anti-apoptotic proteins showed that Bcl-2 was downregulated. These results may suggest that the HBCa-treated epithelial breast cells underwent apoptosis via the intrinsic pathway. This pathway involves the activation of caspase-9 and caspase-3 in response to anticancer chemotherapy, which is closely associated with the increase of the outer mitochondrial membrane permeability, regulated by the Bcl-2 family[38]. It mainly involves caspase-3, which specifically activates the endonuclease CAD and degrades chromosomal DNA within the nuclei, as well as causing chromatin condensation[25]. Previously, we showed that 4-HBZn induced apoptosis via the intrinsic pathway in CLL which is partially abrogated by the caspase-9 inhibitor (Z-LEHD.FMK)[4]. In conclusion, the apoptotic effects of 2-, 3- and 4-HBCa compounds were significantly lesser in the control samples and normal (MCF-10A) breast epithelial cells (MCF-10A) than the corresponding cancer cells (MAD-Mb231 and MCF-7). These compounds induced cell cycle arrest at G0/G1. HBCa compounds also upregulated pro-apoptotic proteins, p53, p21, Bax and caspase-3 and downregulated the anti-apoptotic protein Bcl-2. These results may suggest the involvement of the intrinsic apoptotic mechanism.

Conclusion

The treatment of breast epithelial cells MCF-10A, MDA-MB231 and MCF-7 with 2-, 3-, and 4-HBCa for 48 h induced more apoptosis at 0.5 mmol/L but more secondary necrosis at 2.5 mmol/L. The cytotoxic effect of the higher dose of HBCa could be explained as these compounds may default the apoptotic pathway, leading cell death into necrosis. Therefore, further studies will be required to investigate the stimulation of cell death in breast cancer cells.

Author contributions

Nada M Merghani performed the experiments and contributed to the analysis of the data. The experimental work was supervised by Amal Al-Hazzaa. Eamon JG Mahdi contributed to review and writing of the manuscript, Abigail J Manning contributed to the review and preparation of the manuscript while Chris J Pepper contributed to the design of the study and review of the manuscript. Andea GS Buggins contributed to the design of the study and reviewed of the manuscript. Jassem G Mahdi designed and supervised the overall study and prepared the manuscript.

Conflict of interest

The authors declared no potential conflict of interest with respect to the research, authorship, and/or publication of this article.

References

1. WHO. Cancer country profiles [Internet]. 2014. Available from: www.who.int.
2. GLOBCAN. Estimated cancer incidence and mortality for breast cancer in 2012 [Internet]. 2012 [cited 2015 July 12]. Available from: http://globocan.iarc.fr.
3. Coleman MP, Quaresma M, Berrino F, et al. Cancer survival in five continents: a worldwide population-based study (CONCORD). Lancet Oncol 2008; 9(8): 730–756.
4. Pepper C, Mahdi JG, Buggins AGS, et al. Two novel aspirin analogues show selective cytotoxicity in primary chronic lymphocytic leukaemia cells that is associated with dual inhibition of Rel A and COX-2. Cell Prolif 2011; 44: 380–390.
5. Looi CY, Arya A, Cheah FK, et al. Induction of apoptosis in human breast cancer cells via caspase pathway by vernodalin isolated from *Centratherum anthelminticum* (L.) seeds. PLOS One 2013; 8(2): e56643.
6. Jia T, Zhang L, Duan Y, et al. The differential susceptibilities of MCF-7 and MDA-MB-231 cells to the cytotoxic effects of curcumin are associated with the PI3K/Akt-SKP2-Cip/Kips pathway. Cancer Cell Int 2014; 14(1): 126.
7. Cragg GM, Newman DJ. Plants as a source of anti-cancer

doi: 10.18282/amor.v1.i2.35

agents. J Ethnopharmacol 2005; 100(1-2): 72–79.
8. Baron JA. Epidemiology of non-steroidal anti-inflammatory drugs and cancer. Prog Exp Tumor Res 2003; 37: 1–24.
9. Elwood PC, Gallagher AM, Duthie GG, et al. Aspirin, salicylates, and cancer. Lancet 2009; 373(9671): 1301–1309.
10. Mahdi JG, Alkarrawi MA, Mahdi AJ, et al. Calcium salicylate-mediated apoptosis in human HT-1080 fibrosarcoma cells. Cell Prolif 2006; 39(4): 249–260.
11. Mahdi JG, Al-Musayeib NM, Mahdi EJ, et al. Pharmacological importance of simple phenolic compounds on inflammation, cell proliferation and apoptosis with a special reference to β-D-salicin and hydroxybenzoic acid. Eur J Inflamm 2013; 11(2): 327–336.
12. Mahdi JG, Al-Musayeib NM, Mahdi EJ, et al. The anti-proliferation and pro-apoptotic activities of hydroxybenzoate calcium complexes in HT-1080 human fibrosarcoma cells. Eur J Oncol 2014; 19(1): 21–33.
13. Mahdi JG, Mahdi AJ, Mahdi EJ, et al. Morphological modulation of human fibrosarchoma HT-1080 cells by hydroxybenzoate compounds during apoptosis. Adv Mod Oncol Res 2015; 1(1): 68–75.
14. Mandlekar S, Yu R, Tan TH, et al. Activation of caspase-3 and c-Jun NH_2-terminal kinase-1 signaling pathways in tamoxifen-induced apoptosis of human breast cancer cells. Cancer Res 2000; 60(21): 5995–6000.
15. Crissman HA, Steinkamp JA. Rapid, simultaneous measurement of DNA, protein, and cell volume in single cells from large mammalian cell populations. J Cell Biol 1973; 59(3): 766–771.
16. Mahdi JG, Pepper CJ, Alkarrawi MA, et al. Sub-millimolar concentration of the novel phenol-based compound, 2-hydroxy benzoate zinc, induces apoptosis in human HT-1080 fibrosarcoma cells. Cell Prolif 2010; 43(1): 95–102.
17. McQuitty RJ. Metal-based drugs. Sci Prog 2014; 97(Pt 1): 1–19.
18. Galanski M. Recent developments in the field of anticancer platinum complexes. Recent Pat Anticancer Drug Discov 2006; 1(2): 285–295.
19. Galanski M, Keppler BK. Searching for the magic bullet: anticancer platinum drugs which can be accumulated or activated in the tumor tissue. Anticancer Agents Med Chem 2007; 7(1): 55–73.
20. Shaili E. Platinum anticancer drugs and photochemotherapeutic agents: recent advances and future developments. Sci Prog 2014; 97(Pt 1): 20–40.
21. Gerl R, Vaux DL. Apoptosis in the development and treatment of cancer. Carcinogenesis 2005; 26(2): 263–270.
22. Tannock IF, Lee C. Evidence against apoptosis as a major mechanism for reproductive cell death following treatment of cell lines with anti-cancer drugs. Br J Cancer 2001; 84(1): 100–105.
23. Hirsch T, Marchetti P, Susin SA, et al. The apoptosis-necrosis paradox. Apoptogenic proteases activated after mitochondrial permeability transition determine the mode of cell death. Oncogene 1997; 15(13): 1573–1581.
24. Zeiss CJ. The apoptosis-necrosis continuum: insights from genetically altered mice. Vet Pathol 2003; 40(5): 481–495.
25. Elmore S. Apoptosis: a review of programmed cell death. Toxicol Pathol 2007; 35(4): 495–516.
26. Orrenius S, Nicotera P, Zhivotovsky B. Cell death mechanisms and their implications in toxicology. Toxicol Sci 2011; 119(1): 3–19.
27. Zong WX, Thompson CB. Necrotic death as a cell fate. Genes Dev 2006; 20(1): 1–15.
28. Waring P. Redox active calcium ion channels and cell death. Arch Biochem Biophys 2005*;* 434(1)*:* 33–42.
29. Eguchi Y, Shimizu S, Tsujimoto Y. Intracellular ATP levels determine cell death fate by apoptosis or necrosis. Cancer Res 1997; 57(10): 1835–1840.
30. Mattiolo P, Barbero-Farran A, Yuste VJ, et al. 2-Phenylethynesulfonamide (PES) uncovers a necrotic process regulated by oxidative stress and p53. Biochem Pharmacol 2014; 91(3): 301–311.
31. Liou GY, Storz P. Reactive oxygen species in cancer. Free Radic Res 2010; 44(5): 479–496.
32. Siemankowski LM, Morreale J, Briehl MM. Antioxidant defenses in the TNF-treated MCF-7 cells: selective increase in MnSOD. Free Radic Biol Med 1999; 26(7–8): 919–924.
33. Kasten MM, Giordano A. pRb and the cdks in apoptosis and the cell cycle. Cell Death Differ 1998; 5(2): 132–140.
34. Pucci B, Kasten M, Giordano A. Cell cycle and apoptosis. Neoplasia 2000; 2(4): 291–299.
35. Gartel AL, Feliciano C, Tyner AL. A new method for determining the status of p53 in tumor cell lines of different origin. Oncol Res 2003; 13(6–10): 405–408.
36. Vassilev LT, Vu BT, Graves B, et al. *In vivo* activation of the p53 pathway by small-molecule antagonists of MDM2. Science 2004; 303(5659): 844–848.
37. Zhu J, Zhao C, Zhuang T, et al. RING finger protein 31 promotes p53 degradation in breast cancer cells. Oncogene 2015; doi: 10.1038/onc.2015.260.
38. Fulda S, Debatin KM. Extrinsic versus intrinsic apoptosis pathways in anticancer chemotherapy. Oncogene 2006; 25(34): 4798–4811.

doi: 10.18282/amor.v1.i2.35

Advances in Modern Oncology Research

doi: 10.18282/amor.v1.i2.44

ORIGINAL RESEARCH ARTICLE

Association between *PER3* length polymorphism and onco-hematological diseases and its influence on patients' functionality

María Belén Cerliani[1], Juan Antonio Gili[2], Walter Hernán Pavicic[1], Graciela Klein[3], Silvia Saba[3], Silvina Mariel Richard[1*]

[1]Laboratorio de Citogenética y Mutagénesis, Instituto Multidisciplinario de Biología Celular (IMBICE, CONICET-CCT La Plata-CICPBA), Buenos Aires, Argentina

[2]Laboratorio de Epidemiología Genética (ECLAMC-CEMIC-CONICET), Buenos Aires, Argentina

[3]Unidad de Diagnóstico, Tratamiento y Sostén de Enfermedades Hematológicas, Hospital Interzonal General de Agudos Prof. Dr. Rodolfo Rossi, La Plata, Buenos Aires, Argentina

***Abstract*:** Circadian clock gene *PER3* and its length polymorphism may have a role in oncogenesis as clock genes act as key regulators of cell cycle and DNA repair pathways. The polymorphism may affect the condition of patients who show disrupted circadian rhythm due to tumor development. The aim was to assess the association between *PER3* polymorphism and onco-hematological diseases, and analyze whether this variant has an impact on patient's functionality. We conducted a case-control study on 125 patients with onco-hematological diseases and 310 control patients. *PER3* allelic variants were detected by using polymerase chain reaction. Sociodemographic data and information on patient's habits and functionality were obtained through questionnaire. Genotypes 4/5 + 5/5 showed an odd ratio (OR) = 1.39, with no statistical significance. However, those genotypes were associated with a two-fold increase in the risk of acute/chronic lymphoblastic/myeloblastic leukemia, taken all together. The occurrence of "changes in humor during last two months" was significantly associated with onco-hematological diseases. "Fatigue on awakening" and "self-reported snore" were associated with cases carrying the 4/5 or 5/5 genotypes. The results suggested that *PER3* polymorphism may have a role in the risk of leukemia, and might be a possible marker for individual differences in susceptibility to sleep disruption. This work provides insights for the identification of individuals at high risk of cancer, and those who are more susceptible to circadian disruption, which may decrease the physiological defenses against the tumor.

***Keywords*:** *PER3*; polymorphism; hematologic cancer; circadian rhythm; case-control study

***Citation*:** Cerliani MB, Gili JA, Pavicic WH, et al. Association between *PER3* length polymorphism and onco-hematological diseases and its influence on patients' functionality. Adv Mod Oncol Res 2015; 1(2): 132–140; http://dx.doi.org/10.18282/amor.v1.i2.44.

*Correspondence to: Silvina M. Richard, Camino General Belgrano y 526, Tolosa, La Plata, B1906APP Buenos Aires, Argentina, srichard@imbice.gov.ar.

Received: 18th September 2015; **Accepted:** 31st October 2015; **Published Online:** 2nd December 2015

The circadian system regulates metabolism and energy homeostasis on a daily basis in order to maintain vital processes and prepare the organism to respond to predictable/daily environmental conditions[1]. Accordingly, most of the mammalian physiology is regulated at some points by the main circadian clock which is located at the hypothalamic suprachiasmatic nuclei (SCN). Circadian coordination is known to be

extremely important for healthy physical and mental function, as many diseases display disruption of circadian rhythms[2,3]. Several studies have reported circadian alterations in cancer patients and tumor-bearing animals[4,5]. Moreover, current data have suggested that this disruption could be more than a consequence of cancer development and it may act as a risk factor[6,7]. In 2007, the International Agency for Research on Cancer (IARC, World Health Organization) concluded that shiftwork that involves circadian disruption is probably carcinogenic to humans (Group 2A)[8]. Besides the core clock at the SCN, peri- pheral tissues also have circadian clocks which show internal desynchronization under pathological conditions[9].

At molecular level, the circadian clock involves transcriptional-translational negative feedback loops, rhythmic production and degradation of protein complexes that turn off their own production[10,11]. Some circadian genes involved in the loop also control the transcription of other genes, such as clock-controlled genes (*CCG*), which represent 2%–10% of the mammalian genome[12]. Although the majority of the *CCG* show tissue-specific expression patterns, a few sets of them are expressed in multiple organs and encode key regulators of the cell cycle, deoxyribonucleic acid (DNA) damage/repair pathways, and cell death[6,13].

Period (*PER*) genes are part of the core of the mechanism involved in the circadian clocks. Period circadian clock 3 (*PER3*) is a member of the *PER* family, and in humans it contains a variable number tandem repeat (VNTR) polymorphism, consisting of a 54-bp coding region repeated 4 or 5 times[14]. These repeats are of interest because it included numerous potential phosphorylation sites. Thus, they could affect post-translational modification and stability of the protein. Several studies hypothesized that *PER3* VNTR polymorphism may alter the susceptibility to cancer[15]. Moreover, variants in the circadian genes (*CRY2*, *PER1*, *NPAS2* and *CSNK1E*) have been associated with different types of cancer, including non-Hodgkin lymphoma, prostate and breast cancer[16-20]. Studies on the expression patterns of circadian genes (*PER3* and *CCG*) show that there are significant differences between tumor tissue and the normal one adjacent to the tumor[21-22]. All these data show a possible role of *PER3* and its allelic variants in oncogenesis, and its potential use as a susceptibility biomarker.

As mentioned above, many physiological processes are affected by the tumor development, resulting in disrupted circadian rhythms in cancer patients. On the other hand, the central clock regulates sleep, mood, food intake and attention[23]. The connection between cancer, clock and behavior is quite relevant, given that living with cancer is emotionally exhausting. In fact, cancer patients undergo sickness behavior, a cluster of symptoms that include lethargy, depression, fever, hyperalgesia and decreased social interaction, which might be the result of both the disease and the treatment[24]. *PER3* has been reported to play a role in modulating sleep homeostasis in humans[25]. Thus, the VNTR polymorphism may have an impact on the patient's performance while facing changes in the circadian rhythm.

According to the Atlas of Cancer Mortality published by the Ministry of Health[26], the onco-hematologic diseases (leukemia, lymphomas and multiple myeloma) were the cause of over 18,500 deaths in Argentina from 2007–2011. These disorders exhibit an incidence of almost 850,000 cases/year worldwide, as reported by the IARC in its previous GLOBOCAN 2012 report[27]. In recent years, only a few studies addressed the connection between blood cancer and circadian rhythm, since most of the work on the topic focused on breast, prostate and colon cancers.

The aim of this work is to study the association between the VNTR of *PER3* and onco-hematological diseases, and analyze whether this variant has an impact on the patient's functionality in terms of fatigue, sleep and humor, among other variables.

Materials and methods

A case-control study consisting of 125 patients with onco-hematological diseases and 310 control patients was conducted. All the participants were recruited between June 2013 and March 2015 at the Unit of Diagnosis, Treatment and Support for Hematological Diseases of Hospital Prof. Dr. Rodolfo Rossi (La Plata, Buenos Aires, Argentina).

The cases included patients diagnosed with acute lymphoblastic leukemia (ALL, $N = 10$), acute myeloblastic leukemia (AML, $N = 18$), chronic lymphoblastic leukemia (CLL, $N = 10$), chronic myeloblastic leukemia (CML, $N = 20$), multiple myeloma (MM, $N = 29$), Hodgkin lymphoma (HL, $N = 18$) and non-Hodgkin lymphoma (NHL, $N = 20$). The controls were patients frequently visiting the unit for routine checks of disorders unrelated to cancer, or preoperative blood analyses. All the participants resided in Argentina. Cases and controls with previous history of cancer or pathologies which are closely related to onco-hematological diseases were excluded from the study.

Patients participated in this study upon signing an informed consent. A questionnaire was used to obtain

doi: 10.18282/amor.v1.i2.44

sociodemographic data and information about habits and functionality of patients (previous 2 months), such as changes in weight (± 5 kg), changes in appetite (either increase or decrease), changes in humor (worse or better), presence of physical/mental fatigue, difficulty in sleeping (especially when trying to fall asleep), fatigue on awakening, waking up several times at night, early morning awakening and difficulty to fall asleep again, snoring, and good sleep quality. All the surveys were conducted by the same person. Blood samples were collected and kept in tubes with ethylenediaminetetraacetic acid (EDTA). Then, the DNA was extracted from whole blood using salting out methods.

The detection of *PER3* allelic variants was performed by PCR, using the primers 5′-TGGTCCCAGCAGTGAGAGT-3′ forward and 5′-CCAGATGCTGCTCTACCTGAACC-3′ reverse. Reaction conditions were as follows, in a final volume of 15 µL: 1× buffer, 50 ng DNA, 0.25 mmol/L each primer, 200 µmol/L dNTPs, 1.5 mmol/L $MgCl_2$, 0.45 U *Taq* Platinum Polymerase (Life Technologies) and H_2O up to 15 µL. The PCR cycling consisted of an initial denaturation at 95°C for 5 min, followed by 30 cycles at 95°C for 1 min, followed by annealing at 57°C for 1 min and elongation at 72°C for 1 min, with a final extension at 72°C for 5 min. The products (261 bp and 315 bp) were visualized in 2% (w/v) agarose gels, stained with GelRed (Biotium Inc.).

Odds ratio (OR) and confidence interval at 95% (CI95%) were calculated to assess the association between each variable studied and hematological disease. Chi-square (Chi^2) test was applied to obtain the statistical significance of the association. Analyses were performed with STATA 11.1[28] and Epidat 4.0[29]. Allele and genotype frequencies were calculated and tested for Hardy-Weinberg equilibrium using GenAlEx 6.5[30,31]. *P*-values ≤0.05 were considered statistically significant. The sample size of this study achieved 80% power to detect an OR = 2.00.

Ethics statement

All the procedures performed in studies involving human participants were in accordance with the ethical standards of the institutional and/or national research committee and together with the 1964 Helsinki declaration and its later amendments or comparable ethical standards. The informed consent was obtained from all participants in this study and this study was approved by the ethics committee of the hospital.

Results

Study population

In this association study, a total of 125 cases were compared to 310 controls, and they were all patients from the Hospital Prof. Dr. Rodolfo Rossi. Demographic characteristics are listed in *Table 1*. The missing data for each variable were not included in the analysis or detailed in the tables. The maximum number of missing data in a variable was 18, representing 4.14% of the samples. The height and weight data were excluded due to >10% missing data. There was no significant difference in the mean age of cases and controls. Women showed lower risk of the disease compared to men (OR = 0.52, CI95% 0.34–0.82, $p = 0.003$). Higher levels of education (>12 years) were significantly related with an increased risk, compared to those who completed primary school or less (OR = 3.68, CI95% 1.82–7.40, $p < 0.001$ adjusted for age and sex). Marital status did not show relation with the disease.

PER3 polymorphism

Genotype and allele frequencies for the VNTR of *PER3* were in accordance with Hardy-Weinberg equilibrium (*Table 2*). Considering the 4/4 genotype as reference, genotype 4/5 and the homozygous 5/5 did not show association with hematological cancer (OR = 1.50, CI95% 0.95–2.35 and OR = 1.80, CI95% 0.84–3.95, respectively). The trending *p*-value was 0.039.

Genotypes 4/5 and 5/5 analyzed together showed an OR = 1.39, with no statistical significance ($p = 0.175$ adjusted for age, sex, educational level and city of residence). However, those genotypes were associated with a two-fold increase in the risk of ALL, CLL, AML and CML, taken all together (OR = 1.99, CI95% 1.06–3.74, $p = 0.032$ adjusted for age, sex, educational level, and city of residence). There was no significant association between the polymorphism and the other diseases (MM, HL and NHL data are not shown).

Functionality

With respect to functionality variables evaluated in the questionnaire, only “changes in humor” showed significant associations with the onco-hematological diseases under study (*Table 3*, OR and *p* values adjusted for age, sex, educational level and city of residence). Variables “better mood during the last two months” (OR = 4.28, CI95% 2.00–9.12, $p < 0.001$) and “worse mood” (OR = 2.00, CI95% 1.17–3.42, $p < 0.001$) were significantly associated with the disease.

Impact of *PER3* polymorphism on patient’s behavior

Table 4 shows the distribution of *PER3* genotypes in

doi: 10.18282/amor.v1.i2.44

Table 1 Demographic characteristics of the population under study

	Cases *N* = 125	Controls *N* = 310	OR (CI95%)	*p*
	Mean (SD)	Mean (SD)		
Age (years)	48.5 (16.6)	51 (18.5)	–	0.507
	N (%)	*N* (%)		
Sex				
Male	74 (59.2)	134 (43.2)	Ref.	0.003
Female	51 (40.8)	176 (56.8)	0.52 (0.34–0.82)	
Education				
⩽7 years (completed primary school or less)	55 (44.0)	174 (56.3)	Ref.	
12 years (completed secondary school)	48 (38.4)	115 (37.2)	1.2 (0.73-1.95)	<0.001[a]
>12 years (completed college)	22 (17.6)	20 (6.5)	3.68 (1.82–7.40)	
Marital status				
Single	27 (21.6)	79 (25.5)	Ref.	
Partner/Married	86 (68.8)	162 (52.3)	1.7 (0.99–2.95)	0.055[a]
Divorced/Separated	5 (4.0)	27 (8.7)	0.64 (0.21–1.90)	0.420[a]
Widowed	7 (5.6)	42 (13.5)	0.75 (0.27–2.13)	0.595[a]

a: Adjusted for age and sex. OR (CI95%): odds ratio and confidence interval 95%. Ref: reference category. SD: standard deviation. $p < 0.05$ considered statistically significant.

Table 2 Association between *PER3* polymorphism and onco-hematological diseases. Genotype and allele frequencies for the VNTR are also shown

PER3 polymorphism	Cases *N* = 120 *N* (%)	Controls *N* = 297 *N* (%)	OR (CI95%)	*p*	Chi^2 & *p* trend
	N (%)	*N* (%)			
Allele frequencies					
4-rep	0.69	0.76	–	–	–
5-rep	0.31	0.24			
Genotype frequencies					
4/4	58 (48.3)	176 (59.3)	Ref.		
4/5	50 (41.7)	101 (34.0)	1.50 (0.95–2.35)	0.077	4.26
5/5	12 (10.0)	20 (6.7)	1.82 (0.84–3.95)	0.130	*p* trend = 0.039
4/4	58 (48.3)	176 (59.3)	Ref.	0.175[a]	–
4/5 + 5/5	62 (51.7)	121 (40.7)	1.39 (0.86–2.25)		
LMC/LLC/LMA/LLA (*N* = 58)					
4/4	23 (39.7)	176 (59.3)	Ref.	0.032[a]	–
4/5 + 5/5	35 (60.3)	121 (40.7)	1.99 (1.06–3.74)		

a: Adjusted for age, sex, educational level and city of residence. OR (CI95%): odds ratio and confidence interval 95%. Ref.: reference category. $p < 0.05$ considered statistically significant.

controls and cases for each behavior variables analyzed. Variables “fatigue on awakening” and “self-reported snore” were associated with cases carrying the 4/5 or 5/5 genotype ($p = 0.003$ and $p = 0.036$ respectively, adjusted for age and sex). The rest of the variables included in the questionnaire did not show statistically significant associations.

Discussion

Patients who go through an oncologic disease may undergo circadian disruption as a reaction of physiology to tumor presence or as the result of endocrine response to physical/emotional demands of the illness. Cancer patients take longer time to fall asleep, wake up more often, spend more time in bed and nap more frequently than healthy individuals[32,33]. On the other hand, genetic, environmental or behavioral factors may favor circadian disruption, predisposing patients to tumor development[34]. Several studies have demonstrated that long-term night shiftwork is a prognostic value for breast cancer[35,36].

doi: 10.18282/amor.v1.i2.44

Table 3 Association between functionality variables and onco-hematological diseases

	Cases *N* = 125	Controls *N* = 310	OR (CI95%)	*p*
	N (%)	*N* (%)		
Weight				
No changes	50 (42.0)	140 (47.0)	Ref.	
Increase/decrease <5 kg	31 (26.0)	84 (28.2)	1.03 (0.61–1.74)	0.902
Increase/decrease ≥5 kg	38 (32.0)	74 (24.8)	1.43 (0.86–2.38)	0.161
Appetite				
No changes	72 (60.0)	188 (62.1)	Ref.	
Increase	20 (16.7)	58 (19.1)	0.9 (0.50–1.60)	0.721
Decrease	28 (23.3)	57 (18.8)	1.28 (0.75–2.17)	0.355
Humor				
No changes	50 (41.0)	163 (53.8)	Ref.	
Better mood	22 (18.0)	24 (7.9)	4.28 (2.00–9.12)	<0.001[a]
Worse mood	50 (41.0)	116 (38.3)	2.00 (1.17–3.42)	0.001[a]
Physical/mental fatigue				
No	60 (48.0)	128 (41.4)	Ref.	0.211
Yes	65 (52.0)	181 (58.6)	0.77 (0.49–1.19)	
Fatigue on awakening				
No	77 (62.1)	199 (64.6)	Ref.	0.623
Yes	47 (37.9)	109 (35.4)	1.11 (0.71–1.75)	
Difficulty sleeping				
No	67 (53.6)	175 (56.8)	Ref.	0.541
Yes	58 (46.4)	133 (43.2)	1.14 (0.73–1.77)	
Waking up several times at night				
No	44 (35.2)	122 (39.3)	Ref.	0.420
Yes	81 (64.8)	188 (60.7)	1.19 (0.76–1.89)	
Early morning awakening				
No	95 (99.0)	207 (96.7)	Ref.	0.252
Yes	1 (1.0)	7 (3.3)	0.31 (0.01–2.49)	
Snore				
No	44 (36.4)	100 (34.8)	Ref.	0.769
Yes	77 (63.6)	187 (65.2)	0.94 (0.59–1.50)	
Good sleep quality				
Yes	66 (54.1)	159 (51.3)	Ref.	0.599
No	56 (45.9)	151 (48.7)	0.89 (0.57–1.39)	

a: Adjusted for age, sex, educational level and city of residence. OR (CI95%): odds ratio and confidence interval 95%. Ref: reference category. $p < 0.05$ considered statistically significant.

In our study, behavior variables such as fatigue, difficulty in sleeping, waking up several times at night or changes in appetite or weight did not associate with hematological cancer. This is probably because the study was hospital-based and more than 75% of the control patients were taking medication at the time of the inter- view, e.g., for different cardiologic or gastric disorders (data not shown). Moreover, a survey including >1,700 individuals from Buenos Aires (Argentina), Sao Pablo (Brazil), and Mexico DF (Mexico) showed that 2/3 of interviewed people experienced some type of sleeping difficulty during the previous year, and more than 25% individuals were moderately/severely affected[37]. Among them, the most common sleep disturbances reported within the last 12 months were: waking in the middle of the night (65%), waking up tired (55%), difficulty in sleeping and restarting it after an interruption (50%), or waking up too early (35%)[37].

doi: 10.18282/amor.v1.i2.44

Table 4 Distribution of *PER3* genotypes among cases and controls, and its association with functionality variables

	Cases		Controls		$p^{a,b}$
	4/4	4/5 + 5/5	4/4	4/5 + 5/5	
Weight					
No changes	22 (40.7)	27 (45.0)	69 (40.8)	62 (53.5)	
Increase/decrease <5 kg	12 (22.2)	18 (30.0)	53 (31.4)	28 (24.1)	0.318
Increase/decrease ≥5 kg	20 (37.1)	15 (25.0)	47 (27.8)	26 (22.4)	
Appetite					
No changes	32 (57.2)	35 (59.3)	101 (58.7)	80 (67.8)	
Increase	12 (21.4)	8 (13.6)	36 (20.9)	19 (16.1)	0.180
Decrease	12 (21.4)	16 (27.1)	35 (20.4)	19 (16.1)	
Humor					
No changes	21 (37.5)	26 (42.6)	87 (50.9)	69 (58.0)	
Better mood	12 (21.4)	10 (16.4)	16 (9.4)	8 (6.7)	0.561
Worse mood	23 (41.1)	25 (41.0)	68 (39.7)	42 (35.3)	
Physical/mental fatigue					
No	29 (50.0)	27 (43.6)	69 (39.4)	54 (44.6)	0.159
Yes	29 (50.0)	35 (56.4)	106 (60.6)	67 (55.4)	
Fatigue on awakening					
No	42 (72.4)	31 (50.8)	108 (61.7)	83 (69.2)	0.003
Yes	16 (27.6)	30 (49.2)	67 (38.3)	37 (30.8)	
Difficulty sleeping					
No	31 (53.4)	31 (50.0)	94 (53.7)	75 (62.5)	0.168
Yes	27 (46.6)	31 (50.0)	81 (46.3)	45 (37.5)	
Waking up several times at night					
No	21 (36.2)	21 (33.9)	66 (37.5)	53 (43.8)	0.335
Yes	37 (63.8)	41 (66.1)	110 (62.5)	68 (56.2)	
Early morning awakening					
No	42 (100.0)	48 (98.0)	118 (97.5)	82 (95.4)	0.990
Yes	0	1 (2.0)	3 (2.5)	4 (4.60)	
Snore					
No	25 (44.6)	19 (31.2)	47 (29.2)	43 (38.0)	0.036
Yes	31 (55.4)	42 (68.8)	114 (70.8)	70 (62.0)	
Good sleep quality					
Yes	32 (55.2)	31 (52.5)	87 (49.4)	67 (55.4)	0.320
No	26 (44.8)	28 (47.5)	89 (50.6)	54 (44.6)	

a: *p*-values for interaction between functionality variables and *PER3* genotype were estimated using a logistic regression model extended to include the interaction term. b: Adjusted for age and sex. $p < 0.05$ considered statistically significant.

In fact, sleeping difficulties affect a significant proportion of people living in urban areas who are experiencing social jet-lag and night light pollution[38,39]. Since these disturbances are even worse for chronic diseases, we did not observe significant differences between cases and controls in our study. However, “feeling positive or negative changes in humor” was significantly associated with onco-hematological diseases ($p < 0.001$ adjusted for age, sex, educational level and city of residence). Several factors in a cancer patient should be noted, such as history and family background, physical and psychological impact of the illness, psychic resources and medical care. Cancer patients often suffer from adjustment disorders and anxiety generated by the diagnosis, prognosis, the

doi: 10.18282/amor.v1.i2.44

wait for results, family conflicts, fear of recurrence and death, abnormal metabolic states and drugs, such as corticosteroids[40]. Therefore, patient's mood will depend on the interaction between all these factors in a more complex scenario than any other chronic diseases. In fact, the depression in cancer patients is twice as likely compared to the patients hospitalized due to other medical problems[40].

In the present study, the VNTR polymorphism of *PER3* increased the risk of onco-hematological diseases by 39%. During the analysis of leukemia separately from the rest of the conditions, the genotypes 4/5 and 5/5 were observed to be associated with a statistically significant increased risk (OR = 1.99, CI95% 1.06–3.74, p = 0.030 adjusted for age, sex, educational level and city of residence). Individual studies showed no conclusive results for the above-mentioned polymorphism[19,20,41]. A meta-analysis carried out by Geng and colleagues[15] combining three retrospective studies (2,492 cancer patients and 2,749 controls) reported that individuals with 5 repetition alleles had 17% increased risk of cancer compared to individuals with the 4 repetition alleles. However, this association was not statistically significant. A study on an American population reported a significantly higher risk of breast cancer among premenopausal women with the 5 repetition alleles[16], but a larger replication with Chinese samples did not show significant association results[20]. So far, there are no studies which evaluate the possible association between the VNTR with any of the blood cancers.

When we analyzed the distribution of *PER3* genotypes among controls and cases, we found that cancer patients with the 4/5 or 5/5 genotypes had greater fatigue on awakening. Voinescu et al.[42] focused on *PER3* genotypes and applied a battery of questionnaires to a population with self-reported sleep problems, finding that homozygotes for the 5 alleles showed difficulties in getting up more frequently than those with the 4 alleles or heterozygotes. In another study, a group of 24 healthy volunteers were subjected to sleep deprivation. It was observed that during the morning hours of the second day of sleep deprivation which was approximately 2–6 h after the melatonin peak, the performance (working memory, attention and psychomotor performance) deteriorated significantly in 5/5 individuals, whereas the decline was lower in 4/4 ones[25,43]. Based on the available data described above, our results suggest that cancer patients with 4/5 or 5/5 genotype may suffer fatigue more intensely, since they combine circadian disruption from the pathology itself with an increased susceptibility to sleep deprivation due to *PER3* genotype. It is important to take into account that our results were obtained with a non-validated questionnaire and more accurate approaches could be achieved using validated tools.

Case-control studies, as other population analyses, should also consider the ethnic composition of the group under study as allele frequencies vary among different populations. For the same reason, caution should be exercised when extrapolating results from one population to another.

Conclusion

All these data show that the VNTR of *PER3* may have a role in the risk of leukemia, and it may be a significant marker for individual differences in sleep, vulnerability to sleep disruption and circadian phase misalignment. The investigations aimed at elucidating the molecular connection between circadian genes and carcinogenesis will be helpful in identifying individuals at a higher risk or more susceptible to circadian disruption. It is worth to note that circadian disruption may decrease the physiological defenses against the tumor.

Acknowledgments

We thank the hospital's technical staff for their help in attending the patients for sampling. Beatriz Tosti is thanked for providing language help and Juan José Chiesa for helpful comments on this manuscript. This study was supported by grants from the "Consejo Nacional de Investigaciones Científicas y Técnicas" (PIP-634 to SMR and Scholarship Grant to MBC) and the "Instituto Nacional del Cáncer" (grant no. R.M. 493: Asistencia financiera a proyectos de investigación en cáncer de origen nacional II, to Pavicic WH).

Conflict of interest

The authors declared no potential conflict of interest with respect to the research, authorship, and/or publication of this article.

References

1. Levi F, Schibler U. Circadian rhythms: mechanisms and therapeutic implications. Annu Rev Pharmacol Toxicol 2007; 47: 593–628.
2. Mongrain V, Cermakian N. Clock genes in health and diseases. J Appl Biomed 2009; 7(1): 15–33.
3. Golombek DA, Casiraghi LP, Agostino PV, et al. The times they're a changing: Effects of circadian desynchronization on physiology and disease. J Physiol Paris 2013;

doi: 10.18282/amor.v1.i2.44

107(4): 310–322.
4. Mormont MC, Lévi F. Circadian-system alterations during cancer processes: A review. Int J Cancer 1997; 70(2): 241–247.
5. Davidson AJ, Straume M, Block GD, et al. Daily timed meals dissociate circadian rhythms in hepatoma and healthy host liver. Int J Cancer 2006; 118(7): 1623–1627.
6. Fu L, Lee CC. The circadian clock: Pacemaker and tumour suppressor. Nat Rev Cancer 2003; 3(5): 350–361.
7. Van Dycke KCG, Rodenburg W, van Oostrom CTM, et al. Chronically alternating light cycles increase breast cancer risk in mice. Curr Biol; 2015; 25(14): 1932–1937.
8. IARC Monographs on the Evaluation of Carcinogenic Risks to Humans: Painting, Firefighting and Shiftwork. IARC Working Group. IARC Press 2010; 561–764.
9. Hastings MH, Reddy AB, Maywood ES. A clockwork web: Circadian timing in brain and periphery, in health and disease. Nat Rev Neurosci 2003; 4(8): 649–661.
10. Takahashi JS, Hong HK, Ko CH, et al. The genetics of mammalian circadian order and disorder: Implications for physiology and disease. Nat Rev Genet 2008; 9(10): 764–775.
11. Reppert SM, Weaver DR. Coordination of circadian timing in mammals. Nature 2002; 418(6901): 935–941.
12. Panda S, Antoch MP, Miller BH, et al. Coordinated transcription of key pathways in the mouse by the circadian clock. Cell 2002; 109(3): 307–320.
13. Yu EA, Weaver DR. Disrupting the circadian clock: Gene-specific effects on aging, cancer, and other phenotypes. Aging (Albany NY) 2011; 3(5): 479–493.
14. Archer SN, Robilliard DL, Skene DJ, et al. A length polymorphism in the circadian clock gene *Per3* is linked to delayed sleep phase syndrome and extreme diurnal preference. Sleep 2003; 26(4): 413–415.
15. Geng P, Ou J, Li J, et al. Genetic association between *PER3* genetic polymorphisms and cancer susceptibility: A meta-analysis. Medicine (Baltimore) 2015; 94(13): 1–6
16. Zhu Y, Brown HN, Zhang Y, et al. *Period3* structural variation: A circadian biomarker associated with breast cancer in young women. Cancer Epidemiol Biomarkers Prev 2005; 14(1): 268–270.
17. Zhu Y, Stevens RG, Leaderer D, et al. Non-synonymous polymorphisms in the circadian gene *NPAS2* and breast cancer risk. Breast Cancer Res Treat 2008; 107(3): 421–425.
18. Hoffman AE, Yi CH, Zheng T, et al. CLOCK in breast tumorigenesis: genetic, epigenetic, and transcriptional profiling analyses. Cancer Res 2010; 70(4): 1459–1468.
19. Chu LW, Zhu Y, Yu K, et al. Variants in circadian genes and prostate cancer risk: A population-based study in China. Prostate Cancer Prostatic Dis 2008; 11(4): 342–348.
20. Dai H, Zhang L, Cao M, et al. The role of polymorphisms in circadian pathway genes in breast tumorigenesis. Breast Cancer Res Treat 2011; 127(2): 531–540.
21. Oshima T, Takenoshita S, Akaike M, et al. Expression of circadian genes correlates with liver metastasis and outcomes in colorectal cancer. Oncol Rep 2011; 25(5): 1439–1446.
22. Chen ST, Choo KB, Hou MF, et al. Deregulated expression of the *PER1*, *PER2* and *PER3* genes in breast cancers. Carcinogenesis 2005; 26(7): 1241–1246.
23. Kalsbeek A, Palm IF, La Fleur SE, et al. SCN outputs and the hypothalamic balance of life. J Biol Rhythm 2006; 21(6): 458–469.
24. Myers J. Proinflammatory cytokines and sickness behavior: Implications for depression and cancer-related symptoms. Oncol Nurs Forum 2008; 35(5): 802–807.
25. Viola AU, Archer SN, James LM, et al. *PER3* polymorphism predicts sleep structure and waking performance. Curr Biol 2007; 17(7): 613–618.
26. Ministry of Health, National Cancer Institute. Atlas of Cancer Mortality, Argentina 2007–2011 [Spanish: Ministerio de Salud, Instituto Nacional del Cáncer. Atlas de Mortalidad por Cáncer, Argentina 2007–2011]; 2011. p. 45–48.
27. IARC. GLOBOCAN 2008 – Section of Cancer Information [Internet]. [cited 2012 Dec 3]. Available from: http://globocan.iarc.fr/Pages/fact_sheets_cancer.aspx
28. StataCorp. Stata Statistical Software: Release 11. College Station, TX: StataCorp LP.; 2009.
29. Epidat: program for epidemiological data analysis. Version 4.0. Regional Health, Government of Galicia, Spain; Pan American Health Organization (PAHO- WHO); CES University, Colombia [Spanish: Epidat: programa para análisis epidemiológico de datos. Versión 4.0. Consellería de Sanidade, Xunta de Galicia, España; Organización Panamericana de la salud (OPS-OMS); Universidad CES, Colombia].
30. Peakall R, Smouse PE. GenAlEx 6: Genetic analysis in Excel. Population genetic software for teaching and research. Mol Ecol Notes 2006; 6: 288–295.
31. Peakall R, Smouse PE. GenAlEx 6.5: Genetic analysis in Excel. Population genetic software for teaching and research–an update. Bioinformatics 2012; 28(19): 2537–2539.
32. Pati AK, Parganiha A, Kar A, et al. Alterations of the characteristics of the circadian rest-activity rhythm of cancer in-patients. Chronobiol Int Informa Clin Med 2007; 24(6): 1179–1197.
33. Parker K, Bliwise D, Ribeiro M, et al. Sleep/wake patterns of individuals with advanced cancer measured by ambulatory polysomnography. J Clin Oncol 2008; 26(15): 2464–2472.
34. Eismann EA, Lush E, Sephton SE. Circadian effects in

doi: 10.18282/amor.v1.i2.44

cancer-relevant psychoneuroendocrine and immune pathways. Psychoneuroendocrinology; 2010; 35(7): 963–976.
35. Davis S, Mirick DK, Stevens RG. Night shift work, light at night, and risk of breast cancer. J Natl Cancer Inst 2001; 93(20): 1557–1562.
36. Schernhammer ES, Speizer FE, Walter C, et al. Rotating night shifts and risk of breast cancer in women participating in the nurses' health study. J Natl Cancer Inst 2001; 93(20): 1563–1568.
37. Blanco M, Kriber N, Cardinali DP. Survey on sleep difficulties in an urban Latin American population [Spanish: Encuesta sobre dificultades del sueño en una población urbana latinoamericana]. Rev Neurol 2004; 39(2): 115–119.
38. Roenneberg T, Kantermann T, Juda M, et al. Light and the human circadian clock. Handb Exp Pharmacol 2013; 217: 311–331.
39. Wittmann M, Dinich J, Merrow M, et al. Social jetlag: Misalignment of biological and social time. Chronobiol Int: J Bio Med Rhythm R 2006; 23 (1–2): 497–509.
40. Sala V. Psychiatric and psychological interconsultation in cancer patients [Spanish: La interconsulta psiquiátrica y psicológica en pacientes con cáncer]. Rev Colomb Psiquiatr. 2002; 31(3): 225–236.
41. Karantanos T, Theodoropoulos G, Gazouli M, et al. Association of the clock genes polymorphisms with colorectal cancer susceptibility. J Surg Oncol 2013; 108(8): 563–567.
42. Voinescu BI, Coogan AN. A variable-number tandem repeat polymorphism in *PER3* is not associated with chronotype in a population with self-reported sleep problems. Sleep Biol Rhythms 2012; 10(1): 23–26.
43. Dijk DJ, Archer SN. PERIOD3, circadian phenotypes, and sleep homeostasis. Sleep Med Rev 2010; 14(3): 151–160.

doi: 10.18282/amor.v1.i2.44

Advances in Modern Oncology Research

doi: 10.18282/amor.v1.i2.37

ORIGINAL RESEARCH ARTICLE

Threshold-based parametric analysis of diffusion-weighted magnetic resonance imaging at 3.0 Tesla to identify men with prostate cancer

Diarmaid C Moran[1,2], Laure Marignol[1*], Andrew J Fagan[3], Ruth Dunne[3], Antoinette S Perry[4], Dearbhail O'Driscoll[3], Eoin Gaffney[5], Thomas H Lynch[2], James FM Meaney[3], Donal H Hollywood[1]

[1]Applied Radiation Therapy Trinity, Trinity College Dublin, Dublin, Ireland
[2]Department of Urology, St James's Hospital, Dublin, Ireland
[3]Centre for Advanced Medical Imaging, St James's Hospital, Trinity College Dublin, Dublin, Ireland
[4]Prostate Molecular Oncology Group, Trinity College Dublin, Dublin, Ireland
[5]Department of Pathology, St James's Hospital, Dublin, Ireland

***Abstract*:** The aim of this study is to determine the accuracy of three apparent diffusion coefficient (ADC) threshold values in detecting prostate cancer (PCa) prior to prostate biopsy. Sixty men with clinical suspicion of PCa underwent endorectal diffusion-weighted magnetic resonance imaging (DW-MRI) at 3.0 Tesla (T). Three ADC threshold values (tADC: 1.0, 1.2 and 1.4 × 10^{-3} mm^2/s) were sequentially applied to ADC maps for the detection of malignant lesions in the prostatic peripheral zone (PZ). Segment-based and patient-specific PCa detection performance of these tADC values was correlated with the histopathological results from the subsequent 12-core transrectal ultrasound (TRUS)-guided biopsy. Mean of ADC and area size of the identified malignant region of interests (ROIs) were recorded. Accuracy for PCa detection was assessed by receiver operating characteristic curves. 1.0 × 10^{-3} mm^2/s of tADC provided 79% sensitivity, 97% specificity and 93% positive predictive value for PCa. Area size of the malignant ROI was a good independent factor for PCa detection (Area under curve, AUC = 0.85). ROI area size 0.2 cm^2 was identified as the best performing cut-off values for the detection of PCa. Refined detection criteria combining area size ≤0.2 cm^2 and ADC <1.0 × 10^{-3} mm^2/s increased the detection performance. In conclusion, threshold-based parametric evaluation of DW-MRI at 3.0 T can detect PZ PCa accurately prior to biopsy.

***Keywords*:** diffusion-weighted magnetic resonance imaging (DW-MRI); prostatic neoplasm; early detection of cancer; receiver operating characteristic (ROC) curve; histology

***Citation*:** Moran DC, Marignol L, Fagan AJ, et al. Threshold-based parametric analysis of diffusion-weighted MRI at 3.0 Tesla to identify men with prostate cancer. Adv Mod Oncol Res 2015; 1(2): 141–150; http://dx.doi.org/10.18282/amor.v1.i2.37.

*Correspondence to: Laure Marignol, Applied Radiation Therapy Trinity, Discipline of Radiation Therapy, Trinity Centre for Health Sciences, St James's Hospital, Dublin 8, Ireland, marignol@tcd.ie.

Received: 7th October 2015; **Accepted:** 6th November 2015; **Published Online:** 4th December 2015

Prostate cancer (PCa) patients are treated with a risk-adjusted patient-specific method that is designed to improve the control of cancer while reducing the risk of treatment-related effects. There is a growing demand for individualized treatment plans, which necessitates the accurate characterization of the location, extent and aggressiveness of the tumor[1]. By following the European Association of Urology Guidelines, diagnosis of PCa is based on transrectal ultrasound (TRUS)-guided biopsy performed in patients with either an elevated prostate specific antigen (PSA) and/or an abnormal clinical examination (digital rectal examination

(DRE))[2]. However, only 25%–30% of men with a moderately elevated PSA (4–10 ng/mL) have prostate cancer confirmed at biopsy and therefore many biopsies may ultimately prove unnecessary[3]. In order to reduce the unnecessary biopsy rate, new clinical tools and strategies are required. There has been a great interest in determining the presence or absence of tumor non-invasively with combined anatomical and functional magnetic resonance imaging (MRI)[4].

MRI is well-validated for local staging of PCa using qualitative assessment, including high-resolution T2-weighted (T2W) images once the diagnosis has been established by TRUS biopsy[5]. The combination of T2W imaging and functional techniques have also been proposed for detection purpose[6]. Amongst the three functional parametric techniques available, diffusion-weighted (DW)-MRI has substantial advantages over the other two, i.e., dynamic contrast enhanced-MRI and magnetic resonance spectroscopy (MRS), because it does not require intravenous contrast and is relatively simple to implement. The software also generates apparent diffusion coefficient (ADC) maps. Variations in cellular structure between benign and malignant tissue manifest as differences in water diffusion. These differences can be exploited to improve PCa detection either qualitatively or quantitatively by measuring changes in ADC to potentially measure the aggressiveness of the tumor[7].

There is a poor agreement on the value of 3.0 Tesla (T) over 1.5 T, the use of an endorectal coil (ERC), image acquisition parameters and data processing[8]. Other unresolved issues include variations in the appearance of different parts of the prostate on T2W imaging, inhomogeneous diffusion characteristics within different parts of the prostate, particularly at the prostatic base where increased cellularity may result in area-specific ADC values and the absence of an absolute cut-off value differentiating benign from malignant tissue[5]. Finally, the relevance of abnormalities detected on DW-ADC maps in treatment algorithms either in the absence of proven tumor on TRUS or in patients with low Gleason score on biopsy remains controversial.

ADC maps are readily used for the parametric analysis of DW-MRI, although the diffusion characteristics within the prostate are inhomogeneous[9]. No consensus exists for the cut-off ADC value differentiating benign from malignant prostate tissue and factors such as increased cellularity at the prostatic base which result in area-specific ADC values must be considered[10]. ADC values below 1.0×10^{-3} mm^2/s[9,11-14], 1.2×10^{-3} mm^2/s[15] and 1.4×10^{-3} mm^2/s[16,17] have all been correlated to the presence of PCa. In this study, we evaluated the objective parametric assessment of ADC maps acquired at 3.0 T using these three predetermined cut-off levels to determine whether ADC values could independently predict presence or absence of tumor as compared to TRUS biopsy.

Materials and methods

Study design

60 consecutive patients with clinical suspicion of PCa (abnormal screening of PSA/DRE) were recruited in this study based on the Institutional Review Board protocol (*Table 1*). Exclusion criteria included a history of PCa, previous prostate biopsy and standard contraindication to MRI. After informed and written consent, patients underwent DW-MRI at 3.0 T with an ERC. All patients had 12-core TRUS-guided biopsy within one week of MRI without knowledge of the imaging results. Image analysis and histological assessment were carried out independently.

Table 1 Patient demographics and clinical characteristics

	Biopsy positive	Biopsy negative
Number	33 (55%)	27 (45%)
Age (years)		
Median	59	57
Range	49–73	46–69
Clinical stage (digital rectal examination)		
T1	23 (70%)	
T2	6 (18%)	
⩾T3	4 (12%)	
Gleason score (all scores: $N = 86$)		
3+3	18 (21%)	
3+4	28 (33%)	
4+3	22 (26%)	
4+4	10 (12%)	
4+5	6 (7%)	
5+4	0	
Serum prostate specific antigen (ng/mL)		
0–4	2 (6%)	3 (11%)
4.1–10	22 (67%)	17 (63%)
>10	9 (27%)	7 (26%)
AUC	0.56 ($p = 0.42$)	

Biopsy technique and histopathological interpretation

Two 15 mm cores were taken from each of 6 peripheral zone (PZ) segments (base, mid-gland and apex on each

doi:10.18282/amor.v1.i2.37

side) using a standard TRUS approach. Cores were processed, analyzed and reported according to the international guidelines[18]. The final pathological report (standard institutional report) documented histological findings according to where the cores were taken from.

Image acquisition

All MRI scans were performed on a Philips Achieva 3.0 Tesla scanner (Philips Medical Systems) using a 6-channel surface coil placed on the lower abdomen in combination with a disposable ERC (Medrad Inc.), inflated with a 100% (w/v) barium sulphate suspension. High-resolution T2W images of the prostate and seminal vesicles were acquired in 3 planes while DW images were acquired in axial orientation using 6 b-values (0, 50, 150, 300, 500 and 800) (*Table 2*). ADC maps were generated automatically with the manufacturer's software using all b-values except b = 0, to avoid perfusion-related effects. Scan-time for T2W and DW-imaging was 10 and 6 minutes, respectively.

Data processing

Parametric analysis was performed on a dedicated workstation using OsiriX image processing software (Version 3.9.1). The prostate was virtually divided into six segments: (base, mid gland and apex bilaterally) to match the segment-based biopsy sampling procedure. *Figure 1* shows the image for each step of the data analysis process. The peripheral and transition zone as identified on T2W axial image within each segment (*Figure 1A*) was manually delineated (*Figure 1B*). Threshold ADC (tADC) values of 1.0, 1.2 and 1.4 × 10^{-3} mm^2/s were sequentially applied to the delineated region (central zone excluded). All pixels with values above tADC were removed from the image. Remaining pixels with an ADC at or below tADC were evaluated as a ROI for a candidate malignant lesion and that segment was labeled as "DW malignant" (*Figure 1C*). When ROIs overlapped two (or more) segments, both (or all) were reported as "DW malignant". Segments within which no pixels at or remained below threshold values were labeled as "DW benign".

Prostate cancer detection performance

The results of DW-MRI based assessment of segments as "DW malignant" or "DW benign" were compared to the histopathological report for this segment obtained at biopsy. "DW malignant" segments correlating with a positive biopsy result were considered as truly malignant. "DW benign" segments correlating with a negative biopsy result were considered as truly benign. The ability of DW-MRI in detecting PCa was analyzed in two ways: 1) segment-by-segment (6 segments per patient, $N = 360$), and 2) patient-by-patient ($N = 60$). Patients with at least one DW malignant segment were labeled as having PCa. For each analysis, the sensitivity, specificity, positive predictive value (PPV), negative predictive value (NPV) and accuracy for the detection of PCa were calculated for each tADC value. Accepting the biopsy result as gold standard, a receiver operating characteristic (ROC) curve analysis was performed to evaluate the accuracy of PSA alone and each tADC value in detecting PCa.

ROI for candidate malignant lesions

Location, area size, mean ADC and standard deviation of ROI identified as candidate malignant lesions at each tADC were recorded. Mean ADC and area size values were compared between truly malignant and benign segments (Mann-Whitney test). Mean ADC values were correlated to Gleason score (Pearson correlation). An ROC curve analysis was performed to evaluate the accuracy of ROI area size in detecting PCa. The best cut-off value was determined by identifying the largest sensitivity and specificity product value obtained from each ROC curve.

Refined detection criteria

The best performing tADC and best cut-off value for ROI area size were combined to define the refined detection criteria. These criteria were retrospectively applied to evaluate their performance in PCa detection. Sensiti-

Table 2 MRI parameters

Sequence	Repetition time (msec)	Echo time (msec)	Field of view (mm)	Recon resolution (mm)	Flip angle (degrees)	Slice thickness (mm)	Inter-slice gap (mm)
T2-W TSE							
Axial	3831	110	140	0.2 × 0.2 × 3.00	90	3.00	0
Coronal	4540	110	140	0.2 × 0.2 × 3.00	90	3.00	0
Sagittal	4951	110	140	0.2 × 0.2 × 3.00	90	3.00	0
Axial DW-MRI	3746	69	160	1.1 × 1.1 × 2.73	90	2.73	0

doi: 10.18282/amor.v1.i2.37

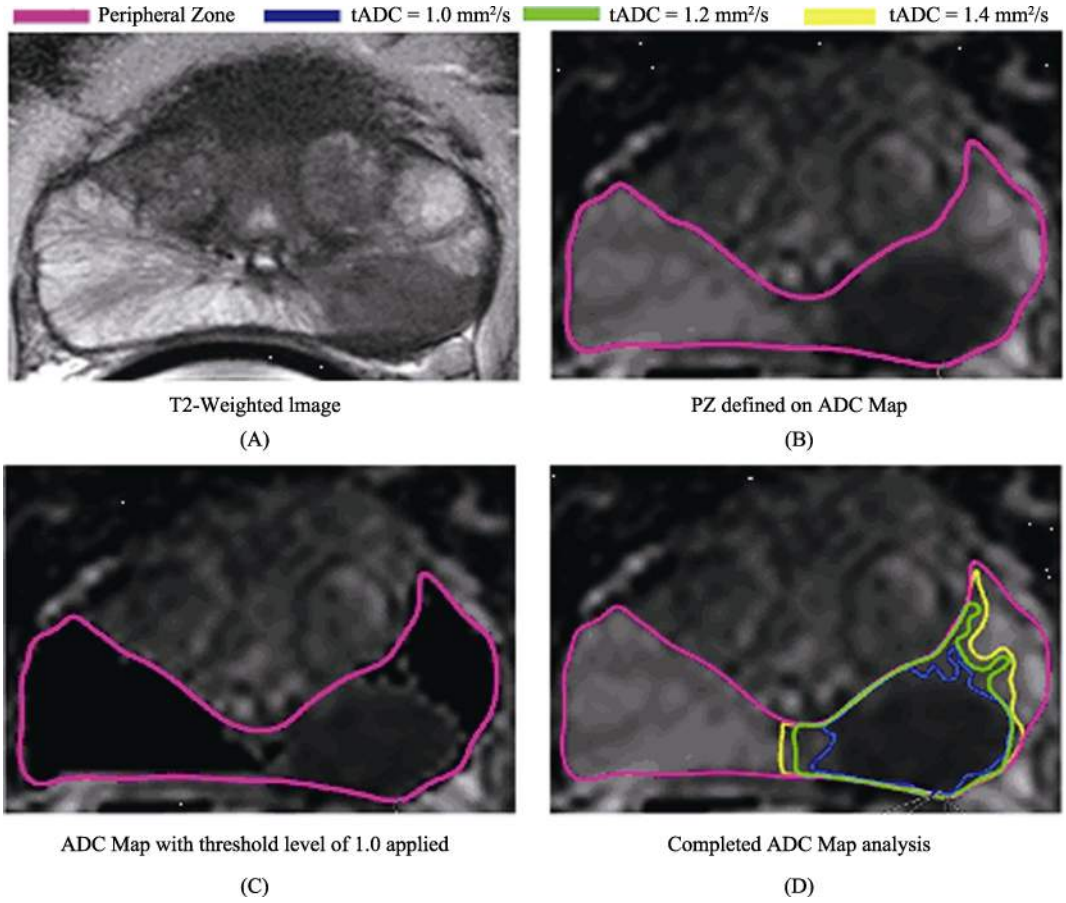

Figure 1 Representative image for each step of the data analysis process. (A) T2-weighted axial image for anatomical identification of the peripheral zone; (B) corresponding apparent diffusion coefficient (ADC) map and outline of the peripheral zone; (C) pixel values above the applied 1.0×10^{-3} mm^2/s tADC appear black on the ADC map, leaving the outline of a potentially malignant lesion; (D) representation of the superimposed lesion area identified at each ADC threshold (tADC) value

vity, specificity, PPV, NPV and accuracy for the detection of PCa were calculated for segment-based and patient- specific analysis.

Statistical analysis

Statistical analysis was performed using Prism, Version 5.01 (GraphPad Software Inc. CA). A p value of <0.05 was considered statistically significant. Data presented as mean ± standard deviation.

Ethics statement

This study received ethical approval from our institution.

Results

Identification of malignant segments

We first analyzed the ADC maps of each generated segment (6/patient, $N = 360$) for the presence of pixels with ADC values below the applied tADC and identified a total of 86 DW malignant segments. The progressive inclusion of pixels with higher ADC values through increased tADC improved the sensitivity for the identification of histologically-confirmed (truly) malignant segments (79% at 1.0×10^{-3} mm^2/s; 91% at 1.2×10^{-3} mm^2/s; 98% at 1.4×10^{-3} mm^2/s) but was associated with loss of specificity (97% at 1.0×10^{-3} mm^2/s; 89% at 1.2×10^{-3} mm^2/s; 71% at 1.4×10^{-3} mm^2/s) (*Table 3*). The lowest tADC of 1.0×10^{-3} mm^2/s yielded the best PPV (79%), while the NPV was high for all the three values (1.0×10^{-3} mm^2/s: 94%; 1.2×10^{-3} mm^2/s: 97%; 1.4×10^{-3} mm^2/s: 99%). Accuracy was the highest at 1.0×10^{-3} mm^2/s (93%). The detection performance was not influenced by the segment location (Chi-square, $p = 0.79$). The ROIs identified in DW malignant segments were next analyzed. The ROIs mean ADC values were significantly lower in DW malignant segments correlating with a positive

doi:10.18282/amor.v1.i2.37

Table 3 Segment-based prostate cancer detection performance of the ADC threshold value

	ADC threshold value ($\times 10^{-3}$ mm^2/s)					
	1.0		1.2		1.4	
	DW malignant	DW benign	DW malignant	DW benign	DW malignant	DW benign
Biopsy-positive	68 (Truly malignant)	18	78 (Truly malignant)	8	84 (Truly malignant)	2
Biopsy-negative	8	266 (Truly benign)	30	244 (Truly benign)	80	194 (Truly benign)
Sensitivity	79% (68/86)		91% (78/86)		98% (84/86)	
Specificity	97% (266/274)		89% (244/274)		71% (194/274)	
Positive predictive value	89% (68/76)		72% (78/108)		51% (80/164)	
Negative predictive value	94% (266/284)		97% (244/252)		99% (194/196)	
Accuracy	93% (334/360)		89% (322/360)		77% (278/360)	

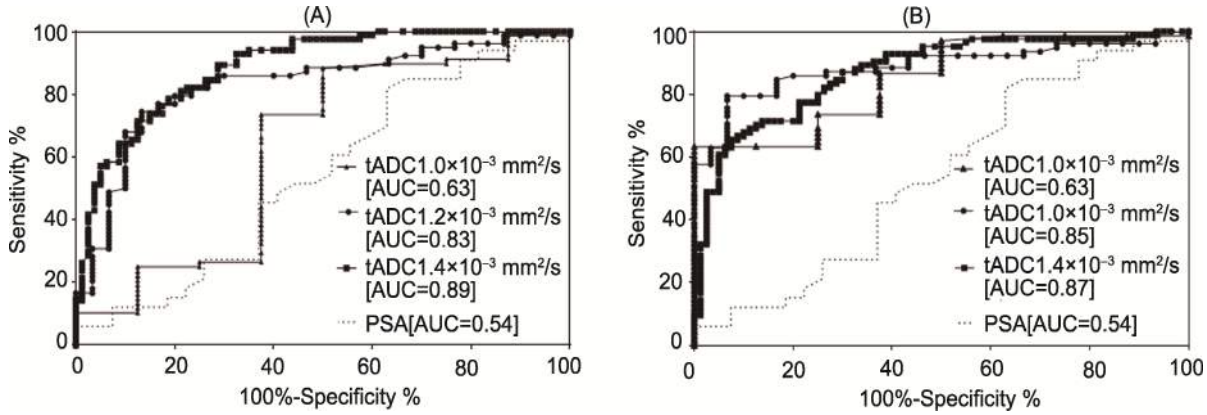

Figure 2 Receiver operating characteristic (ROC) curve for the identification of truly malignant segments following apparent diffusion coefficient threshold values (tADC) analysis at 1.0, 1.2 or 1.4 × 10^{-3} mm^2/s tested by different cut-off points of (A) the mean ADC value and (B) the area size of the identified candidate malignant lesion region of interest (ROI). The ROC curve for prostate specific antigen (PSA) is provided for comparison. Area under curve (AUC) values are provided

biopsy (truly malignant segment) than those correlating with a negative biopsy (truly benign segment) at 1.2 and 1.4 × 10^{-3} mm^2/s (Mann-Whitney; $p < 0.0001$) but not at 1.0 × 10^{-3} mm^2/s ($p = 0.23$). ROC curves showed increasing performance for detection of PCa with increasing tADC value. Detection performance was higher than that of PSA (*Figure 2A*). The area under the curve (AUC) were 0.63 ($p = 0.22$), 0.83 ($p < 0.001$) and 0.89 ($p < 0.001$) at 1.0, 1.2 and 1.4 × 10^{-3} mm^2/s, respectively, compared to 0.54 ($p = 0.56$) for PSA. Mean ADC values were furthermore significantly correlated with Gleason scores 6–8 (3 + 3, 3 + 4, 4 + 3, 4 + 4) at 1.0 × 10^{-3} mm^2/s ($r = -0.9792$, $p = 0.0208$) and 1.2 × 10^{-3} mm^2/s ($r = -0.9819$, $p = 0.0100$) but not at 1.4 × 10^{-3} mm^2/s ($r = -0.9545$, $p = 0.1900$) (*Figure 3*). Significant differences in mean ADC values between the Gleason scores were noted at all threshold values (Mann-Whitney, $p < 0.01$) but the Gleason score specific ADC values could not be established. Similarly, the ROIs area sizes measured at each tADC value were significantly larger in DW malignant segments correlating with a positive biopsy (truly malignant segment) than those correlating with a negative biopsy for tADC of 1.2 and 1.4 × 10^{-3} mm^2/s (Mann-Whitney; $p < 0.0001$) but not 1.0 × 10^{-3} mm^2/s ($p = 0.2328$) (*Table 4*). ROI area size demonstrated a good diagnostic performance (*Figure 2B*), with an AUC of 0.85 ($p = 0.001$) at 1.0 × 10^{-3} mm^2/s, 0.88 ($p < 0.001$) at 1.2 × 10^{-3} mm^2/s and 0.87 ($p < 0.001$) at 1.4 × 10^{-3} mm^2/s.

doi: 10.18282/amor.v1.i2.37

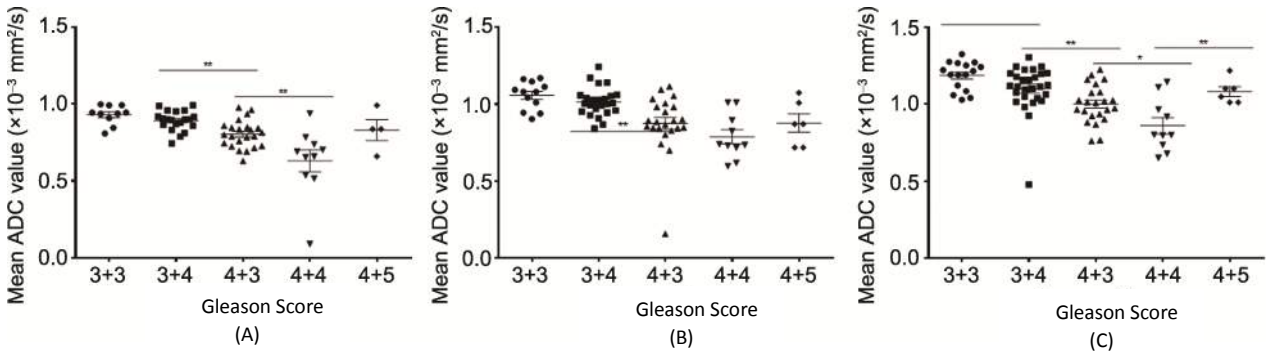

Figure 3 Dot-plots representing the mean ADC value of each identified candidate malignant lesion region of interest (ROI) according to its Gleason Score at ADC threshold (tADC) value of (A) 1.0, (B) 1.2 and (C) 1.4 × 10^{-3} mm^2/s. The mean and standard deviation of the ADC values associated with the ROI for each Gleason Score are presented. The outcomes of Mann-Whitney tests comparing the mean ADC values between Gleason Scores are presented: ***p* < 0.005, **p* < 0.01

Detection of prostate cancer in men

We re-analyzed the data on a patient-specific basis (*N* = 60). The sensitivity for the detection of PCa was high at all three tADC values (94% at 1.0 × 10^{-3} mm^2/s; 94% at 1.2 × 10^{-3} mm^2/s; 100% at 1.4 × 10^{-3} mm^2/s) but specificity was lost with increasing threshold value (98% at 1.0 × 10^{-3} mm^2/s; 70% at 1.2 × 10^{-3} mm^2/s; 26% at 1.4 × 10^{-3} mm^2/s) (*Table 5*). The tADC of 1.0 x 10^{-3} mm^2/s had the highest specificity (98%), PPV (94%), NPV (93%) and accuracy (92%).

Detection performance of refined detection criteria

We finally examined the combination of ROI size and tADC of 1.0 × 10^{-3} mm^2/s since this tADC provided the best balance between sensitivity and specificity, PPV, NPV and accuracy to determine whether the detection criteria for PCa could be refined. Further analysis of the ROC for ROI area size identified 0.20 cm^2 as the best cut-off area size value for the detection of PCa (sensitivity 79.5%; specificity 93.3%; likelihood ratio 11.92). Applying these values (ADC value <1.0 × 10^{-3} mm^2/s with area size <0.20 cm^2) as a refined PCa detection criteria in our cohort, we achieved a sensitivity of 88.3% (76/86), specificity of 99.2 % (272/274), PPV of 97% (69/71) and NPV of 94% (272/289) in segment-based analysis. On patient-specific analysis, these refined detection criteria had a sensitivity of 96.6% (31/33), specificity 88% (24/27), PPV 82% (23/28) and NPV 86% (24/28).

Table 4 Mean apparent diffusion coefficient (ADC) and area size of the region of interest (ROI) of the candidate malignant lesions detected at each threshold level

		ADC threshold value (× 10^{-3} mm^2/s)		
		1.0	1.2	1.4
ADC	All	0.9 ± 0.22	0.98 ± 0.16	1.16 ± 0.17
	Biopsy-positive (Truly malignant)	0.80 ± 0.22	0.94 ± 0.16	1.05 ± 0.16
	Biopsy-negative	0.88 ± 0.12	1.09 ± 0.08	1.27 ± 0.10
	p value (Mann-Whitney)	*p* = 0.2328	*p* < 0.0001	*p* < 0.0001
Area size	All	0.35 ± 0.35	0.50 ± 0.44	0.59 ± 0.49
	Biopsy-positive (Truly malignant)	0.38 ± 0.36	0.63 ± 0.46	0.87 ± 0.51
	Biopsy-negative	0.096 ± 0.07	0.16 ± 0.08	0.30 ± 0.25
	p value (Mann-Whitney)	*p* < 0.0001	*p* < 0.0001	*p* < 0.0001

The mean ± SD were calculated for all tumor regions identified and for those correlating with biopsy-positive and biopsy-negative regions. A Mann-Whitney test was used to compare the mean values between biopsy-positive and biopsy-negative regions.

doi:10.18282/amor.v1.i2.37

Table 5 Patient-based prostate cancer detection performance of the apparent diffusion coefficient (ADC) threshold value

	ADC threshold value ($\times 10^{-3}$ m^2/s)					
	1.0		1.2		1.4	
	Positive	Negative	Positive	Negative	Positive	Negative
Biopsy-positive	30	2	30	2	32	0
Biopsy-negative	2	25	8	19	20	7
Sensitivity	94% (30/32)		94% (30/32)		100% (32/32)	
Specificity	98% (25/27)		70% (19/27)		26% (7/27)	
Positive predictive value	94% (30/32)		79% (30/38)		62% (32/52)	
Negative predictive value	93% (25/27)		90% (19/21)		100% (7/7)	
Accuracy	92% (55/60)		82% (49/60)		65% (39/60)	

Discussion

Current screening and diagnostic tools for PCa have imperfect profiles and may result in men being both under- and over-diagnosed[4]. A reliable, non-invasive and robust diagnostic tool such as MRI could potentially benefit men with suspected PCa[19,20]. As the majority of significant PCas are visible on DW, potential roles include selection of a suitable area for biopsy and incorporation into an image-guided approach where registration of real-time TRUS images with MRI data allows accurate needle placement, thus eliminating the randomness of TRUS-guided biopsy and increasing the likelihood of positive biopsy[21–23]. Although qualitative interpretation of DW images is useful, subjective and has a significant inter-observer variability, it cannot be applied to predict tumor grade[17,24]. On the other hand, ADC values generated from multiple b-values give an objective measurement of tissue diffusion and are a surrogate for tumor aggressiveness[5,25]. The values broadly change inversely with Gleason score and the trend is lower in higher stage of disease, although there are some overlaps between benign and malignant tissue[5,25,26].

Gains in sensitivity with higher tADC values would be expected to be offset by lower specificity and a balance between these outcome parameters is required. To address these issues, we applied three sequential ADC threshold levels (tADC of 1.0, 1.2 and 1.4 $\times 10^{-3}$ mm^2/s) in 360 segments across 60 patients to determine whether quantitative assessment at 3.0 T could identify malignant lesions within the prostatic PZ prior to prostate biopsy. At 1.2 $\times 10^{-3}$ mm^2/sec, the sensitivity and specificity for cancer detection was 91% and 89%, respectively, with a negative predictive value of 97% for segment-based analysis. For patient-specific analysis, the sensitivity and specificity were 94% and 70%, respectively. While tADC of 1.2 $\times 10^{-3}$ mm^2/s gives excellent cancer detection, a significant number of segments with ADC values below this value would be correlated with a negative biopsy.

Potential reasons include overlap of ADC values for tumors and other pathological processes conditions which are also known to restrict diffusion (e.g., chronic inflammation, hyperplasia and calcification)[1,27]. Potentially, sampling error due to the random nature of TRUS biopsy could in part account for this overlap, a factor that has been cited in favor of using MRI to not only identify potential tumors in high risk patients with negative biopsy results but also to guide subsequent biopsy. We also observed that optimal parametric DW-MRI interpretation benefits from the combination of both the mean ADC value and the minimum lesion size. The measurement of the diameter of suspicious tumor lesions on DW-MRI was indeed proposed as an important parameter to consider for the prediction of insignificant PCa[28]. ROC analysis identified an ROI area size of 0.20 cm^2 as the best cut-off for the detection of PCa. Combination of this value with a tADC of 1.0 $\times 10^{-3}$ mm^2/s into a refined detection criteria increased specificity (89% to 99%) and PPV (72% to 97%), albeit at the expense of a slight decrease in both sensitivity and NPV. We observed a significant negative correlation between Gleason score and mean ADC values at all tADC values. While we were unable to determine Gleason score specific ADC values, we observed unexpected mean ADC values in Gleason 9 biopsies (N = 5), which was higher than that of Gleason 8 lesions, though the small patient numbers preclude a meaningful comparison.

Neither the distribution of tumor within segments nor detection performance was statistically different across the 6 prostate segments in our study. Apparently, they differ from few published studies where the prostatic

doi: 10.18282/amor.v1.i2.37

base was associated with higher false positive rates[29]. This may be explained by the higher spatial resolution afforded by 3.0 T imaging, especially with an ERC, which may make definition between prostatic and surrounding tissue less challenging. It also suggests that DW-MRI identifies PZ PCa with a high degree of accuracy independent of tumor location.

Our study has several limitations. We traded the ease of dual-functional sequence MRI without an ERC for a single functional study acquired with an ERC at 3.0 T with the knowledge that it would require additional set-up and physician time, increased cost and some discomforts which might not sit well with screening program philosophy. In the absence of controlled trials and based on the best available information, an advisory group of the European Society of Urogenital Radiology (ESUR) drafted consensus recommendations for screening of PCa with MRI. Faced with differences between centers such as field strength, use of an ERC, use of dynamic contrast-enhancement and spectroscopy, they recommended multi-parametric MRI techniques incorporating two functional techniques (DW-MRI, DCE or spectroscopy) in addition to T2W imaging for screening of PCa. Although the ERC clearly boosts signal, the consensus group noted that the use of an ERC was not essential at 3.0 T due to the signal boost from the higher field strength. Nonetheless, we opted to place an ERC to maximize signal-to-noise in this study in order to compensate for the fact that we adopted a single functional study only (DW-MRI). Although the cost and inconvenience of an ERC are significant, our approach of T2W imaging plus a single functional (DW-MRI) sequence at 3.0 T is simple and can be readily implemented into clinical algorithms, with the longer preparation time and cost of the coil offset by shorter and less complex examination shall avoid the use of contrast agent and spectroscopy which normally require complex post-processing.

While the performance of parametric DW-MRI was robust, our results must be interpreted within the known limitations of 12-core biopsy, which may underestimate the Gleason score in up to 29% of cases[30] and the modest number of patients included in this study. Like most previous studies, our study did not address central gland (central zone) tumors which account for up to 30% of all PCa, however, as TRUS biopsy routinely targets the peripheral gland we were bereft of a reference standard for the central zone[31]. Image and data processing using this objective parametric analysis technique was modestly time-consuming which may hinder its application in routine clinical care. Further evaluation of the constraints associated with this approach is necessary. In the future, automatic color-look-up-tables corresponding to specific ADC values could be developed providing acquisition parameters (field strength, b-values use of specific coils) are standardized[32]. This would aid rapid, objective image review and facilitate rapid identification of malignant lesions by virtue of their ADC values alone or alongside qualitative analysis.

Conclusion

We have shown that parametric DW-MRI at 3.0 T can objectively detect tumor prior to TRUS-guided prostate biopsy. The high NPV of 94% at 1.0×10^{-3} mm^2/s adds further the weight supporting of a DW-MRI role in detecting PCa. Despite its limitations, it is considerably more accurate than PSA alone and a promising tool for not only the screening of peripheral zone PCa but potentially also for characterizing its aggressiveness. This concept is particularly important in the context of over-diagnosis and over-treatment of clinically insignificant cancers. However, large-scale adequately powered randomized and standardized studies are needed to determine whether Gleason score specific ADC values can be established. If this could be achieved, incorporation of ADC values into a diagnostic algorithm in combination with other clinical parameters (such as PSA and DRE) might ultimately allow low-risk patients to forego biopsy. Additionally, patients undergo a policy of active surveillance who observed declination in the ADC values baseline during serial follow-up might signal an imperative for change to active treatment.

Author contributions

Diarmaid C Moran collected the data and together with Laure Marignol conducted the data analysis. Andrew J Fagan developed the image acquisition protocols. Eoin Gaffney conducted pathological assessments.Ruth Dunne, Dearbhail O'Driscoll and James FM Meaney conducted radiological assessments. All the authors were involved in study design and the construction of the patients' cohort.

Acknowledgments

This project was supported by an unconditional educational research grant from Astellas, the St Luke's Institute for Cancer Research and the Health Research Board.

doi:10.18282/amor.v1.i2.37

Conflict of interest

The authors declared no potential conflict of interest with respect to the research, authorship, and/or publication of this article.

References

1. Wolf A, Wender RC, Etzioni RB, et al. American Cancer Society guideline for the early detection of prostate cancer: update 2010. CA Cancer J Clin 2010; 60(2): 70–98.
2. Heidenreich A, Bastian PJ, Bellmunt J, et al. EAU guidelines on prostate cancer. Part 1: screening, diagnosis, and local treatment with curative intent-update 2013. Eur Urol 2014; 65(1): 124–137.
3. Catalona WJ, Richie JP, deKernion JB, et al. Comparison of prostate specific antigen concentration versus prostate specific antigen density in the early detection of prostate cancer: receiver operating characteristic curves. J Urol 1994; 152(6 Pt 1): 2031–2036.
4. Roemeling S, Roobol MJ, Kattan MW, et al. Nomogram use for the prediction of indolent prostate cancer. Cancer 2007; 110(10): 2218–2221.
5. Dickinson L, Ahmed HU, Allen C, et al. Magnetic resonance imaging for the detection, localisation, and characterisation of prostate cancer: recommendations from a Eurpean consensus meeting. Eur Urol 2011; 59(4): 477–494.
6. Sciarra A, Barentsz J, Bjartell A, et al. Advances in magnetic resonance imaging: how they are changing the management of prostate cancer. Eur Urol 2011; 59(6): 962–977.
7. Choi MS, Choi YS, Yoon BI, et al. The clinical value of performing an MRI before prostate biopsy. Korean J Urol 2011; 52(8): 572–577.
8. Cornfeld DM, Weinreb JC. MR imaging of the prostate: 1.5T versus 3T. Magn Reson Imaging Clin N Am 2007; 15(3): 433–448.
9. Kim JH, Kim JK, Park BW, et al. Apparent diffusion coefficient: prostate cancer versus noncancerous tissue according to anatomical region. J Magn Reson Imaging 2008; 28(5): 1173–1179.
10. Morgan VA, Kyriazi S, Ashley SE, et al. Evaluation of the potential of diffusion-weighted imaging in tate cancer detection. Acta Radiol 2007; 48(6): 695–703.
11. Kim CK, Park BK, Han JJ, et al. Diffusion-weighted imaging of the prostate at 3 T for differentiation of malignant and benign tissue in transition and peripheral zones: preliminary results. J Comput Assist Tomogr 2007; 31(3): 449–454.
12. Kim CK, Park BK, Kim B. High-b-value diffusion-weighted imaging at 3 T to detect prostate cancer: comparisons between b values of 1,000 and 2,000 s/mm^2. AJR Am J Roentgenol 2010; 194(1): 33–37.
13. Sato C, Naganawa S, Nakamura T, et al. Differentiation of noncancerous tissue and cancer lesions by apparent diffusion coefficient values in transition and peripheral zones of the prostate. J Magn Reson Imaging 2005; 21(3): 258–262.
14. Tamada T, Sone T, Jo Y, et al. Apparent diffusion coefficient values in peripheral and transition zones of the prostate: comparison between normal and malignant prostatic tissues and correlation with histologic grade. J Magn Reson Imaging 2008; 28(3): 720–726.
15. Kumar V, Jagannathan NR, Kumar R, et al. Apparent diffusion coefficient of the prostate in men prior to biopsy: determination of a cut-off value to predict malignancy of the peripheral zone. NMR Biomed 2007; 20(5): 505–511.
16. deSouza NM, Reinsberg SA, Scurr ED, et al. Magnetic resonance imaging in prostate cancer: the value of apparent diffusion coefficients for identifying malignant nodules. Br J Radiol 2007; 80(950): 90–95.
17. Mazaheri Y, Hricak H, Fine SW, et al. Prostate tumor volume measurement with combined T2-weighted imaging and diffusion-weighted MR: correlation with pathologic tumor volume. Radiology 2009; 252(2): 449–457.
18. Van der Kwast T, Bubendorf L, Mazerolles C, et al. Guidelines on processing and reporting of prostate biopsies: the 2013 update of the pathology committee of the European Randomized Study of Screening for Prostate Cancer (ERSPC). Virchows Arch 2013; 463(3): 367–377.
19. Thompson JE, Moses D, Shnier R, et al. Multiparametric magnetic resonance imaging guided diagnostic biopsy detects significant prostate cancer and could reduce unnecessary biopsies and over detection: a prospective study. J Urol 2014; 192(1): 67–74.
20. Pokorny MR, de Rooij M, Duncan E, et al. Prospective study of diagnostic accuracy comparing prostate cancer detection by transrectal ultrasound-guided biopsy versus magnetic resonance (MR) imaging with subsequent MR-guided biopsy in men without previous prostate biopsies. Eur Urol 2014; 66(1): 22–29.
21. Overduin CG, Futterer JJ, Barentsz JO. MRI-guided biopsy for prostate cancer detection: a systematic review of current clinical results. Curr Urol Rep 2013; 14(3): 209–213.
22. Park BH, Jeon HG, Choo SH, et al. Role of multiparametric 3.0-Tesla magnetic resonance imaging in patients with prostate cancer eligible for active surveillance. BJU Int 2014; 113(6): 864–870.
23. Nishida S, Kinoshita H, Mishima T, et al. Prostate cancer detection by prebiopsy 3.0-Tesla magnetic resonance imaging. Int J Urol 2011; 18(9): 653–658.

doi: 10.18282/amor.v1.i2.37

24. Turkbey B, Pinto PA, Mani H, et al. Prostate cancer: value of multiparametric MR imaging at 3 T for detection—histopathologic correlation. Radiology 2010; 255(1): 89–99.
25. Hambrock T, Hoeks C, Hulsbergen-van de Kaa C, et al. Prospective assessment of prostate cancer aggressiveness using 3-T diffusion-weighted magnetic resonance imaging-guided biopsies versus a systematic 10-core transrectal ultrasound prostate biopsy cohort. Eur Urol 2012; 61(1): 177–184.
26. Verma S, Rajesh A, Morales H, et al. Assessment of aggressiveness of prostate cancer: correlation of apparent diffusion coefficient with histologic grade after radical prostatectomy. AJR Am J Roentgenol 2011; 196(2): 374–381.
27. Liu X, Peng W, Zhou L, et al. Biexponential apparent diffusion coefficients values in the prostate: comparison among normal tissue, prostate cancer, benign prostatic hyperplasia and prostatitis. Korean J Radiol 2013; 14(2): 222–232.
28. Lee DH, Koo KC, Lee SH, et al. Tumor lesion diameter on diffusion weighted magnetic resonance imaging could help predict insignificant prostate cancer in patients eligible for active surveillance: preliminary analysis. J Urol 2013; 190(4): 1213–1217.
29. Morgan V, Kyriazi S, Ashley S, et al. Evaluation of the potential of diffusion-weighted imaging in prostate cancer detection. Acta Radiol 2007; 48(6): 695–703.
30. Corcoran NM, Hong MK, Casey RG, et al. Upgrade in Gleason score between prostate biopsies and pathology following radical prostatectomy significantly impacts upon the risk of biochemical recurrence. BJU International 2011; 108(8b): 202–210.
31. Kim CK, Park BK, Kim B. Diffusion-weighted MRI at 3 T for the evaluation of prostate cancer. AJR Am J Roentgenol 2010; 194(6): 1461–1469.
32. Koo JH, Kim CK, Choi D, et al. Diffusion-weighted magnetic resonance imaging for the evaluation of prostate cancer: optimal b value at 3T. Korean J Radiol 2013; 14(1): 61–69.

doi:10.18282/amor.v1.i2.37

Focus and Scope

Advances in Modern Oncology Research, AMOR, is a peer-reviewed, open-access publication that delivers original research articles, reviews and clinical studies that are significant in all disciplines of modern oncology. With a focus on publishing high quality academic papers, detailing the latest information and research in the field of oncology, AMOR aims to provide a communication and information exchange platform for a broad audience of oncologists, surgeons, medical researchers and professionals. Articles from related fields that are interesting to a broad readership are particularly welcome.

Call for Papers

PiscoMed Publishing Pte Ltd and the Editor-in-chief, Dr. Omar Abdel-Rahman, invite all authors to submit their manuscripts to our journal, *Advances in Modern Oncology Research* (AMOR), for peer review.

AMOR allows immediate visibility and access for research outputs as well as free usage of researchers' results. As the journal is entitled *Advances in Modern Oncology Research*, some relevant topics include but are not limited to:

- Breast cancer
- Thoracic malignancies (including lung cancer, mesothelioma and thymoma)
- Genitourinary cancer (including kidney cancer, prostate cancer and bladder cancer)
- Gastrointestinal cancer (including colorectal cancer, gastroesophageal cancer, hepato-pancreato-biliary cancer)
- Hematological malignancies (including lymphoma, myeloma and leukemia)
- Endocrine cancer
- Head and neck cancer

The journal is well-defined in rendering support to authors, including how:

- Authors may maintain their copyright
- The articles can be shared, re-used and archived without cost
- Being consistent with important open access guidelines, the journal is a compelling addition to the latest archiving procedures
- Immediate processing refers to publication in minimum time. All editorial and publication work are directed towards high-quality results

Submission can be made through the "**Submit Your Manuscript**" icon on the journal home page. By clicking on this, you will be directed to the Online Submission page and Author Guidelines.

Copyright

About the Publisher

PiscoMed Publishing Pte Ltd is an international publisher based in Singapore, with operations in China and Malaysia. Since its inception in 2011, PiscoMed has dedicated itself towards advancing medical research and clinical practice worldwide via the publication of high quality literature, aimed at academics and medical practitioners. Our vision is to transform scientific research findings into quality-assessed communications for the continuous dissemination of new knowledge and state-of-the-art discoveries.

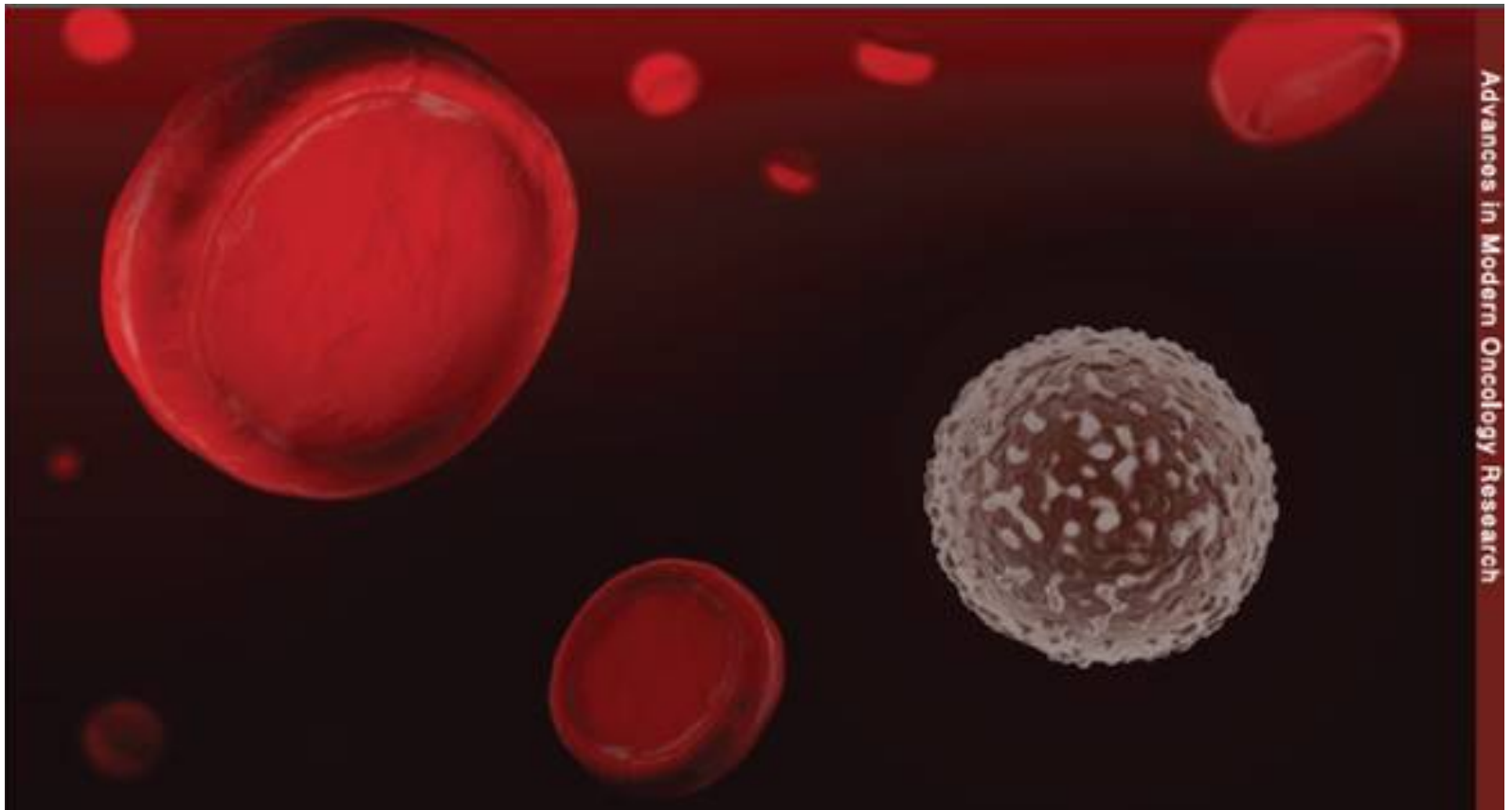

Advances in Modern Oncology Research

Volume 1 | Issue 2 • December 2015

Pisco Med Publishing

ISSN 2424-7847

21 Serangoon North Avenue 5, #03-03, Ban Teck Han Building, Singapore 554864.

www.piscomed.com